

Master thesis submitted in partial fulfillment of the requirements for the degree Master in Biomedical Engineering

DEVELOPMENT OF A MULTI-SENSOR MODULAR ELECTRONIC STETHOSCOPE

Veronika Catharina Schatz

13th of January 2025

Promotor: Prof. Dr. ir Bruno da Silva Gomes

Co-Promotors: Dr. Laurent Segers Assistant: Jerome Vande Velde

Engineering



Acknowledgments

I would like to express my deepest gratitude to my promotor Prof. Dr. ir Bruno da Silva Gomes for guiding me through this master thesis and assisting me in finding creative ideas, new perspectives and above all supporting me in improving my engineering skills. You were always willing to listen to my concerns and helped me find solutions for them. Thank you for making this project possible.

Secondly, I would like to thank my co-promoter Dr. Laurent Segers and assistant Jerome Vande Velde who helped me during the whole course of the thesis. You supported me with exceptional guidance and contributed greatly to this project. I had a great time in the Jungle Lab and I will truly miss it.

Remark On Master's Dissertation and the Oral Presentation

This master's dissertation is part of an exam. Any comments formulated by the assessment committee during the oral presentation of the master's dissertation are not included in this text.

Abstract

Electronic stethoscopes address limitations of auscultation with analog stethoscopes, such as the dependency on the physicians' hearing ability, their experience, and their subjective interpretation. However, currently the electronic stethoscopes on the commercial market fail to exploit the full potential of cutting-edge microphone technology and innovative multi-sensor approaches. This thesis proposes a modular upgrade to an analog stethoscope that incorporates multiple sensor types and features microphone array capabilities. The presented stethoscope was tested for its performance in detecting heart beats but is designed to be applied to other auscultation sites as well. Above that, it can be employed as an educational and potential research platform to promote the development of revolutionary signal processing techniques and artificial intelligence algorithms.

Contents

1	Introduction	5
2	Background 2.1 The Heart	7 8 9 10 11
3	Related Work 3.1 Electronic Stethoscopes in Industry	12 12 17
4	Design Approaches 4.1 Acoustic Sensors	24 24 31
5	Multi-Sensor Modular Design 5.1 Requirements of the Design 5.2 General Design Outline 5.2.1 Analog Front End 5.2.2 Interfacing Layer 5.2.3 Digital Back End 5.2.4 3D Printed Casing 5.3 Demonstrator	33 36 37 44 49 53
6	Experimental Results 6.1 Microphone Characterization in the Anechoic Box 6.1.1 Sensitivity and Noise Floor Measurement 6.1.2 SNR Analysis 6.1.3 Frequency Response 6.1.4 Heart Sound emitted by Loudspeaker 6.2 Microphone Performance on Recording Heart Sounds 6.2.1 Individual Microphone Types applied to Auscultation Points 6.3 Summary of the Findings	55 57 60 61 64 65 65 70
7	Conclusion and Future Work	7 1
8	Societal Reflection	73

List of Tables

2.1	Comparison of features of the four major heart sounds S1, S2, S3, S4 and pathologic heart murmurs. S3 and S4 may be caused by a diseased heart as well and are then referred to as ventricular or atrial gallop respectively [47]. The auscultation points refer to the auscultation scheme illustrated in Figure 2.4	1(11
3.1	Summary of the State-of-the-Art electronic stethoscopes on the commercial market sorted by their release dates and comparison of their features with regard to the herein presented stethoscope. It should be noted that the CardioSleeve is not a classical electronic stethoscope but an add-on device that can improve the examination quality by performing an ECG in parallel to the auscultation process. For the 3M Littman CORE stethoscope no information was found regarding sensor type or filters. However, this information was published in an earlier version of the stethoscope, the Littmann Range. NM: not mentioned, NA: not applicable .	15
3.2	Electronic stethoscopes presented in the scientific literature sorted by year, ECM: electret condenser microphone NM: not mentioned,	22
3.3	Electronic stethoscopes presented in the scientific literature sorted by year (continuation of Table 3.2) ECM: electret condenser microphone NM: not mentioned,	23
4.1	Comparison of acoustic sound acquisition sensors (references: [57], [43])	30
5.1	List of functional requirements, H: hard requirements S: soft requirement	35
5.2	List of non-functional requirements, H: hard requirement, S: soft requirement	35
5.3	Estimated current consumption of the individual PCBs	47
6.1	Coefficients for the linear regression model of Equation 6.1 for the three microphone boards and the commercial reference stethoscope	57
6.2	Noise floor levels per acoustic transducer deduced from the sensitivity curves shown in Figure 6.2	59
6.3	Signal-to-noise-ratios (SNRs) for the developed microphone boards and the commercial reference stethoscope. SNR_{max} represents the maximal SNR that a sensor can achieve and SNR_{max} of the SNR that can be expected for a typical heart sound. The SNR_{max} of the 3M Littmann CORE stethoscope is not available as 3M does not provide the specifications necessary to calculate the SNR.	61

List of Abbreviations

ADC Analog-to-Digital Converter

AI Artificial Intelligence

AV Atrioventricular
BLE Bluetooth Low Energy

BMI Body-Mass-Index

DSP Digital Signal Processor ECG Electrocardiography EMG Electromygraphy

FFT Fast Fourier Transform

FPGA Field-Programmable Gate Array I2S Inter-Integrated Circuit Sound

IC Integrated circuit IoT Internet of Things

ISR Interrupt Service Routine LDO Low-Dropout Regulator LOR List of Requirement MCU Microcontroller Unit

MEMS Micro-Electromechanical Systems

OSR Oversampling Ratio
PC Personal Computer
PCB Printed Circuit Board
PCG Phonocardiography
PDM Pulse Density Modulation
PPG Photoplethysmography

RMS Root-Mean-Square SNR Signal-to-Noise-Ratio

SoC System on Chip

SPI Serial Peripheral Interface SPL Sound Pressure Level UDP User Datagram Protocol

Chapter 1

Introduction

Organs like the heart, lungs, abdomen, or joints emit internal body sounds that can propagate through tissue to the surface of the skin. In medicine, these sounds contain crucial information about a patient's health condition and are an essential tool to diagnose a disease or monitor its progression. Listening to body sounds is called auscultation and is a non-invasive and easy-to-use technique. A doctor performs auscultation by placing the chestpiece of a stethoscope to specific auscultation points on the skin of a patient. The diaphragm of the chestpiece captures vibrations of the skin induced by internal body sounds that propagate through tubes to the ears of a physician [43]. However, the current auscultation procedure is strongly affected by the doctor's hearing abilities and experience, as well as his/her subjective interpretation.

Electronic stethoscopes, available on the commercial market since the early 1990s [43], address these issues by recording body sounds with acoustic sensors and relaying them to the user in an amplified fashion. Today, commercial electronic stethoscopes offer a wide range of functionalities in addition to measuring and amplifying body sounds. The user can specify the target organ to auscultate using pre-configured filters, store recordings to replay them at another time or share them with specialists. Furthermore, some commercial stethoscopes incorporate artificial intelligence (AI) classifiers to automatically identify and categorize a condition.

Despite all their advanced technological features, recent electronic stethoscopes do not enable for simultaneous analog and digital listening modes, as they all incorporate acoustic transducers in the stethoscope tubes that disrupt the natural sound propagation pathway of a conventional stethoscope. This makes it impossible for the user to accurately compare the genuine natural sound and its recording. Moreover, a purely electronic stethoscope becomes inoperative in case the battery is depleted. Paradoxically, the state-of-the-art electronic stethoscopes try to mimic conventional stethoscopes and specifically filter for the human hearing range [9], [23], [66]. Thereby, they disregard valuable diagnostic information outside the human hearing frequency range and do not exploit the full potential of cutting-edge microphone technology.

Conventional stethoscopes are a widely spread instrument. Therefore, this thesis proposes an upgrade of a traditional stethoscope that does not interfere with its ordinary operation mode and that allows for simultaneous analog and digital auscultation. With the prototype, described in this thesis, it is possible to quickly and easily digitalize a conventional stethoscope, thereby giving fully functional analog stethoscopes a new purpose and keeping them from being discarded. Furthermore, the proposed design exploits multiple sensor technologies that offer heterogeneous responses and can thus potentially be suitable for different auscultation sites.

The designed prototype aims to meet the following three scientific goals:

- 1. The presented electronic stethoscope aspires to be employed as an education and potential research platform. The prototype is compatible with multiple computational platforms. Therefore, its application spectrum is versatile. In future works, it can enable to verify the performance of signal processing techniques or newly emerging AI algorithms for disease classification with real body sounds captured with the prototype. Furthermore, it can serve as an educational tool to teach students and professionals about existing microphone technologies and auscultation techniques, thereby potentially reinforcing multi-disciplinary collaboration.
- 2. In the light of environmental pollution, electronic waste has become a serious issue [51]. In order to avoid contributing to this problem, a modular prototype design was chosen that facilitates easy repair or replacement of damaged components without abandoning the whole device. Moreover, multiple acoustic sensor types are employed in the presented prototype that can be arbitrarily exchanged or combined and thus allow for technology comparison. The prototype does not interfere physically with the conventional stethoscope it incorporates, and therefore, the original condition of the stethoscope can be easily restored. These features make the design a sustainable, eco-friendly, and viable option to electrify conventional stethoscopes.
- 3. Lastly, the prototype features microphone array capabilities that enable advanced signal processing algorithms for sensor fusion and potentially drive AI algorithms. In future works, this arrangement can help to locate the sound source and might provide an added value to the diagnosis of diseases.

The herein presented electronic stethoscope is engineered to capture all body sounds of the heart, the lungs, and the abdomen. However, in the course of this thesis, the performance of the prototype is evaluated using the example of heart sounds. The thesis is structured as follows:

The next Chapter 2 provides fundamental information about the conventional stethoscope and how it can be deployed to detect body sounds. Furthermore, it details the origin of body sounds with a special emphasis on heart sounds.

Subsequently, Chapter 3 reviews electronic stethoscopes currently found on the market and in the scientific field and details their key characteristics and advancements.

Chapter 4 details the most common sound acquisition sensors deployed in electronic stethoscopes, along with their benefits and drawbacks. Furthermore, the various mechanical designs of electronic stethoscopes are described.

Chapter 5 outlines the design of the presented prototype. It first defines the functional and non-functional requirements that the device must meet and details the design outline. The hardware components, namely the three microphone types and the software, are explained thereafter.

Chapter 6 presents the experiments performed to evaluate the characteristics of the developed microphones along with their findings. First, the noise floor, sensitivity, signal-to-noise ratio (SNR), and the frequency response of the individual microphone boards were determined in an anechoic box, and then the microphones were exposed to real-life heart auscultation scenarios.

Chapter 7 summarizes the findings and gives an outlook on future works that could be performed with the prototype.

Finally, Chapter 8 contextualizes the implications that the device might have on society.

Chapter 2

Background

The stethoscope is a device that is intended to detect internal body sounds and serves as a diagnostic tool to detect medical conditions [43]. The major body sounds collected with a stethoscope originate from movements of the heart, lungs, joints, or abdomen [43]. The process of listening to these sounds is called "auscultation" and involves placing the chest piece of a stethoscope at the location of interest in order to pick up vibrations of the skin and transmitting them to the ears of the operator [43]. The French physician René Laënnec invented the first stethoscope in 1816 [3]. Since then, the acoustic stethoscope has advanced further and today consists of a chestpiece that picks up vibrations of the patient's skin and a tubing that directs the sound waves to a headset [50]. A sketch of a typical acoustic stethoscope is depicted in Figure 2.1. A chestpiece has a diaphragm and a bell side. The diaphragm is more suited for high-frequency sound and the bell is used for lower frequency sound [49]. However, there exists no standard dimension for chestpieces.

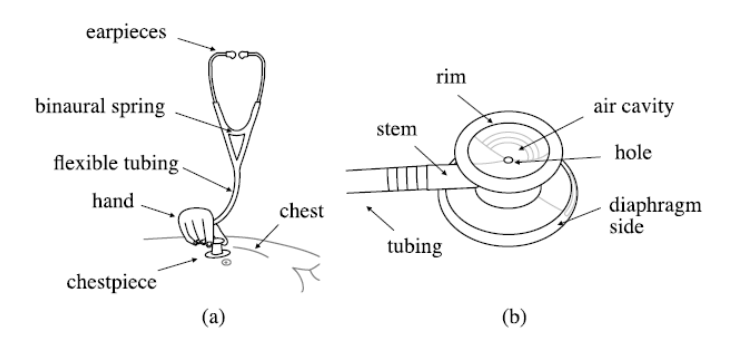


Figure 2.1: Sketch of an acoustic stethoscope [50]. a) Drawing of an exemplary auscultation. The chestpiece is placed in direct contact to the skin and the captured sound waves are transmitted through a flexible tubing to the ears of a physician. b) Drawing of a chestpiece with the "bell side" on top and the "diaphragm side" on the bottom.

In this thesis, the functionality of the developed prototype is evaluated using the example of heart sounds. Therefore, a special focus lies on understanding the heart's anatomy, how heart sounds arise, where they originate from, and how they are made audible with traditional stethoscopes. This chapter provides insight into the basic working principle of the human heart, the typical profile of a heart beat and the standard auscultation process. Additionally, the last

section details other body sounds that can be auscultated with a stethoscope.

2.1 The Heart

The heart can be divided into two halves, the "right heart" and the "left heart" [53]. Both halves consist of an atrium and a ventricle that are separated through atrioventricular (AV) heart valves [53]. The AV valve of the right heart is called the tricuspid valve and the AV valve of the left heart is called the mitral valve [53]. The aortic and the pulmonary valves, also called the semilunar valves, are located between the ventricles and the aorta or the pulmonary artery, respectively [53]. The right heart pumps deoxygenated blood from the body to the lungs (pulmonary circulation), while the left heart pumps oxygenated blood from the lungs to the rest of the body (systemic circulation) [3]. A cardiac cycle consists of two phases: diastole (filling phase) and systole (ejection phase). During diastole, blood is directed towards the ventricles and is ejected during systole [3]. The two phases are determined by the pressure differences between the atria and the ventricles. Figure 2.2 [3] shows changes in ventricular volumes based on alterations in pressure levels. With the onset of systole, the ventricular muscle contracts, causing an increase in ventricular pressure. The AV valve closes when the ventricular pressure exceeds the atrial pressure. The continued increase in ventricular pressure causes the aortic valve to open, leading to the ejection of blood to the circulatory system. The aortic valve closes as the ventricular pressure drops and finally the AV valve opens again and blood passively flows from the atria into the ventricle [3].

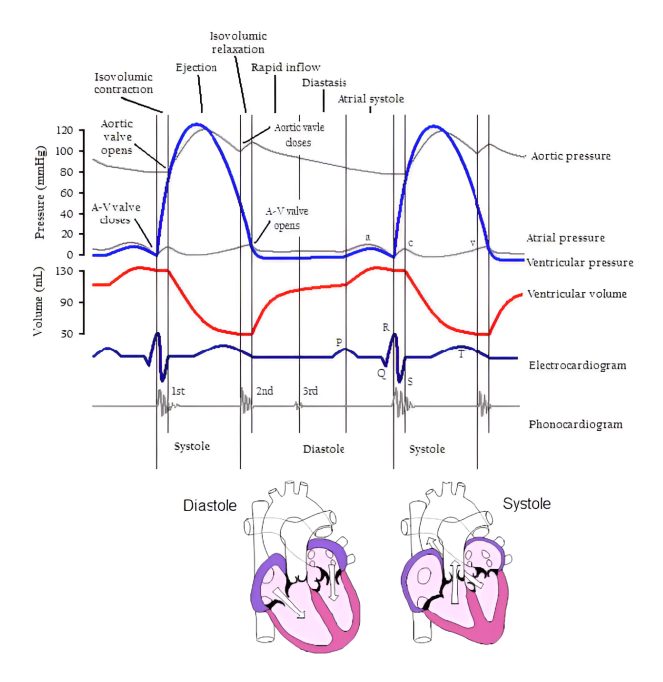


Figure 2.2: Mechanical, electrical and acoustic events occurring in the left heart during a cardiac cycle [3]. The graphs show how pressure differences (blue and light grey) in the left heart impact the left ventricular volume (red) and how electrical (dark blue) and acoustic (dark grey) events relate to it. The first and second heart sounds begin with the closure of the AV valve and the aortic valve respectively.

2.1.1 Heart Sounds

As can be seen in Figure 2.2, the cardiac cycle is accompanied by heart sounds generated through the closing of heart valves or blood flow into the heart [3]. In general, there are four heart sounds: the first two, S1 and S2, can be heard in all healthy hearts. The third heart sound, S3, when heard in a person older than 40 years, indicates a pathology, for example a systolic dysfunction [47]. An audible S4 heart sound can also be considered abnormal [47]. The pathologic S3 and S4 heart sound are also referred to as ventricular or atrial gallop, respectively [47]. The first heart sound, S1, is the highest in amplitude and duration and generates a "crescendo-decrescendo" signal [53]. It is caused by the closure of the tricuspid and mitral valve which is delayed by 20-30 ms ("the split") [3]. The second heart sound S2 results from the closure of the aortic and pulmonary valve likewise separated by a split of approximately 30 ms [3]. The S3 heart sound arises from rapid ventricular filling during early diastole and can be a sign of a diseased heart in adults [3]. The fourth heart sound S4 comes from the contraction of the atria prior to the onset of systole [3]. Other heart sounds different from those four heart sounds are called murmurs and suggest a heart malfunction [3]. A visualization of the four heart sounds over time is called phonocardiogram (PCG) and an example can be seen in Figure 2.3. Systole contains only the S1 heart sound, whereas diastole comprises the S2, S3, and S4 heart sounds.

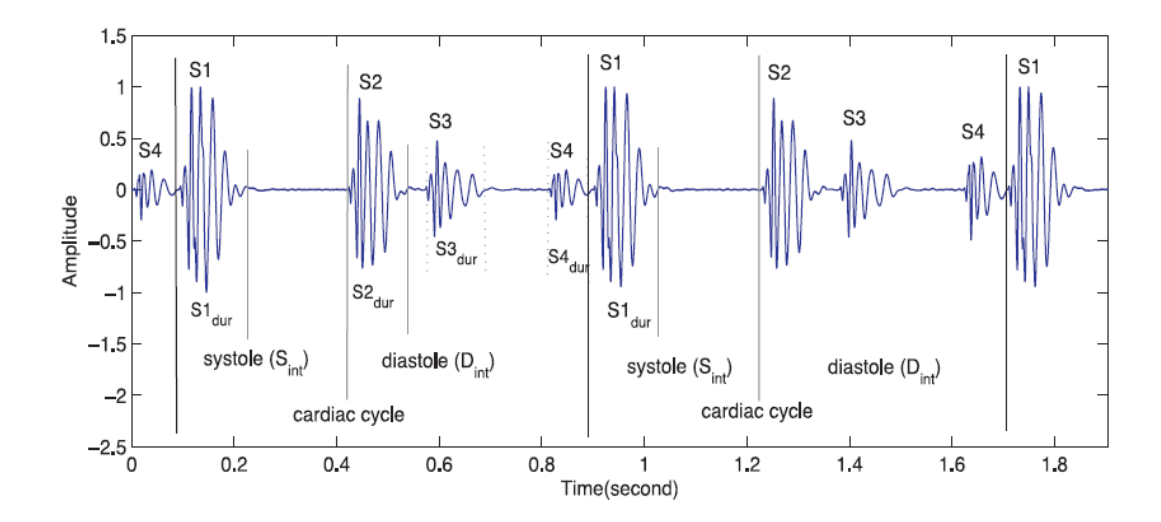


Figure 2.3: Visualization of a typical phonocardiogram showing the four major heart sounds S1, S2, S3 and S4 over time [69]

2.1.2 Auscultation Technique

In order to make those heart sounds audible from a distance from the patient, the stethoscope is placed on one of five dedicated auscultation points [58]. The arrangement of these points on the chest is depicted in Figure 2.4. The auscultation points 1, 2, 4 and 5 allow for detailed listening to sounds originating from the four heart valves individually [58]. Auscultation point 3, the so-called Erb's point, is the spot where the opening and closing of both the aortic and the pulmonary valve can be heard similarly [58]. Table 2.1 summarizes the features of different heart sounds and gives an overview of their frequency distributions. In general, the S1 and S2 heart sounds consist of higher frequency components than the S3 and S4 heart sounds. The major cardiac sounds are low-pitched and the corresponding frequencies lie below 500 Hz. For a more detailed insight into frequency ranges of pathologic heart sounds it is referred to [31].

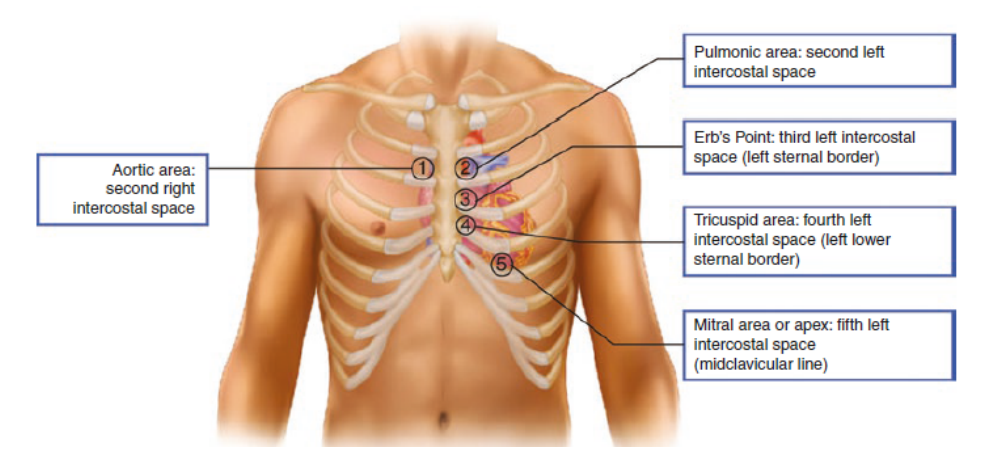


Figure 2.4: Auscultation scheme of the heart. There are five points for listening to sound originating from the aortic valve (point 1), the pulmonic valve (point2), the tricuspid valve (point 4) and the mitral valve (point 5). The Erb's point serves to listen to both semilunar valves similarly [58].

Heart Sound	Origin	Frequency [Hz]	Best heard at Auscultation Point
S1	Closure of AV valves [3]	10-200 [3]	4, 5 [3]
S2	Closure of semilunar valves [3]	50-250 [31]	2, 3 [3]
S3	Vibration of ventricular	20-70 [47]	Left ventricle: 5
59	walls during early diastole [47]	20-10 [41]	Right ventricle: 4 [47]
S4	Vibration of ventricular	20-70 [47]	Left ventricle: 5
54	walls during late diastole [47]	20-70 [47]	Right ventricle: 4 [47]
Systolic murmurs	Diseased heart	50-450 [31]	/
Diastolic murmurs	Diseased heart	45-400 [31]	/

Table 2.1: Comparison of features of the four major heart sounds S1, S2, S3, S4 and pathologic heart murmurs. S3 and S4 may be caused by a diseased heart as well and are then referred to as ventricular or atrial gallop respectively [47]. The auscultation points refer to the auscultation scheme illustrated in Figure 2.4.

2.2 Lung, Bowel and Knee Joint Sounds

The stethoscope is a versatile instrument and can auscultate a wide range of organs besides the heart. For example, the analysis of lung sounds can reveal obstructions in the pulmonary tracts as well as other lung diseases. The breath sounds are a superposition of normal breath sounds during in- and expiration, and adventitious sounds that are caused by pulmonary disorder. The latter can include crackles that appear as explosive sounds during inspiration, wheezes with an almost musical character throughout the whole breath cycle, or cough sounds among others [55]. Typically, lung sounds have frequency components between 60 and 1200 Hz [43].

Auscultation of bowel sounds can pose a patient-friendly, economic and time-efficient alternative to other diagnostic tools to detect abdominal diseases. The sounds can be separated into clicks that are short-time, high-pitched sounds and bursts that take more time. The principal frequencies of the sounds lie between 50 and 1500 Hz [37].

Knee joints consist of three articulating bones, namely femur, tibia and patella. Frictions in the joint induce vibrations that propagate to the surface of the skin and can then be picked up by a stethoscope. This examination is ideal to assess the rehabilitation progress after joint injuries. Frequencies emitted by the knee joints lie between 15 and 21000 Hz [63]. Table 2.2 summarizes the typical frequency ranges for the major body sounds detectable with a stethoscope.

Heart	Lung	Abdomen	Knee Joint	
<= 500 Hz [43]	60 - 1200 Hz [43]	50 - 1500 Hz [37]	15 - 21000 Hz [63]	

Table 2.2: Overview of auscultation sites and their corresponding frequencies

Chapter 3

Related Work

In the last few decades, various electronic and digital auscultation systems emerged in both the scientific field and on the commercial market. This chapter provides a review of the state-of-the-art electronic stethoscopes with a special emphasis on their key contributions. The chapter is subdivided into a first part highlighting commercially available devices and a second part focusing on advances made in the scientific literature.

3.1 Electronic Stethoscopes in Industry

Commercially available electronic stethoscopes generally mimic the physical appearance of a regular stethoscope [36] and follow a similar architecture: An acoustic sensor embedded in the stethoscope captures body sounds, and makes them available either through a loudspeaker on the device or by sending them wirelessly to an external device, for instance, a mobile phone. Furthermore, commercial electronic stethoscopes can be customized regarding their frequency bandwidth and sound amplification factor.

This subsection aims to present the major players on the market that manufacture electronic stethoscopes and focuses on key innovations made across more than three decades. Figure 3.1 aids for visual inspection of the devices mentioned in this chapter, and Table 3.1 gives a detailed insight into their technology specifications, advantages, drawbacks and makes a comparison to the herein presented stethoscope.

One of the first electronic stethoscopes introduced to the industrial market was the E-Scope II presented by Cardionics [8] in 1991. At that time, the chestpiece was equipped with electrocardiography (ECG) electrodes that record an ECG wave pattern [34]. Those were converted into phonocardiography (PCG) signals by a computer embedded in a housing adjacent to the tubing [34]. The user could listen to amplified body sounds through earpieces or through a loud-speaker mounted on the housing [34]. Today, Cardionics additionally incorporates a microphone in their device that acquires sounds directly.

In the following years, other manufacturers such as JABES by GST [23] or Thinklabs' ONE [65] entered the market presenting different system designs. Still, they did not contain any internal wireless transmission module, and hence had to perform all computation, sound storage, and acoustic output on the device. Naturally, this comes at the cost of increased weight and bulkiness. The inventor of the Thinklabs ONE, Clive Smith, found an elegant way around this issue by proposing merely a chestpiece that can be connected to ordinary auxiliary headphones [65]. All electronic components are tightly packed inside the chestpiece, making unwieldly tubing obsolete [59].

Although these stethoscopes still exist on the market, more advanced devices have been introduced in recent years. Nowadays, all devices come with the option for wireless data transmission. Therefore, some manufacturers relinquish the stethoscope tubing completely, such as, eKuore's Pro stethoscope [20]. Others offer a modular system that allows the user to remove the tubing and listen to the sound remotely. This approach is taken, for instance, by Eko Health Inc. with their Eko Core 500 [26]. A key feature of the Eko Core 500 is a built-in ECG that is displayed on the chestpiece during auscultation [26]. Thus, the user can listen to heart sounds and simultaneously inspect the heart's electrical activity. Another noteworthy device is the Littmann CORE published by 3M [1], that offers to switch between amplified and analog listening modes.

Furthermore, manufacturers are beginning to incorporate diagnostic artificial intelligence (AI) into their stethoscopes. For example, Eko Health Inc. published an app that is capable of detecting heart diseases, such as atrial fibrillation or brady- and tachycardia [26]. The Eko app can be connected to the Eko Core 500 [26] as well as the Littmann CORE [1]. Recently, GST has also published the JABES-Analyzer which can classify heart sounds as normal or abnormal and can categorize lung sounds into normal, wheezing, stridor, rhonchi, and crackle sounds [22].

Apart from whole-system stethoscopes, there also exist chestpiece-add-on devices. For example, Rijuven's CardioSleeve [11] can be sandwiched between the chestpiece and the tubing and improves the auscultation quality by additionally measuring and analyzing ECG wave forms [11].

Table 3.1 summarizes the electronic stethoscopes currently available on the market with regard to their technical specifications and compares them to the herein presented stethoscope. It reveals that there is no common standard for filtering bandwidths. Moreover, the current electronic stethoscopes filter for the human hearing range and thereby neglect frequencies beyond that bandwidth that could potentially contain vital diagnostic information. Especially low frequency component below 20 Hz are not considered although Chapter 2 states that cardiac frequencies can lie within that range. The herein presented stethoscope does not contain any high pass filters. Most companies do not publish the sensor type or the amount of sensors they employ so no comparison can be made with regard to the multi-sensor approach taken in this thesis. However, for example, Cardionics and Thinklabs only deploy one transducer, making them thus inferior to the electronic stethoscope outlined here.

Furthermore, when considering an auscultation time of up to five minutes (e.g. for bowel sounds) [6] and an additional automatic power off of 1.5 minutes (as e.g. in the E-Scope II) [9], a battery life of 4-8 hours is not sufficient as this only allows for 37 to 73 auscultation cycles.

This can become especially inconvenient in emergency situations when the system contains a rechargeable battery (e.g. the eKuore Pro), as the device cannot be used during the recharging process. GST tries to overcome this issue by using two AAA batteries to extend the battery life to 100 hours [23], but this makes the device heavier, bulkier, and less sustainable.

The herein presented electronic stethoscope is an upgrade to a conventional stethoscope. Therefore, the device can still be operated in analog mode when the battery needs a recharge.



Figure 3.1: Summary of several commercial stethoscope systems presented on the market. a) The Eko Core 500 (Eko Health Inc.) combines sound measurements with ECG signal acquisition [26], b) The Littmann CORE (3M) offers the possibility to switch between analog and amplified listening modes [1], c) The ONE (Thinklabs) offers five frequency filters to select from [65], d) The E-Scope II (Cardionics) was one of the first electronic stethoscopes on the market [8] together with e) The JABES (GST) [23], f) The Cardiosleeve (Rijuven) is a device that can be located between the stethoscope's tubing and the chest piece to measure ECG during auscultation [11] and g) The eKuore Pro (eKuore) is a wireless stethoscope system powered by a rechargeable battery [20].

Table 3.1: Summary of the State-of-the-Art electronic stethoscopes on the commercial market sorted by their release dates and comparison of their features with regard to the herein presented stethoscope. It should be noted that the CardioSleeve is not a classical electronic stethoscope but an add-on device that can improve the examination quality by performing an ECG in parallel to the auscultation process. For the 3M Littman CORE stethoscope no information was found regarding sensor type or filters. However, this information was published in an earlier version of the stethoscope, the Littmann Range. NM: not mentioned, NA: not applicable

Company & Product name	Release date	Price [€]	Sensor type(s)	Peak Amplification	Bandwidth [Hz]	Battery life [h]	Wireless data transmission
Cardionics - E-Scope II [8]	1991 [34]	413 [12]	PCG derived from ECG waves [34] Microphone [44]	64 x [9]	Heart: 20 - 650 Lung: 70 - 2000 [9]	NM	no [34]
GST - JABES [23]	2003 [23]	222 [64]	NM	20 x [23]	Bell mode: 20 - 200 Diaphragm mode: 200 - 500 Wide mode: 20 - 1000 [23]	100 [23]	(yes)
Rijuven - CardioSleeve [11]	2013 [56]	NM	NA, add- on device [11]	NA	NA	15	yes [11]
Thinklabs - ONE [65]	<2015 [44]	473 [65]	patented capacitive transducer [44], [60]	100 x [65]	Heart: 30 - 500 Bell mode: 60- 500 Lung, heart valve clicks: 80 - 500 Lung: 100 - 1000 Wideband mode: 20 - 2000 [66]	4 [66]	no [66]
eKuore - Pro [20]	2016 [21]	399 [20]	NM	NM	Cardiac: 50 -150 Lung: 50 - 500 Wide range: 40 - 600 [19]	7 [20]	yes [19]
3M - Littmann CORE [1]	2020 [27]	309 [25]	NM Littmann Range: piezoelectric sensor [44]	40 x @ 125 Hz [1]	NM but filters for wide, cardiac and pulmonary [2] Littmann Range: Bell (20-200Hz) Diaphragm (100-500 Hz) Extended mode (20-1000Hz) [44]	8 [25]	yes [25]
Eko Health Inc Eko Core 500 [26]	2023 [27]	402 [26]	NM	40 x [26]	20 - 2000 [24] filters: wide, cardiac, pulmonary [24]	5 [26]	yes [26]

Company & Product name	Certifications	Key characteristic	Drawbacks	Inferiority to herein presented stethoscope
Cardionics - E-Scope II [8]	CE certified [9]	Pediatric Bell [9] Built-in ECG acquisition [34]	Bulky, heavy (1.3 kg) [8] No wireless data transmission [5]	No analogue listening option Only one microphone type No wireless data transmission Filters for human hearing range Inoperable in case of battery depletion
GST - JABES [23]	CE certified FDA certified ISO certified [23]	Very long battery life Connectable to JABES-AI classifier	Bulky Wireless data transmission only in combination with an external Bluetooth modules [22]	No analogue listening option No embedded wireless data transmission Filters for human hearing range Inoperable in case of battery depletion
Rijuven - CardioSleeve [11]	FDA Cleared [11]	Built-in 3 lead ECG acquisition Analysis of heart rhythm and heart murmur detection [11]		not applicable
Thinklabs - ONE [65]	FDA Cleared [67]	Large variety in filter selection	No analogue listening option	No analogue listening option only one microphone type Filters for human hearing range Inoperable in case of battery depletion
eKuore - Pro [20]	FDA approved [21]	No tubes		No analogue listening option Filters for human hearing range Inoperable in case of battery depletion
3M - Littmann CORE [1]	FDA Cleared CE Marked ISO 13485 Certified MDSAP Certified HIPAA Compliant [25]	Feature to switch between analog and amplified listening Active noise cancellation Pediatric diaphragm Tunable diaphragm technology connects to EkoApp [1]	limited exam recordings [1]	Only one transducer type Limited exam recordings Filters for human hearing range Inoperable in case of battery depletion
Eko Health Inc Eko Core 500 [26]	FDA Cleared ISO 13485 MDSAP HIPAA GDPR [26]	Eko App: cardiac disease detection Built in 3-lead ECG Active noise cancellation [26]	ECG waveform variations depending on auscultation site [41]	No analogue listening option Filters for human hearing range Inoperable in case of battery depletion

3.2 Electronic Stethoscopes in Scientific Literature

This section is dedicated to providing a detailed overview of electronic stethoscopes found in the scientific literature with a special focus on advances made in the last decade. The following text is structured by the targeted body sounds, namely joint sounds, bowel sounds, lung sounds, and heart sounds. At the end of this section, a short review of papers that combine body sounds with other biosignals is given. Some excerpts from the scientific publications highlighted below are shown in Figure 3.2 and are likewise categorized by their application. Finally, Tables 3.2 and 3.3 summarize the key specifications of the literature presented in the following.

Joint Sounds

Teague et al. [63] proposed an example of a wearable knee joint sound acquisition unit to continuously evaluate the rehabilitation process after a musculoskeletal injury. For this purpose, they collect sound using three microphone types simultaneously, namely a piezoelectric film, an electret microphone and a MEMS microphone. The authors chose to employ a piezoelectric film because it can be attached directly to the skin and detects vibrations induced by sound waves propagating from the knee joint to the surface of the skin, making it less prone to ambient noise. However, in case the film detaches from the skin, sound recordings are no longer possible, and valuable information is lost. To compensate for this issue, the authors propose the addition of an electret and a MEMS microphone that can sense skin vibrations even from a distance. They placed the piezoelectric film proximally and the electret and MEMS microphone laterally to the joint and secured them with tex tape. The orientation of the sensors is shown in Figure 3.2a). Furthermore, the authors equipped the setup with an inertial measurement unit that was used to calculate the angles of the knee joint during flexion and extension. The acoustic sensors were compared in terms of SNR and frequency range. For both metrics, the electret and the MEMS microphones scored better than the piezoelectric film because the latter was more susceptible to interface noise such as the tex tape rubbing on the skin.

Bowel Sounds

The abdomen does not produce sounds constantly. Since classical auscultation at the doctor's office generally occurs during a limited time span, potentially at a moment of bowel silence, physicians might lose significant information crucial for giving a diagnosis. To address this problem, Wang et al. [70] developed a patch to monitor bowel sounds continuously and in real-time. The patch is made of a flexible printed circuit board (PCB) that conforms with the curved surface of the skin making long-term wearing comfortable and user-friendly. The prototype and a typical auscultation scenario can be seen in Figure 3.2b). The patch holds a MEMS microphone to sense bowel sounds and a Bluetooth chip to send them to an external mobile phone for inspection and analysis. The MEMS microphone is intentionally separated from the rest of the electronic circuit to enhance the board's flexibility and bending capabilities. This is indicated by the red rectangle in the image on the right.

Lung Sounds

Li et al. [46] developed a system to continuously monitor breathing sounds with an integrated classification algorithm that analyzes the frequency components of lung sounds. The device consists of a sound acquisition unit that detects breathing sounds and wirelessly sends them to an external host system via Bluetooth. The sound acquisition unit comprises a condenser microphone mounted behind a regular stethoscope bell and can be embedded into an elastic band wrapped around the chest. An illustration of this setup can be seen in

Figure 3.2h). The host system serves for data storage, visualization, and wheezing sound detection.

Yilmaz et al. [76] are currently developing another wearable prototype for lung sound inspection. Their ultimate goal is to integrate multiple acoustic sensors in a vest to enable continuous breathing monitoring. The authors claim that with a wearable device, the limitations of electronic stethoscopes, such as improper positioning of the sensor or insufficient pressure on the skin, can be overcome. As a sound transducer, the authors opted for a piezoelectric film embedded in a silicone rubber that is in direct contact with the skin. This improves the stability of the transducer and acts as a natural barrier against ambient noise. Furthermore, the authors paid careful attention to acoustically match the impedance of the transducer to the human skin. Both the the silicone rubber and the piezoelectric film have acoustic impedances comparable to those of the human body.

Inspired by the COVID19 pandemic that required medical personnel to wear protective suits and consequently impaired the auscultation process, Yang et al. [75] have developed a contactless auscultation device for heart and lung sounds. The authors found a simple and cost-efficient way to electrify a regular stethoscope chestpiece by placing a collar microphone behind its stem. A Rapsberry Pi receives the acoustic data and forwards it to a loudspeaker or sends it over WiFi to a PC for further processing and analysis. A schematic of the whole setup is visualized in Figure 3.2i). With this approach, they made the need for earpieces obsolete, which can be a great advantage in terms of hygiene and allows the user to wear protective clothing. The cost of all components used does not exceed more than 94 \\$. Therefore, the presented auscultation device poses a low-cost alternative to the more expensive commercial stethoscopes.

In 2023 Soo Hyun Lee et al. [42] developed a wearable, flexible patch that continuously monitors respiratory function in real-time. The patch can be glued to the patient's back with medical adhesive as shown in Figure 3.2j). A flexible PCB holds all relevant components for capturing lung sounds: A battery powering a microcontroller unit (MCU) and a MEMS microphone with a pulse density modulated (PDM) interface. The MCU samples data from the microphone and communicates with an external mobile device that can visualize the data and re-play the recorded sound in real-time. The electronic circuit is protected by a skin-colored cover that functions as a barrier against surrounding noise. Holes in the cover give access to the charging port of the battery and a switch to turn off the device. Furthermore, recorded signals can be analyzed by a machine learning algorithm that can distinguish between heart and lung sounds. Due to its compact design, the authors suggest that the patch could be suited especially for children who are too young to perform a regular pulmonary function test.

Heart Sounds

Cowdhury et al. [10] proposed a portable stethoscope that is wirelessly connected to a binary classifier algorithm. A system block diagram of their prototype can be seen in Figure 3.2c). An electret microphone is mounted in a regular stethoscope tubing close to the chestpiece and transmits acoustic signals to an analog-front end where the signal is filtered, pre-amplified and digitized. An RFDuino microcontroller sends the signals to a PC for further processing and heart sound classification.

In 2019, Weidong Wang et al. [72] developed a custom-built piezoresistive MEMS sensor for heart auscultation. For this purpose the authors designed a Wheatstone bridge with two of four resistors made up of a piezoelectric material. When a sound wave pushes on the center mass of the MEMS sensor, the resistors of the Wheatstone bridge are being

deformed leading to a change in resistance value and consequently to a voltage change. In order to protect the sensitive MEMS microphone, the setup is encapsulated in a plastic casing with a sound transparent textile at the position of the transducer. An image of the final prototype is shown in Figure 3.2g). All electronics are contained in the plastic casing and manage the filtering, amplifying and converting of the detected heart sounds to a digital format before sending them via Bluetooth to an external PC.

Further advances in electronic auscultation can be achieved by deploying multiple microphones in an array. For example, Tian Wang et al. [71] arranged 16 electret condenser microphones in a 4 x 4 array for recording heart sounds. The authors state that choosing microphone arrays increases the amplitude of the total signal output, enhances sensitivity and further enlarges the auscultation area therefore providing more accurate heart sound recordings. A flow chart of the proposed sound acquisition process is shown in Figure 3.2e). A Field-Programmable Gate Array (FPGA) samples heart beat signals from the 16 individual microphones synchronously. The authors opted for an oversampling approach to spread quantization noise over a large frequency range and thereby reduce noise present in the targeted cardiac frequency spectrum. The FPGA filters and subsequently digitizes the signals and sends them to an MCU that further applies digital filters and displays the heart beats on a screen. In fact, with the oversampling approach and the microphone array arrangement the authors achieved an SNR increase by 7 dB and a noise reduction by 3 dB as compared to sampling from one individual microphone. In a future work, they aim to integrate a flat and flexible version of this prototype in a garment to support heart monitoring.

To address the drawbacks that come with high expenses for a commercial electronic stethoscope, Minh et al. [48] propose a low-cost stethoscope by modifying a conventional stethoscope. They mount an electret microphone to the stem of a regular chestpiece. The collected heart sound is filtered and amplified in two stages by consecutive operational amplifiers. Subsequently, the signals are converted into a digital format by the analog-to-digital-converter (ADC) integrated in an Arduino UNO R3. This minimalistic approach comprises only very few low-cost components while achieving results comparable to that of a commercial electronic stethoscope.

Combined Body Signals

Some researchers exploited the fact that auscultation always requires placing a sensor to the targeted body part anyway and therefore combined their systems with other biosensors. For example, Park et al. [54] presented a light-weight, ergonomic prototype that can simultaneously measure heart sounds and pulse and that can be seen in Figure 3.2d). The proposed stethoscope comes in the shape of a computer mouse to establish a convenient grip and is supposed to be held by the patients themselves. The front side that is attached to the chest is equipped with a digital MEMS microphone mounted behind a stethoscope bell. Additionally, an integrated OLED screen informs the user about the detected heart rate. On the back of the stethoscope, a finger holder and a photoplethysmography (PPG) sensor can be found. When a patient pushes the bell to the chest, his or her middle finger is guided by the finger holder precisely to the location of the PPG sensors that takes pulse measurements. Both biosignals are sampled in parallel by a processor to ensure synchronization and are transmitted over Bluetooth. To evaluate the user comfort, the authors performed EMGs during an auscultation experiment. For this purpose, they attached EMG sensors on certain muscle groups on the lower arm that hold the prototype or a conventional stethoscope respectively. The results reveal that more effort was needed to perform auscultation with the regular stethoscope. This is likely because the prototype

weighs about 3 times less than a regular stethoscope. In a future work, the authors aim to exploit their multi-signal approach for an accurate disease classification algorithm.

Lee et al. [41] combined heart sound monitoring with electrocardiography (ECG) measurements. Heart sounds and ECG waveforms have a strong correlation: The R-peak of the ECG appears at the same time as one can hear the first heart sound (S1). Likewise the second heart sound (S2) can be heard towards the end of the T-wave. Providing these two associated body signals to a heart sound classifier concurrently can improve its performance and consequently lead to more accurate predictions of cardiac diseases. A typical auscultation scenario with the presented prototype can be seen in Figure 3.2f). Two hardware subsystems sample simultaneously: First, an electret microphone that converts heard sounds into electrical signals, and second, an ECG patch that measures the electrical activity of the heart. The signals are synchronized with a synchronization algorithm that compensates for package loss during wireless transmission. Finally, the aligned signals are displayed on a mobile phone and can be analyzed by a heart murmur classification algorithm.

Other researches present universal electronic stethoscopes that can be applied to both heart and lung by providing dedicated filters for both body sounds. Such an approach has, for example, been taken by Wu et al. [74]. In their presented prototype one can switch between analog filters for the lung and for the heart. Furthermore, the authors have investigated different strategies for installing a condenser microphone. The one with the lowest noise amplitude was an arrangement of two stethoscope heads attached back to back that each incorporated a microphone. The setup was encapsulated by a cylindrical container made of cork to shield it from ambient noise. Additionally, they deployed one microphone for capturing heart or lung sounds and the other microphone for sensing environmental noise. The noise signal was then subtracted from the body sound signal by passing them through a differential amplifier.

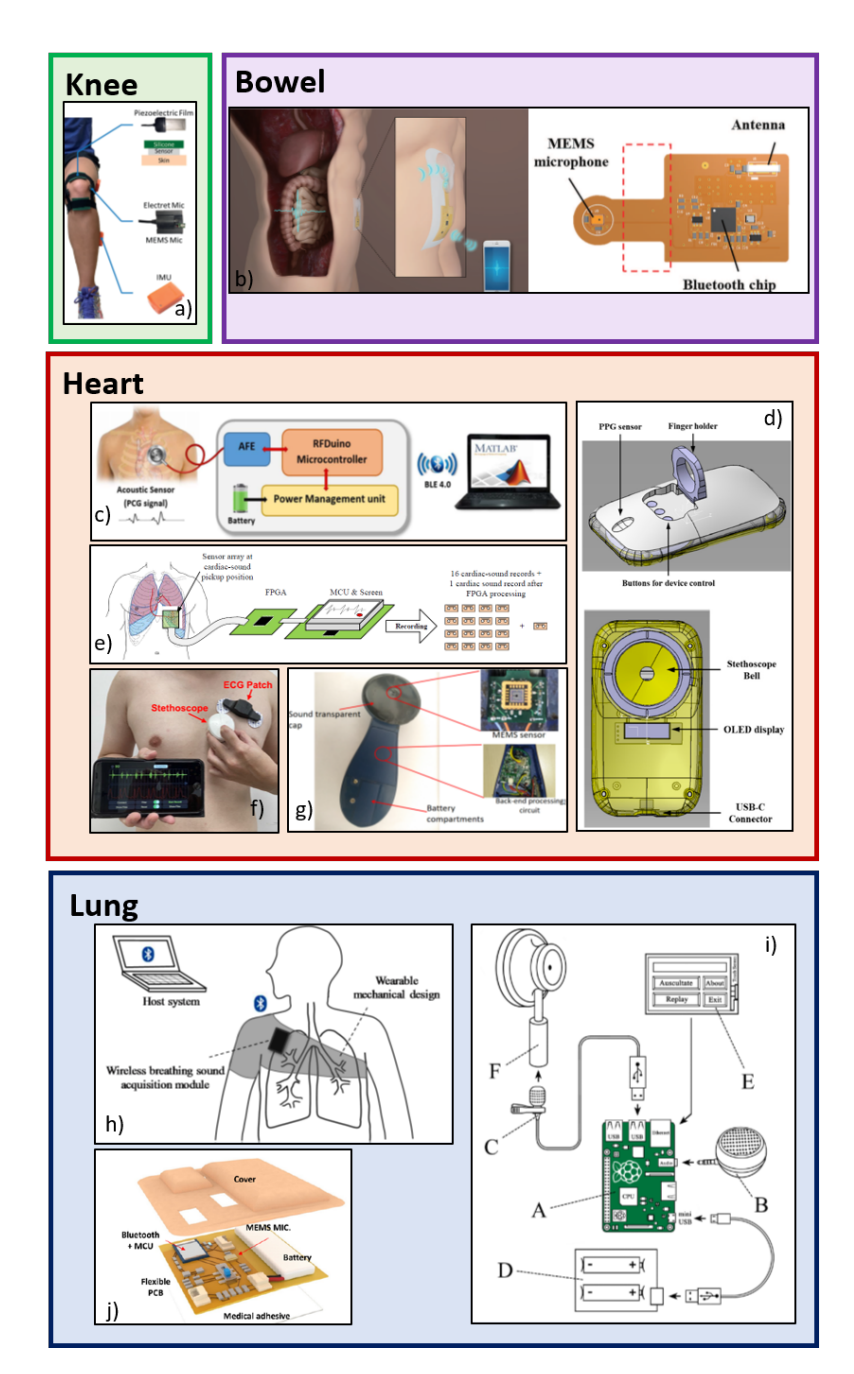


Figure 3.2: Summary of several stethoscope systems presented in scientific literature and comparison of their features. a) A wearable joint monitoring system [63], b) A skin-attached monitoring device for bowel sound evaluation [6], c) A block diagram of a heart sound acquisition and classification system [10], d) A stethoscope system measuring heart sounds from the chest and PPG from a finger [54], e) A system using an array-based arrangement of microphones [71], f) A monitoring device that combines heart sound measurements and ECG waveform acquisition [41], g) A measurement device utilizing a piezoresistive transducer mounted behind a soundtransparent cap [72], h) A wearable device for continuous breathing monitoring [46], j) A skin-attached flexible PCB for observation of lung sounds [42], i) A low-cost, easy-to-mount sound acquisition system using a Raspberry Pi as a core [75]

Table 3.2: Electronic stethoscopes presented in the scientific literature sorted by year, ECM: electret condenser microphone NM: not mentioned,

Ref.	Year	Application	Device Type	Sensor Type	Number of Acoustic Sensors	Sampling Rate [kHz]	Frequency Bandwidth [Hz]	Wireless Communication
[63]	2016	Knee	wearable	piezoelectric film, ECM, analog MEMS	1 per sensor type	piezo & MEMS: 50 electret: 44.1	piezo: 15k - 21k electret: 7k - 16k	NM
[46]	2017	Lung	wearable	ECM	1	2,048	150-1000	Bluetooth
[10]	2019	Heart	chestpiece with mircophone	ECM	1	2	20-600	BLE
[72]	2019	Heart	custom-built electronic stethoscope	custom-built analog MEMS	1	1	20-600	Bluetooth
[70]	2019	Abdomen	wearable	analog MEMS	1	2	<= 600	Bluetooth
[76]	2020	Lung	wearable	piezoelectric film	1	5	100-1600	yes
[71]	2021	Heart	custom-built electronic stethoscope	ECM	4x4	8	<= 4000	NM
[75]	2021	Lung	modified conventional stethoscope	collar microphone	1	NM	NM	WiFi
[74]	2022	Heart & Lung	modified conventional stethoscope	ECM	2 1 for ambient noise	44,1	heart: <= 400, lung: 100-2000	NM
[33]	2022	Heart & Lung	custom-built electronic stethoscope	custom-built piezoelectric transducer	72	NM	1-20.000	Bluetooth

Table 3.3: Electronic stethoscopes presented in the scientific literature sorted by year (continuation of Table 3.2) ECM: electret condenser microphone NM: not mentioned,

Ref.	Year	Application	Device Type	Sensor Type	Number of Acoustic Sensors	Sampling Rate [kHz]	Frequency Bandwidth [Hz]	Wireless Communication Type
[54]	2022	Heart	custom-built electronic stethoscope	digital MEMS	1	NM	20-400	Bluetooth
[48]	2023	Heart	modified conventional stethoscope	ECM	1	NM	20-200	Bluetooth
[41]	2023	Heart	custom-built electronic stethoscope	ECM	1	2	20-300	Bluetooth
[42]	2023	Lung	wearable	digital MEMS	1	NM	heart: 20-200 lung: 50-500	Bluetooth

Chapter 4

Design Approaches

The literature analysis in the previous chapter revealed that published electronic stethoscopes differ predominantly in two aspects: the type of sound acquisition sensor deployed and the mechanical design of the electronic stethoscope. Consequently, this chapter is dedicated to provide fundamental knowledge about these aspects, starting with the sound acquisition sensors followed by the physical appearance of electronic stethoscopes.

4.1 Acoustic Sensors

Various acoustic sensors can be deployed for an electronic stethoscope, but all have advantages and disadvantages. In general, the sensors can be separated into air microphones that capture airborne signals, and contact microphones that have to be placed in direct contact with a surface to sense its vibrations. The following details the sound transduction mechanisms of the acoustic sensors along with their benefits and drawbacks to enable for an informed microphone type selection.

Electret Condenser Microphone

An example of capacitive microphones are electret condenser microphones [57]. They consist of a fixed backplate and a flexible diaphragm that form a capacitor [57]. Any movement of the membrane results in a change in capacitance relative to the deflection of the membrane and, ultimately, in a change in output voltage [68]. Electret condenser microphones typically come with an integrated junction field effect transistor (JFET) that matches the high output impedance of the capacitor to the circuit interfacing the microphone as e.g. amplification stages or analog-to-digital converters (ADCs) [68] (compare Figure 4.1). The standard operational circuit of an electret condenser microphone comprises a resistance and a capacitor [68]. The microphone is powered over the resistance connected to the voltage supply and the capacitor blocks the DC components of the signal output.

Electret condenser microphones can be purchased at low cost [68] in the range of a few cents and are a few millimeters up to a centimeter large. They provide a relatively flat frequency response (compare as an example Figure 4.2) but are typically unable to pick up very low frequencies as needed for detecting low frequency components of heart sounds. Furthermore, the electret microphone shows a low sensitivity, and therefore its output voltage has to be amplified and filtered before it can be digitized by an ADC [68].

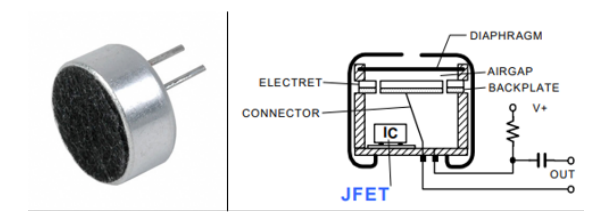


Figure 4.1: Visualization of the electret condenser microphone. Left: The CMA-4544PF-W as an example of a typical electret condenser microphone [15]. Right: Cross-section of an electret condenser microphone and its typical operational circuit consisting of a resistor and a capacitor [68]

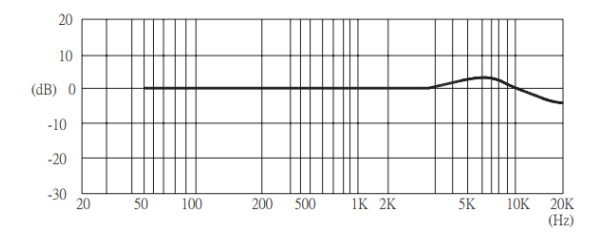


Figure 4.2: Frequency response of the CMA-4544PF-W as indicated in the datasheet [15]. The frequency response is almost flat for all audible frequencies.

Piezoelectric Transducer

These kinds of sensors exploit the piezoelectric effect. This phenomenon appears when a piezoelectric crystal is deformed (e.g., through audio vibration of a membrane) and generates charges on conductive plates surrounding the piezoelectric material. The hereby evolving potential is proportional to the incoming sound wave and is measured as an output signal [57]. A visualization of the piezoelectric phenomenon can be seen in Figure 4.3. A force F causes a displacement of charges in a molecule that ultimately leads to the creation of an electrical field and, thereby, a voltage change across the piezoelectric material.

As a piezoelectric material one can use e.g. ceramics like lead zirconium titanite, zinc oxide or aluminium nitride [43]. In the structure of the transducer, this piezoelectric ceramic is sandwiched between two electrodes, as can be seen in Figure 4.4 [7].

In conventional auscultation scenarios, the chestpiece is placed in direct contact with the skin to pick up vibrations induced by internal body sounds. Similarly, piezoelectric microphones can detect vibrations of the skin, making them particularly appropriate for use in electronic stethoscopes [43].

An advantage of piezoelectric transducers is that they do not need to be actively driven by a power source due to their intrinsic voltage creation capability. However, as their output is analog, the signals have to be digitized with an ADC. Furthermore, [44] points out that sounds captured with a piezoelectric transducer are different in tonality than sounds heard with an acoustic stethoscope, and [76] states that piezoelectric elements need careful stabilization to operate effectively.

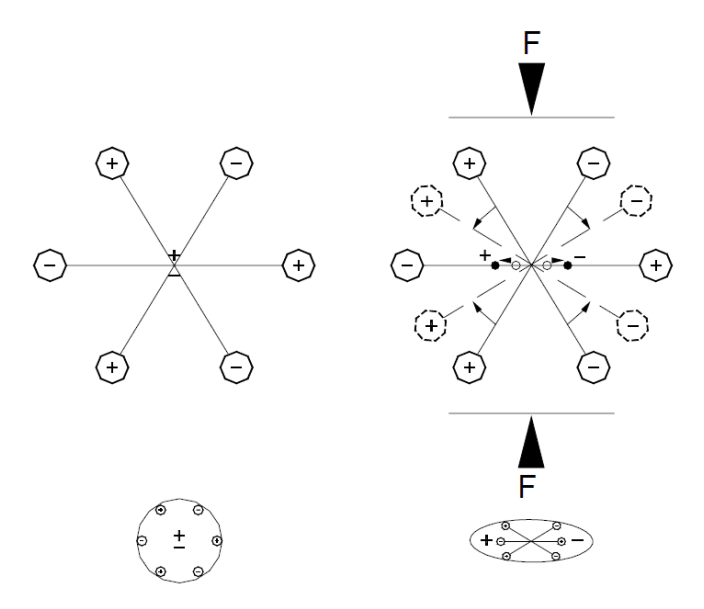


Figure 4.3: Illustration of the piezoelectric effect on the molecular basis, from [4]. Left: the molecule is neutrally charged as positive and negative charges cancel each other out. Right: a force F deforms the piezoelectric crystal causing a displacement of charges and therefore a dipole.

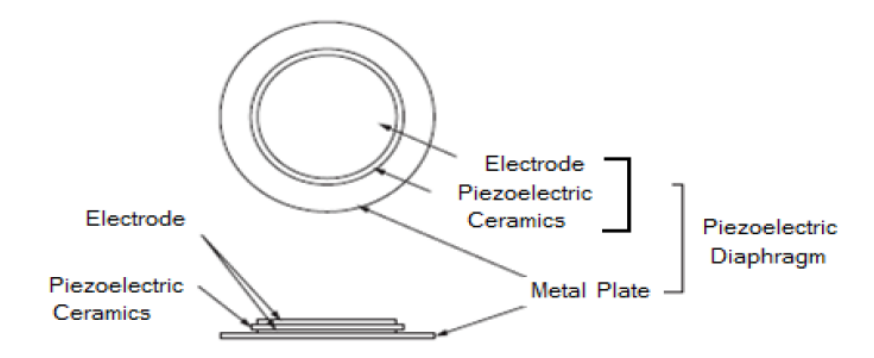


Figure 4.4: Schematic of a piezoelectric transducer switched between a metallic backplate and an electrode [7]

Optical Microphone

The working principle of optical microphones lies in sensing variations in the properties of a light beam in response to acoustic sound waves [57]. These changes can include the light beam's intensity, its phase or its polarization [57]. An exemplary setup of a fiber optic microphone can be seen in Figure 4.5. An incident light beam is guided through an optic fiber and is reflected by a diaphragm [57]. The properties of the reflected light beams are modulated by the diaphragm's vibrations [57]. A photodetector senses these changes in light properties and converts them to an electrical signal [57].

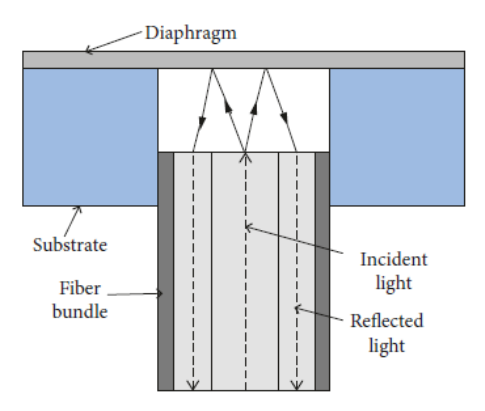


Figure 4.5: Illustration of the working principle of an optical microphone [57]. The properties of the incident light beam are altered in response to the vibrations of the diaphragm. A photodetector captures the reflected light beam and converts it into an electrical signal.

Since the transduction mechanism of optical microphones is purely based on light modulation, they are less prone to interferences by electric or magnetic fields [43]. However, their need for an external reference light source makes the microphone's design complex and its output voltage sensitive to oscillations [57]. While optical microphones are predominantly found in public safety and military technology [43], some researchers have tested their performance in sensing body sounds [77], [29].

Microelectromechanical System (MEMS) Microphone

Microphone development has been revolutionized by the introduction of microelectrome-chanical system (MEMS) technology miniaturizing devices and therefore making them light-weight and of a compact size [57]. Nowadays, MEMS microphones can be found in manifold configurations exploiting various working principles such as piezoelectric, piezore-sistive, capacitive, and optical MEMS microphones [57]. The most popular MEMS microphone types are capacitive microphones that translate the motion of a membrane into a capacitance and ultimately into an electrical signal [57], similar to the working principle of the electret condenser microphone. However, unlike electret condenser microphones, the MEMS technology offers microphones in the millimeter scale down to a few hundred micrometers in size [57].

Figure 4.6 shows the typical appearance of a MEMS microphone, along with a crosssection of a capacitive MEMS microphone that illustrates how sound waves pass through the perforated backplate and consequently deflect the diaphragm, leading to a change in capacitance [57]. MEMS microphones come with several advantages over the previously discussed acoustic sensors ranging from their compact size to a low power consumption, in particular, due to optimized current consumption of typically less than 0.25 mA [52]. Furthermore, MEMS microphones offer a flat frequency response down to 20 Hz, as can be seen in Figure 4.7. The output of MEMS microphones can be analog or digital. Digital MEMS microphones provide the output directly in a digitized form and therefore require a minimum number of components to which they need to be connected. This ultimately leads to a smaller size of manufactured printed circuit boards (PCB) and an increased ease of usage. Furthermore, the authors [39] suggest that digital outputs might be less susceptible to interferences of surrounding devices than analog outputs. There exist two popular digital interface protocols for audio data: the Inter-Integrated Circuit Sound (I2S) protocol and the pulse-density modulation (PDM) standard [45]. The former is established with three lines of data transfer, namely the clock line SCK, the word select line WS that denotes the microphone (left or right channel) addressed to place data onto the data line SD [61]. In contrast to that, the PDM protocol consists of only 2 signal lines, SCK and SD [45]. The captured audio data is sent as a bit stream with the density of subsequent zeros and ones encoding the amplitude of the recorded signal [61]. Consequently, signals sent over the PDM protocol require a decoding step before their data can be accessed, while data send over the I2S standard can be obtained immediately [61].

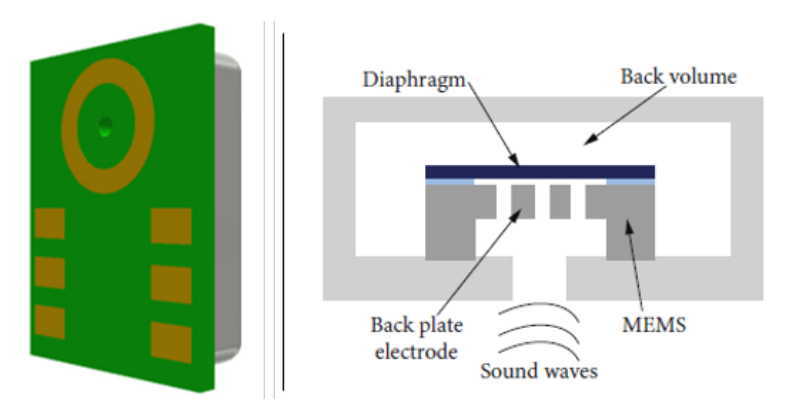


Figure 4.6: Visualization of a MEMS microphone. Left: The DMM-4026-B-I2S-R as a typical example for a digital MEMS microphone [16]. Right: Cross-section of a typical capacitive MEMS microphone [57]. Sound waves transmit through the perforated backplate and consequently move the diaphragm resulting in a change in capacitance between the diaphragm and the back pate electrode.

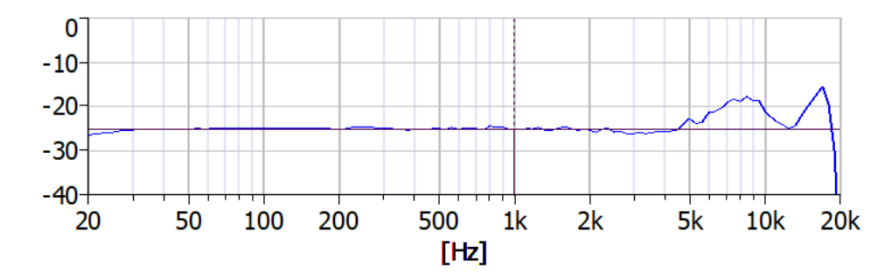


Figure 4.7: Frequency response of the DMM-4026-B-I2S-R as indicated in the datasheet [16]. The frequency response is nearly flat for frequencies between 20 Hz and 5 kHz

Table 4.1: Comparison of acoustic sound acquisition sensors (references: [57], [43])

Microphone Type	Measured Signal	Output Signal	Advantages	Disadvantages	
Electret Condenser	Capacity	Voltage	highly-sensitive	prone to ambient noise & motion artifacts	
Electric Condenser	Capacity	, orașe	flat frequency response	signals needs to be digitized	
Piezoelectric Transducer	Deformation of a	Voltage	wide dynamic range	signals needs to be digitized	
i lezoeiectric fransducei	piezoelectric crystal	vonage	no power supply necessary	critical stabilization of piezoelectric element	
Fiber Optic	Light intensity	Voltage or current	immune to magnetic & electric field interferences	sensitive to fluctuations of reference light	
Fiber Optic	Light intensity	voltage of current	minute to magnetic & electric field interferences	signals needs to be digitized	
	Application- Application-dependent dependent		small and compact size		
MEMS			light-weight	1 4:	
WEMS			optimal for arrangement in microphone arrays	complex design	
			low-power consumption		

4.2 Mechanical Design

While commercially available electronic stethoscopes try to mimic the appearance of conventional stethoscopes, researchers have investigated a wide range of mechanical designs, as can be seen in Figure 3.2. The literature review in Section 3 revealed that electronic stethoscopes can come in a wide variety of mechanical designs. For example, in the form of a wireless chestpiece, a wearable device for continuous real-time monitoring, or by modifying a conventional stethoscope. This subsection is dedicated to classifying the mechanical design of electronic stethoscopes proposed in the literature by highlighting the shape of sound acquisition modules and the implementation of the acoustic transducer.

Physical Appearance of the Electronic Stethoscope

The most straightforward strategy to design an electronic stethoscope is to integrate an acoustic sensor in a traditional stethoscope, as done by Jain et al. [30]. The authors claim that the microphone can be placed anywhere in the stethoscope tube or earpieces. This modular approach is a promising low-cost alternative to generally expensive electronic stethoscopes found on the market. Furthermore, it has the advantage of restoring the original state of the stethoscope and making it easy to repair damaged electronics. Several other researchers have proposed complementing conventional stethoscope chestpieces with acoustic transducers [10], [75], [48], [74], among others.

Naturally, the mechanical design of the stethoscope depends on its application. A device for listening to joint sounds might differ from the setup for auscultating the heart. However, not only does the targeted body sound determine the stethoscope's physical appearance. Researchers have also taken other aspects into consideration, such as user comfort or the combination of multiple biosignals. For example, Park et al. [54] proposed an ergonomic stethoscope chest piece in the shape of an ordinary computer mouse, arguing an improved ease of operation and comfort. The authors also incorporated both a photoplethysmogram (PPG) sensor and a MEMS microphone to simultaneously capture the pulse and heart sounds. They attached a finger holder to the device, which guarantees additional stability of the stethoscope on the chest wall.

Other multi-signal acquiring stethoscopes come in the form of wearable devices such as the ones presented by the authors of [36], [42], [46], [40]. For example, Klum et al. [36], [35] presented a multimodal patch that synchronously performs an ECG, a pneumography, and an actigraphy in addition to capturing body sounds. By simultaneously providing multiple body signals, they aim to contribute to a successful disease diagnosis and therapy. The authors of [36], [42], and [40] propose wearable devices in the form of a stethoscope patch that can be directly attached to the skin. In contrast to that, Li et al. [46] incorporate their sound acquisition module in an elastic band that exerts sufficient pressure to maintain a stable connection between the module and the skin, and Yilmaz et al. [76] aim to integrate their prototype in a dedicated vest for real-time and continuous monitoring of heart signals.

The shape of electronic stethoscopes is also influenced by the amount of acoustic sensors deployed. An arrangement of microphones in an array enables to localize the origin of acoustic events through beamforming [52]. Furthermore, it can increase the sensitivity and signal-to-noise ratio (SNR), consequently leading to an improved sound quality [71]. Jia et al. [33], [32] propose an array arrangement in a honeycomb architecture to increase the fill factor compared to a rectangular array arrangement. Wang et al. [71] opted for a 4 x 4 rectangular array arrangement to increase the sound pick up area and to facilitate the alignment of the individual microphones. However, the amount of microphones deployed in an array needs careful design considerations to compromise an enlarged pick up area

and improved sensitivity with power consumption, size, and weight of the developed device [52].

Location of the acoustic sensor

The position of the acoustic sensor is closely tied to the type of transducer deployed. While contact microphones, such as piezoelectric transducers, have to be in direct contact with the vibrating skin, air microphones like electret condenser microphones or capacitive MEMS microphones need a diaphragm as an interface to the skin [76]. However, the evolving air cavity between the diaphragm and the microphone exposes air microphones to a higher level of ambient noise [44].

Wodicka et al. [73] examined the impact of this air cavity by varying the distance between the skin and an electret microphone. They compared the resulting frequency responses of the microphone predicted by an acoustic model and verified their findings with lung sounds from an artificial and a human chest. Their findings show that shorter cavity depths yield increased measurement sensitivity, especially for frequencies higher than 400 Hz.

In another publication by the same authors [38], they investigated how the shape of this air cavity influences the quality of captured lung sounds. For this purpose, they manufactured a plastic air chamber in cylindrical and conical shape with a constant depth of 2 mm and diameters varying between 5, 8, 10, and 15 mm and attached it to an electret microphone. As a metric of comparison, they chose the power spectra of inspiratory lung sounds. Their findings show that the contact area between the air chamber and the skin in relation to the volume in the chamber is a significant factor and should be maximized. Therefore, they suggest an air chamber with a conical shape and a diameter between 10 and 15 mm. In their study, the authors also propose puncturing the air chamber to avoid pressurization at the microphone's position. However, they also mention that this perforation can cause an increase in noise picked up from the environment.

An example of the installation of a contact microphone is provided by Yilmaz et al. [76]. They suggest using silicone as an interfacing material between a piezoelectric transducer and the human skin. The silicon creates a natural barrier to ambient noise, improves impedance matching between the transducer and the human skin, and additionally stabilizes the transducer.

In contrast to that, Teague et al. [63] propose to bring a piezoelectric film in direct contact to the skin and covering it with a piece of silicone.

Chapter 5

Multi-Sensor Modular Design

In the previous two chapters, state-of-the-art electronic stethoscopes were described and classified for both commercial devices and systems presented in the scientific literature. This chapter is dedicated to describing the electronic stethoscope developed within the scope of this thesis and is divided into three parts: The first section explains and reasons about the requirements that the design has to meet, resulting in the final design outline in the second part detailing the hardware and software components.

5.1 Requirements of the Design

From the findings of the previous chapters, a functional and a non-functional list of requirements (LOR) were derived and are shown in Tables 5.1 and 5.2, respectively. Functional requirements comprise technical specifications that are crucial for the operation of the electronic stethoscope. Non-functional requirements define characteristics that influence the design but are irrelevant for its basic functionality. Additionally, the tables contain hard requirements (H) that have to be fulfilled and soft requirements (S) that are "nice-to-have"-features. The reasons for the specifications in the functional and non-functional LORs are explained in the following text. The enumeration corresponds to the requirement number (No.) in Tables 5.1 and 5.2, respectively.

Functional Requirements

- 1. Most importantly, the electronic stethoscope must be able to accurately capture various body sounds. With regard to Table 2.2, the desired frequency range is fixed to frequencies lower than 2 kHz.
- 2. From Chapter 4.1, it becomes evident that every microphone type has strengths and weaknesses. For example, piezoelectric transducers have the advantage of capturing the genuine, unattenuated signal but need careful stabilization [76] and might alter the tone quality of the captured sound [44]. In contrast to that, air microphones, like electret condenser microphones or MEMS microphones, are more sensitive to ambient noise but are simpler to attach to the skin. The following three acoustic sensors should be incorporated into the design in order to exploit the benefits of multiple microphone types:

- An electret condenser microphone is deployed because it has been proven to accurately measure the body sounds such as the heart beat [10], [71], [74], [48], [41].
- A piezoelectric transducer is used because it picks up the original vibrations of the skin.
- A digital MEMS microphone is incorporated because of its compact size and low power consumption and to integrate an advanced type of microphone technology.

Furthermore, the microphones should be arranged in an array of four to increase the sensitivity, signal-to-noise ratio (SNR) and enable for beamforming and sensor fusion in a future work.

- 3. Ideally, the electronic stethoscope should be powered by a rechargeable battery to limit costs and the ecological footprint. However, this is an advanced feature and is therefore marked as a soft requirement.
- 4. The device should communicate with the operator. Naturally, providing the recorded body sound to the user is a hard requirement. If a rechargeable battery is incorporated into the prototype, informing the user about its charge level adds value to the design.
- 5. The prototype should send captured body sounds wirelessly to an external device that post-processes and stores the data. However, these specifications are considered soft requirements.

Non-Functional Requirements

- 1. The electronic stethoscope should be a modification of a typical analog stethoscope, as it has been demonstrated by multiple research papers found in the literature [75], [74], [48]. However, the prototype should also work on its own. Thereby, the user can choose between analog and digital listening modes and compare their quality and features. Furthermore, the device can still be used in analog mode if electronic components are non-functional due to power depletion.
- 2. There must be an option to arbitrarily exchange transducer types. This yields three main advantages: First, regarding environmental pollution and public health, electronic waste has become a serious issue [51]. To avoid contributing to this problem, damaged microphones can be easily replaced and potentially repaired instead of abandoning the device as a whole. Secondly, this approach helps in debugging the electrical circuits. Lastly, it enables the user to compare the microphone's performances. Above that the user should be able to freely select the type of computational platform he or she wants to use. This allows for effortless exchange of technologies, and therefore, the proposed device can act as an education and potential research platform, for example, to evaluate designed signal processing techniques or AI algorithms.
- 3. The cost of the prototype is a soft requirement and should be competitive with commercial alternatives.
- 4. To further promote the device's sustainability factor, a rechargeable battery with a minimum battery life of 4 h should be deployed, and the system should be automatically shut off after 3 minutes. However, these features are considered soft requirements.
- 5. The size of the prototype should not add more than 4 cm to a classical chestpiece to conform with the surface area of a typical human chest.
- 6. Last but not least, the weight of the electronic stethoscope should not exceed 700 g to offer a convenient and ergonomic auscultation experience.

H/S	No.	Description	Specification	
1. Body Sound Acquisition				
H	1.1	Frequency range	$<=2000~\mathrm{Hz}$	
			Electret Condenser Microphone	
Н	1.2	Transducers	Piezoelectric Transducer	
			MEMS Microphones	
Н	1.3	Number of transducers	Four in an array arrangement	
S	2	Power Supply Rechargeable Battery		
S	3	Ambient Noise Reduction	SNR increase by $>= 10 dB$	
	4	Outputs		
S	4.1	Battery Life Indication	Inform user about low battery status	
Н	4.2	Obtained Body Signals	Provide body sound to user	
	5	Data Processing		
S	5.1	Wireless Data Transmission	Distance $\leq 50 \text{ m}$	
S	5.2	Processing	External	
S	5.3	Memory	External	

Table 5.1: List of functional requirements, H: hard requirements S: soft requirement

H/S	No.	Description	Specification
	1.	Design	
Н	1.1	Upgrade for Digitization of an	
11	1.1	analog stethoscope chestpiece	1
H	1.2	Stand-alone device	
S	1.3	Switching option between	
۵ ا	1.0	analog and digital auscultation	
	2.	Modularity	
H	2.1	Transducers	Replacement possibility
Н	2.1	Interesponability	Compatibility to several
111	2.1	Interoperability	computational platforms
S	3	Cost	Low-cost
	4	Environment	
S	4.1	Rechargeable battery	
S	4.2	Battery life	>= 4 h
S	4.3	Auto shut off	3 min
S	5	5. Geometry	<= 4 cm
	υ.		additional to the analog chestpiece
	6	Ergonomy	
S	6.1	Weight	<= 700 g

Table 5.2: List of non-functional requirements, H: hard requirement, S: soft requirement

5.2 General Design Outline

In the light of the LORs provided in the previous section, the proposed design of the developed stethoscope is described in this section.

The design should be an add-on device to a traditional stethoscope without disturbing the analog auscultation process. A sketch of the basic setup can be seen in Figure 5.1 (left). The add-on device is attached to a conventional stethoscope chestpiece and incorporates an array of four acoustic sensors. The user can freely choose which kind of acoustic sensor she or he wants to use. The device offers three types of transducers, an electret condenser microphone, a piezoelectric transducer, and a MEMS microphone. Detected body sounds can be transmitted wirelessly, for example, to a personal computer (PC). The whole setup is encapsulated by a casing consolidating the components and protecting the device from mechanical damage.

The proposed device consists of three essential layers, as depicted in Figure 5.1 (right)

- Analog front end: comprises the three acoustic sensors deployed.
- Interface layer: consists of a main board that collects measured data and converts analog signals into digital signals using an analog-to-digital converter (ADC).
- Digital back end: is compatible with a wide range of computational platforms such as Microcontroller Units (MCU), Field-Programmable Gate Arrays (FPGA), System on Chip (SoC) or Digital Signal Processors (DSP).

The platform is powered through a dual-channel buck converter that supplies the main board with 3.3 V and the circuits of the acoustic sensors with 5 V.

In accordance with the signal flow path, the following subsections detail the analog front end, the interface layer, and the digital back end, with a special emphasis on their modular functionality.

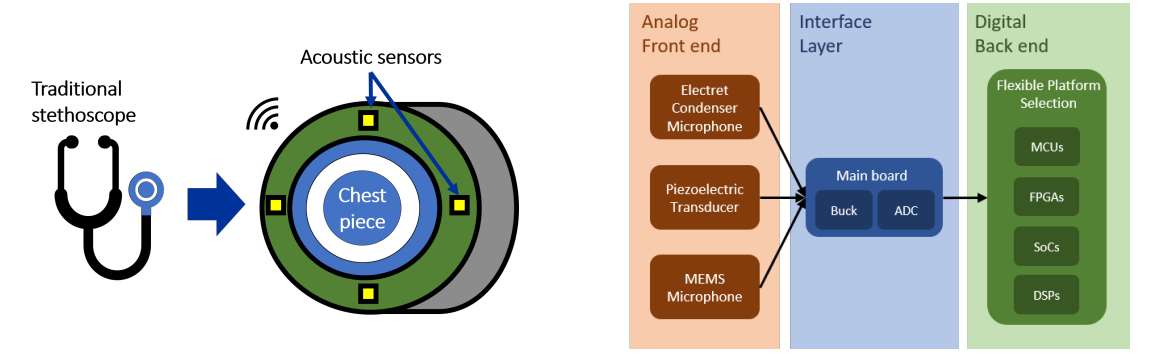


Figure 5.1: Left: Schematic of the chest piece add-on device. The device surrounds the chest piece marked in blue. Acoustic sensors arranged in an array of four are highlighted in yellow. Right: System design of the developed electronic stethoscope. The analog front end consists of three acoustic sensors that transmit data to the interfacing layer represented by a main board. The main board is powered by a buck converter and features an ADC that digitizes the signals received from the analog front end. The back end offers a flexible platform selection, and the operator of the device is free to choose the system most appropriate for her or his application.

5.2.1 Analog Front End

The prototype features three acoustic sensor types, namely, an electret condenser microphone, a piezoelectric transducer, and a MEMS microphone. Each of these transducers was manufactured on a dedicated printed circuit board (PCB) because the MEMS microphone is a surface-mount-device. Although this comes at the cost of a bulky design and additional costs, this approach was chosen to allow for easy interchange between the sensors and replacement of the boards. In the following text, the front end PCBs are explained in detail by reasoning about the electronic components used and describing the developed circuits.

Electret Condenser Microphone Board

Condenser microphones have been used frequently in literature and have proved to be capable of accurately capturing heart sounds, see e.g. [10], [74], [41], [71] among others. Consequently, these microphones can be used as a reference to compare the performance of other microphone types. In addition, electret condenser microphones are very cost-effective. Therefore, an electret condenser microphone is one of the three acoustic sensors employed in the design.

The CMA-4544PF-W microphone [15] is an omnidirectional electret condenser microphone and promises a flat frequency response curve between 50 Hz and 2 kHz that covers the body sound frequencies specified in the LOR. It offers a sensitivity of -44 dBV at 94 dB sound pressure level (SPL) and an SNR of 60 dBA at 1 kHz. Its power consumption is determined by a current consumption of maximally 0.5 mA and an operating voltage between 3 and 10 V.

The circuit designed to operate the electret condenser microphone is shown in Figure 5.2, and a simulation of the corresponding Bode diagram of this circuit is depicted in Figure 5.3. The CMA-4544PF-W electret condenser microphone is connected through a resistor of 2.2 k Ω to a 5 V voltage supply. The DC component of the output signal is removed when passing the coupling resistor of 10 μ F. Subsequently, the signal is amplified by the first active low-pass filter with amplification factor 10 and cutoff frequency $f_c = \frac{1}{2\pi * \sqrt{100k}\Omega * 820pF} \simeq 1.94$ kHz. Simultaneously, the signal is referenced to be around 1.25 V to stay within the range of voltages that the ADC on the interface layer expects. In the second amplification stage, the signals are low-pass-filtered once more at a cutoff frequency of $f_c = \frac{1}{2\pi * \sqrt{4.7k}\Omega * 15nF} \simeq 2.6$ kHz and are amplified by a customizable amplification factor that can be adjusted with a trimmer potentiometer.

In performed tests, it became apparent that the 50 Hz mains hum distorts the signals captured by the electret condenser microphone. Consequently, a passive notch filter with this target frequency is incorporated directly after the second amplification stage. The values of the components deployed in this filter were carefully chosen, and their actual values need to stay within the tolerances indicated in the schematic. The effect of this notch filter can be observed in Figure 5.3 where the behavior of the notch is simulated for multiple combinations of component values within the tolerance ranges. The simulations reveal that the effective notch frequency falls between 49.6 Hz and 50.6 Hz.

Finally, the signal is low-pass filtered by a second-order Sallen-Key filter with a cutoff frequency of $f_c = \frac{1}{2\pi * \sqrt{82k\Omega * 180k\Omega * 1nF*470pF}} \simeq 2$ kHz and transmitted to the main board for further processing and digitization.

The breakout board was intermediately tested with an oscilloscope for its ability to sense heart beats from the five auscultation points. During these tests, it was recognized that the signals were captured more effectively when a tube was added on top of the electret microphone. This reduced surrounding noise and increased the amplitudes of the detected heart beats. The impact of multiple tube lengths was tested, and the best results were achieved with a tube length of 2 cm.

Figure 5.4 depicts the breakout board produced that holds the electret condenser microphone. The board is 30.4 mm in length and 17.1 mm in width.

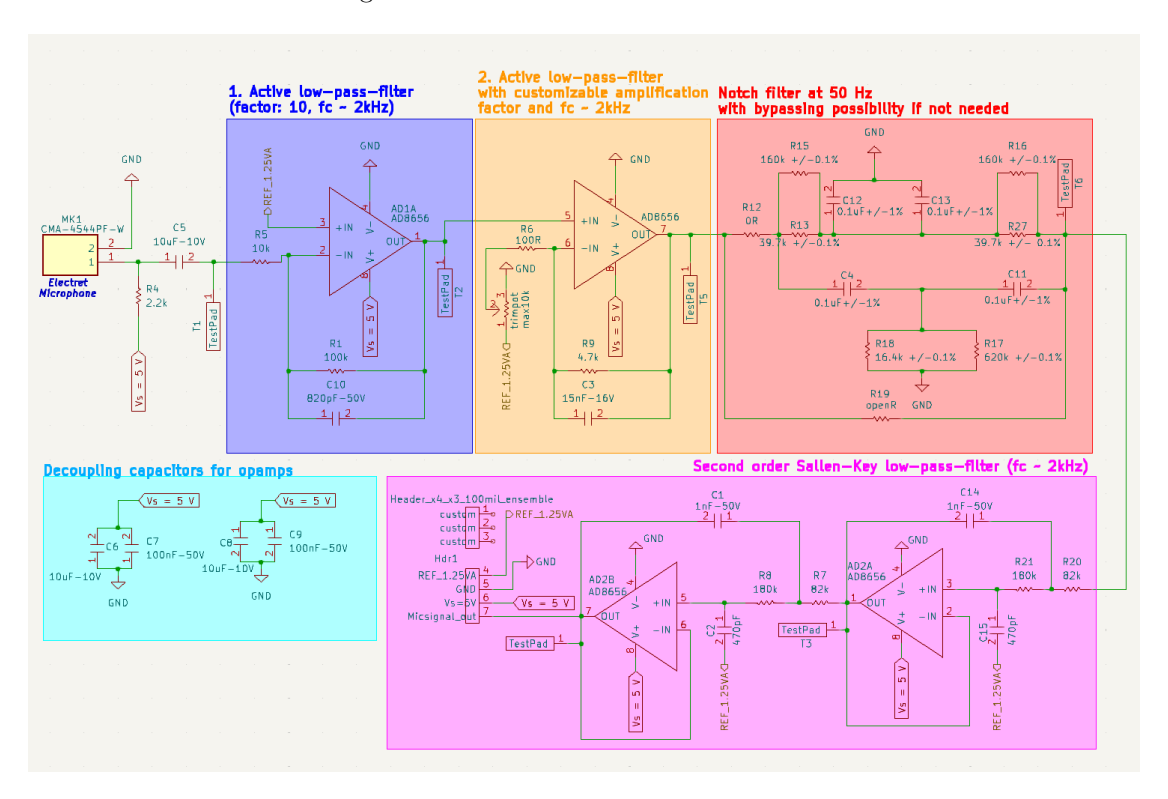


Figure 5.2: Electrical circuit that interfaces the electret condenser microphone (CMA - 4544PF - W). The microphone is powered with the typical application circuit presented in Figure 4.1. The output signal is amplified by a factor of at least 470 (blue and orange box) and subsequently filtered by a notch filter (red box) and a low pass filter (pink box) with target frequencies of 50 Hz and 2 kHz, respectively.

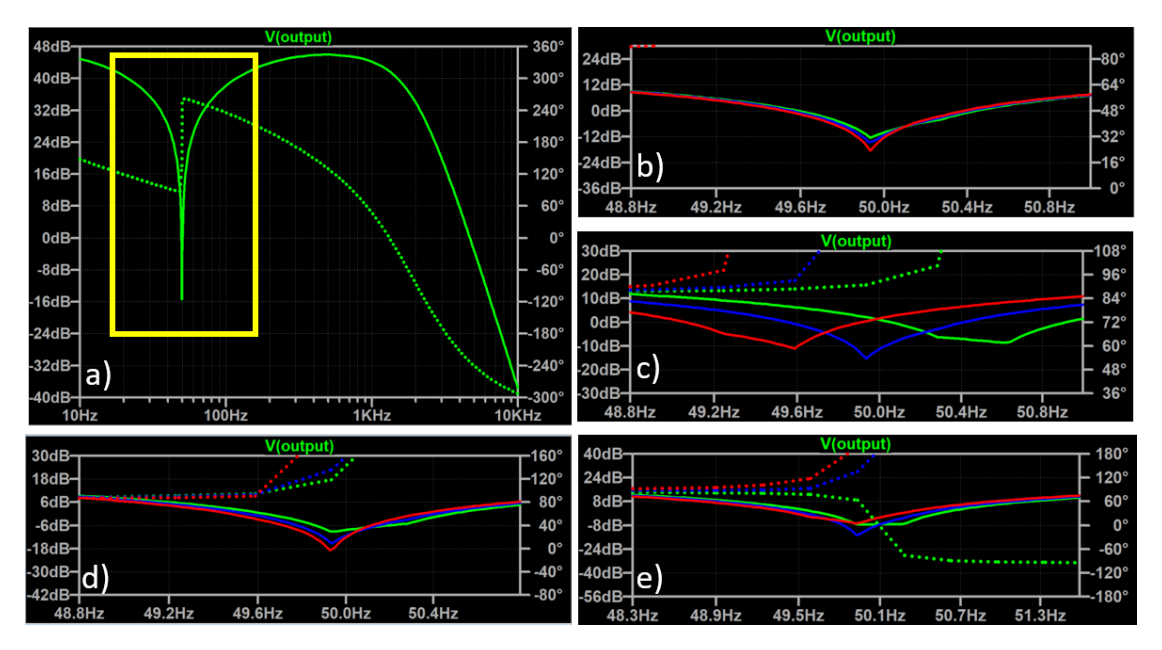


Figure 5.3: Frequency response of the circuit interfacing the electret condenser microphone shown in Figure 5.2 simulated with LTSpice. The solid line shows the magnitude plot and the dashed line represents the phase plot. a) Frequency response of the entire electrical circuit for the norm values indicated in the schematic. A sharp attenuation can be seen at the target notch frequency of 50 Hz and a gradual decrease in amplification for frequencies higher than the cutoff frequency of 2 kHz. b)-e) are magnifications of the area highlighted with a yellow rectangle. b) Varying values of R13 and R27 within their tolerance ranges: green: -0.1 %, blue: norm value (39.7k), red: +0.1 %, c) Varying values of C12, C13, C4 and C11 within their tolerance ranges: green: -1 %, blue: norm value (0.1uF), red: +1 %, d) Varying values of R15 and R16 within their tolerance ranges: green: -0.1 %, blue: norm value (160k), red: +0.1 % e) Varying value of R18 within its tolerance range: green: +0.1 %, blue: norm value (16.4k), red: -0.1 %. It can be noted that the effective notch frequency for all simulations lies in the range between 49.6 Hz and 50.6 Hz.

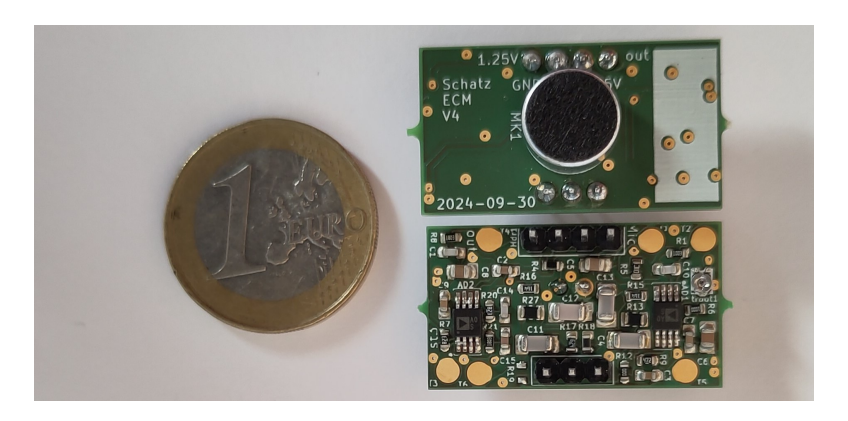


Figure 5.4: Photograph showing the front and back sides of the developed electret microphone board with a one-euro coin for scale reference. The breakout board is 30.4 mm long and 17.1 mm wide.

Piezoelectric Transducer Board

Piezoelectric transducers cannot be considered a typical microphone because their working principle relies on converting mechanical stress rather than sound waves into electrical signals. However, body sounds propagate through the body to the chest's surface and induce skin vibrations. Therefore, piezoelectric transducers are the ideal choice to pick up those vibrations and thereby mimic the behavior of a traditional stethoscope diaphragm.

For these reasons, the second acoustic sensor incorporated in the prototype is a piezoelectric element, namely the CEB-20D64 manufactured by Same Sky [14]. The CEB-20D64 is a typical piezoelectric disc with two wire leads carrying the voltage changes when the transducer is deformed. It is 20 mm in diameter and has a resonance frequency of 6.5 kHz.

Figure 5.5 shows the electrical circuit that interfaces the piezoelectric transducer. The acoustic signals are fed into a differential amplifier to obtain the voltage differences between the backplate of the transducer and the piezoelectric material. This stage features passive low-pass filters for both differential inputs at a cutoff-frequency fc of $f_c = \frac{1}{2\pi*100pF*1M\Omega} \simeq 1.6$ kHz and an amplification factor of 1000. Additionally, the sensed signals are referenced around 1.25V to stay within voltage ranges expected by the ADC in the interface layer.

This first stage is followed by a buffer amplifier with a unity gain of 1. This stage might not be needed in a future PCB design but has shown to stabilize the circuit in a previous version. There is a possibility of bypassing this stage if desired. Finally, the signal is filtered by an active Sallen-Key low-pass-filter with a cutoff frequency of $f_c = \frac{1}{2\pi * \sqrt{82k\Omega * 180k\Omega * 1nF*470pF}} \simeq 2 \text{ kHz}$.

The circuit was simulated in LTSpice, and the corresponding Bode-diagram can be seen in Figure 5.6. The pink line represents the frequency response after the signals passed the differential amplifier. The green line shows how the Sallen-Key filter of the last stage contributes in attenuating frequencies above 2 kHz.

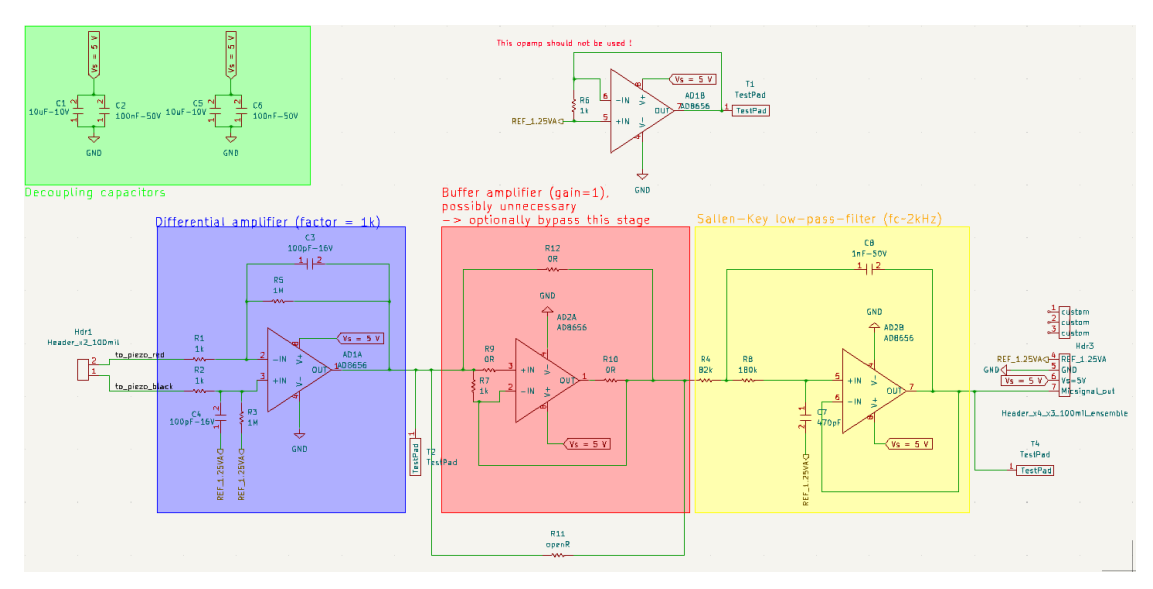


Figure 5.5: Electrical circuit that interfaces the piezoelectric transducer (CEB-20D64). The signal is captured with a differential amplifier (blue box) that provides the difference between the backplate of the transducer and the piezoelement. Then a buffer amplifier (red box) with gain 1 follows. There is a bypassing possibility to this stage. Lastly, the signals are filtered with a Sallen-Key low pass filter (yellow box).

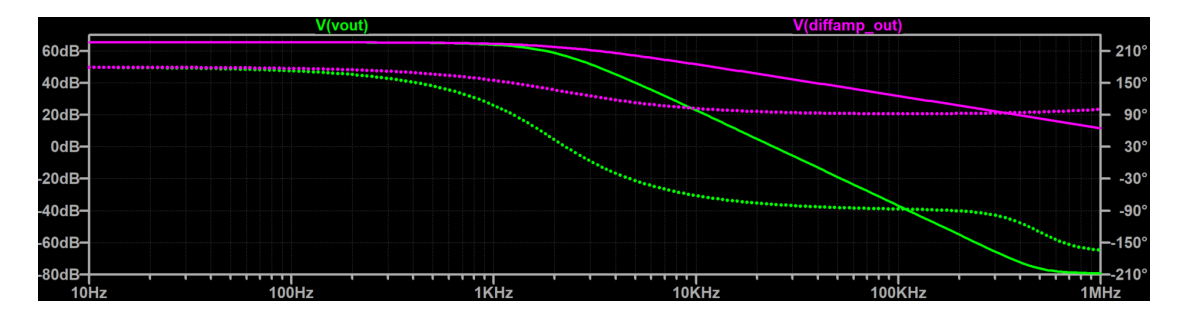


Figure 5.6: Frequency response of the schematic interfacing the piezoelectric transducer generated in LTSpice. The solid line shows the magnitude plot, and the dashed line represents the phase plot. Pink lines: Frequency response directly after the first differential amplifier stage; green lines: Frequency response at the final output of the electric circuit shown in Figure 5.5.

During preliminary tests of the circuit given in Figure 5.5, it became apparent that the piezoelectric transducer needs to be encapsulated in a casing due to two reasons: First, the transducer consists of a conductive material, and the measured signal gets distorted when in direct contact with the electrically conductive human skin. Secondly, the piezoelectric effect is based on the compression of the piezoelectric material, hence transducer's backside must be fixated. Multiple casing designs were tested and can be found in the Appendix A along with their findings. Figure 5.7 shows an image of the final encapsulated piezoelectric transducer. The transducer is glued with superglue to the lower part and the upper part of the casing. The lower part fixes the outer surface of the transducer while leaving a cavity below the transducer. In case of mechanical stress, the top part presses the transducer into the cavity. In response to this deformation, the wire leads of the piezoelectric element experience a voltage change.

The final physical appearance of the encapsulated piezoelectric transducer, along with its PCB is shown in Figure 5.8. The developed PCB has a width of 17.0 mm and a length of 20.4 mm.

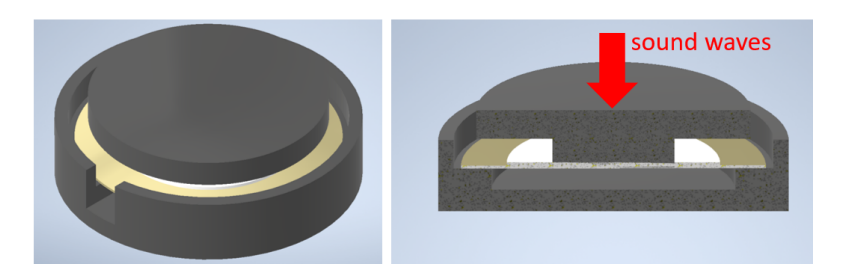


Figure 5.7: Piezoelectric transducer (gold-white) encapsulated by a casing consisting of two black parts. Left: Isometric view on the assembly, a notch is left open for the wires of the transducer. Right: cross-section of the setup, sound waves exert forces on the center of the transducer, leading to its deformation and, ultimately, to an electric signal



Figure 5.8: Photograph showing the front and back sides of the developed PCB and the casing of the piezoelectric transducer with a one-euro coin for scale reference. The breakout board is 20.4 mm long and 17.0 mm wide.

Digital MEMS Microphone Board

MEMS microphones offer a light-weight and compact alternative to the previously presented transducers. They generally operate on low power consumption and are easy to install. Digital MEMS microphones, in particular, convert analog audio signals internally into a digital form, thereby making audio data immediately available without the need for intermediate filtering, amplification, or conversion steps. This property makes them less susceptible to noise and interference from surrounding devices.

A digital MEMS microphone, namely the DMM-4026-B-I2S-R [16], was selected as the third candidate of acoustic transducer to capture body sounds. Furthermore, choosing a digital microphone increases the variety of investigated acoustic sensors. The output of the chosen microphone is formatted with the I2S standard. It was specifically opted for this standard, as it transmits data over a dedicated data line, making audio data directly available to access without any complex decoding steps, as opposed to the PDM standard. Furthermore, the DMM-4026-B-I2S-R promises a flat frequency response ranging from 20 Hz to 20 kHz, thus covering all audible frequencies (see Figure 4.7). The microphone provides an 18-bit precision resolution, a sensitivity of -26 dBV at 94 dB SPL, and an SNR of 64 dBA at 1 kHz. Its power consumption is composed of a voltage supply of 1.8 V and a current consumption of 820 - 1000 µA.

The DMM-4026-B-I2S-R microphone is operated as suggested by the datasheet and the circuit is shown in Figure 5.9. Since the microphone breakout boards are all supplied with 5 V and the DMM-4026-B-I2S-R requires a rated voltage of 1.8 V, the low-dropout regulator (LDO) NCP164CSN180T1G [17] was deployed to scale down the input voltage to the required level. The microphone is interfaced through the I2S standard with three lines, namely clock SCK, word select WS, and the data line SD that transmits audio data to the interface layer. When the microphone's Left/Right LR pin is pulled low, the signal is outputted in the left channel of the transmitted word. Vice versa, when the LR pin is set high, the signal is outputted in the right channel. Right and left channels can be addressed by placing 0 Ω resistors on the pads of R3 or R4, respectively.

The PCB holding the MEMS microphone is 13.02 mm long and 17.1 mm wide and can be inspected in Figure 5.10.

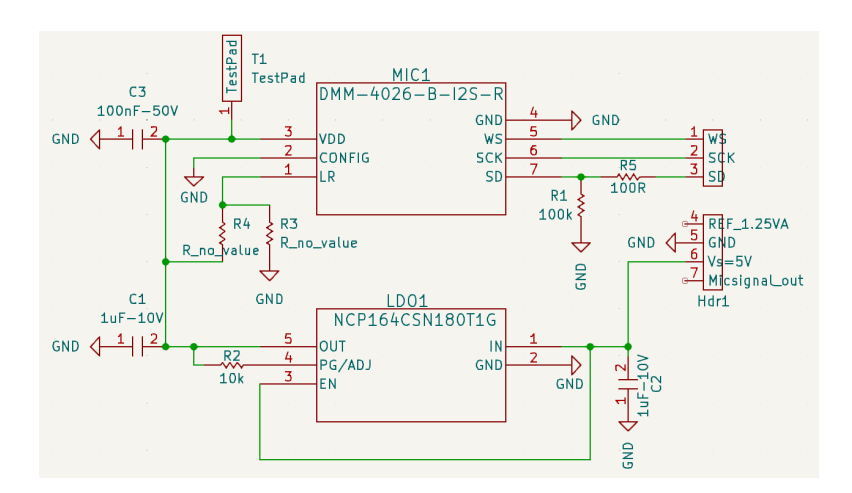


Figure 5.9: Electrical circuit that interfaces the digital MEMS microphone (DMM-4026-B-I2S-R). The schematic was designed according to the recommendations in the datasheet [16]. The resistors R3 and R4 determine the channel selected. To enable the right channel, set 0 Ω to R4 and remove R3, to enable the left channel set 0 Ω to R3 and remove R4. The LDO NCP164CSN180T1G [17] regulates the 5 V input voltage down to the rated voltage of the digital MEMS microphone of 1.8 V.

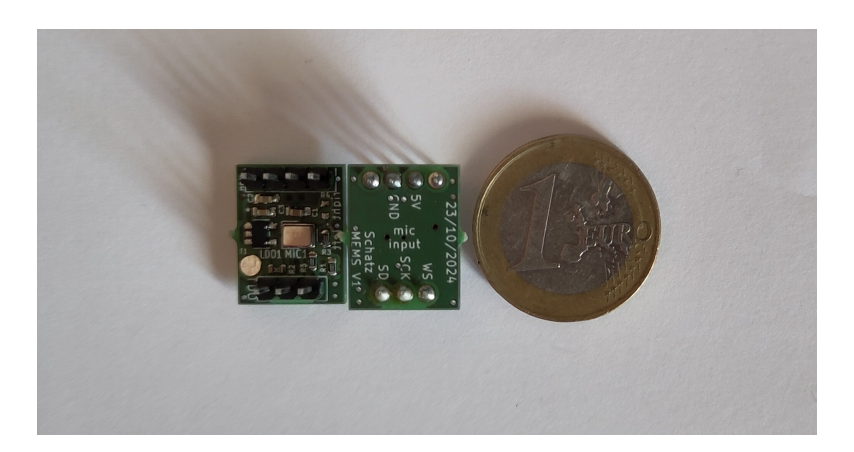


Figure 5.10: Photograph showing the front and back sides of the developed digital MEMS board with a one-euro coin for scale reference. The breakout board is 13.02 mm long and 17.1 mm wide.

5.2.2 Interfacing Layer

The second layer in the signal transmission path is represented by a main board that acts as an interface between the analog front end and the digital back end. Its main task is to convert analog data with an ADC to digital signals that can be interpreted by the back end. The main board provides headers in the Arduino UNO R3 standard, which allows every back-end device with the same format to be connected. A buck converter powers the circuitry of the main board with 3.3 V and the circuits of the microphone boards with 5 V. Ones again, to promote modularity of the design, the buck converter is manufactured on an individual PCB and can be easily replaced in case of damage.

The following text explains the functionality of the main board and the buck converter in detail.

Main Board

Audio data from the individual microphone boards explained prior to this section is received through female pin headers to which the microphone breakout boards can be attached. As can be seen in Figure 5.11, there are four of these interface headers marked with red rectangles. Each is represented by a 1x4 pin header and a 1x3 pin header. The 1x4 pin header supplies the microphone boards with voltage and manages the communication with the analog microphones, while the 1x3 pin header establishes the I2S interface between the digital microphones and the back end. This arrangement serves two main purposes: first, it avoids accidentally switching the orientation of the microphone breakout boards when plugging them onto the main board, and second, this design allows for keeping analog and digital voltage planes separated on the PCB, thereby reducing noise and interferences. Additionally, it guarantees a secure connection of the microphone breakout boards to the main board. Furthermore, the PCB is designed in a circular shape to mimic the appearance of a traditional stethoscope chest piece, and because it is more space-saving than e.g. a rectangular shape with the same microphone array arrangement. The diameter of the PCB is 96 mm, leaving enough room in its center to mount a traditional stethoscope chestpiece with a 47 mm diameter.

The principal task of the main board is to receive audio data from the individual microphone breakout boards and convert it to a format that that the back end can interpret. The outputs of the digital microphone are instantly structured in the I2S format and can therefore be forwarded without any further processing steps to the back end. For analog signals from the electret microphone and the piezoelectric transducer, the main board has an ADC, namely the ADS131A04 [28], that digitizes the signals and sends them over Serial Peripheral Interface (SPI) to the back end. The ADS131A04 can be configured in multiple SPI modes, such as asynchronous interrupt and synchronous master or slave mode. The PCB of the main board is designed in a flexible configuration that allows for switching between SPI modes through minor changes, in essence, by exchanging the resistors R1-R6 on the PCB. Figure 5.12 shows the interface diagram using the example of the asynchronous SPI interface. This communication includes a DRDY line that indicates the time point when data is ready to be sampled, a CS line that starts the data read out, a clock line SCK, and two lines MISO and MOSI for the data exchange between ADC and the back end device. The digital MEMS microphones are immediately interfaced to the back end device.

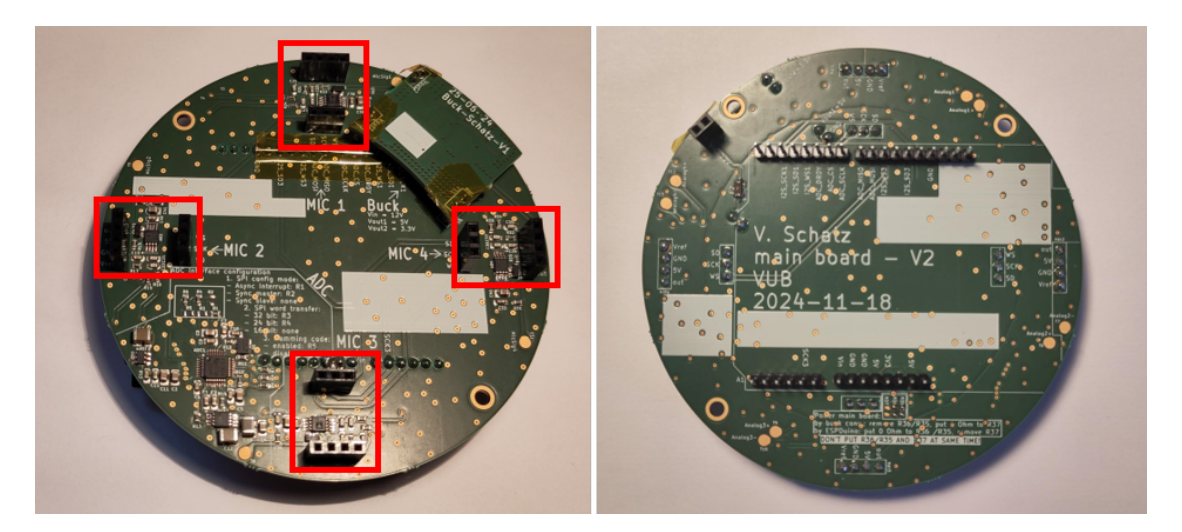


Figure 5.11: Photograph showing the front and back sides of the developed main board. The front side shows the headers, highlighted by red rectangles, to which the microphone boards can be attached, as well as the PCB of the buck converter that powers the whole setup. The main board is 96 mm in diameter and the microphone interfacing headers are arranged such that there is enough room for a generic analog stethoscope chestpiece in the center of the PCB. The back side shows the physical interface to the back end with the Arduino UNO R3 standard.

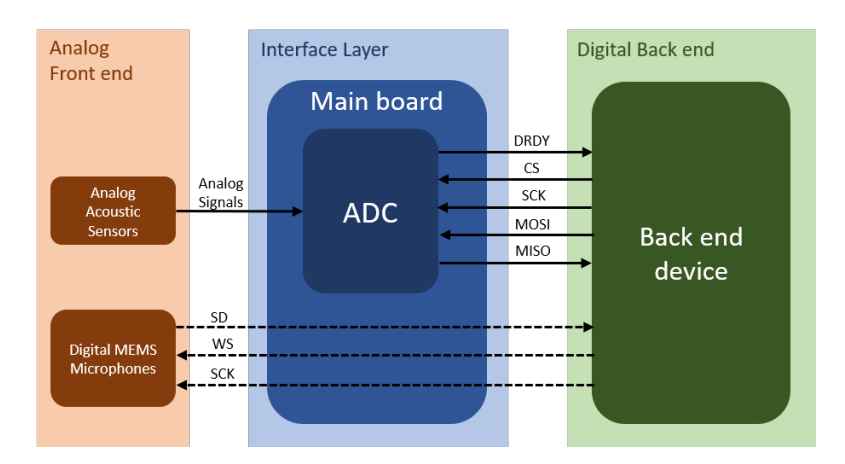


Figure 5.12: Interfacing diagram between analog front, main board and digital back end. The analog signal conversion is shown in solid lines, and the digital signal transmission is shown in dashed lines. The analog signals from the electret condenser microphone and piezoelectric transducer are converted with an ADC to digital data. The ADC communicates over asynchronous SPI with the digital back end. The DRDY line indicates that data is ready to be sampled. The CS line initializes the data read out, SCK is the clock line, MOSI is the line for data sent from the back end to the ADC, and MISO is the line for data sent from the ADC to the back end. The SPI mode can be changed through minor changes on the PCB and in the firmware of the back end. The main board establishes the I2S communication between the back end and the digital MEMS microphones. SD is the data line, WS is the word select line that addresses a specific microphone channel, and SCK is the clock line.

The ADS131A04 is a four-channel delta-sigma ADC with a data rate of up to 128 kSPS and a high resolution of 24 bits ensuring superior accuracy, which is crucial for audio applications. This ADC was explicitly chosen for three main reasons: First, it features the delta-sigma-method that oversamples the analog signal at a much higher frequency than the Nyquist rate, consequently reducing the risk for aliasing and promising little presence of noise in the converted signal. Secondly, it offers a wide range of programmable features such as the oversampling ratio (OSR) or the digital gain setting for individual ADC channels. And finally, because it runs on a low power consumption of 7.2 mW.

The inputs of the ADS131A04 have to lie between 0 V and 2.5V. Therefore, the circuits of the two analog microphones have to output signals that oscillate around a voltage reference of $1.25~\rm V~(=2.5~\rm V~/2)$ and do not exceed $0.25~\rm V~$ and $2.25~\rm V~$ to create a buffer. The ADC comes in a differential input pin configuration which further helps rejecting common-mode noise, i.e. noise present at both the positive and the negative analog input pins. According to the ADC's datasheet [28], the signals at the positive and negative input pins have to be phase-shifted by 180 degrees. For this purpose, the schematic shown in Figure 5.13 was designed. At the bottom of the figure, one can inspect the AC analysis of this circuit simulated in LTSpice. Indeed, the two outputs Analog_1- and Analog_1+ are out-of-phase by 180 degrees. The signals of all four channels are treated equally and are subsequently fed into the ADC to be digitized.

All other pins of the ADC are interfaced as suggested in its datasheet [28].

The main board is powered by a dual-channel buck converter (see the following Section 5.2.2). The outputs of the buck converter are separated from the rest of the electrical circuit by fuses to protect the components from possible over currents.

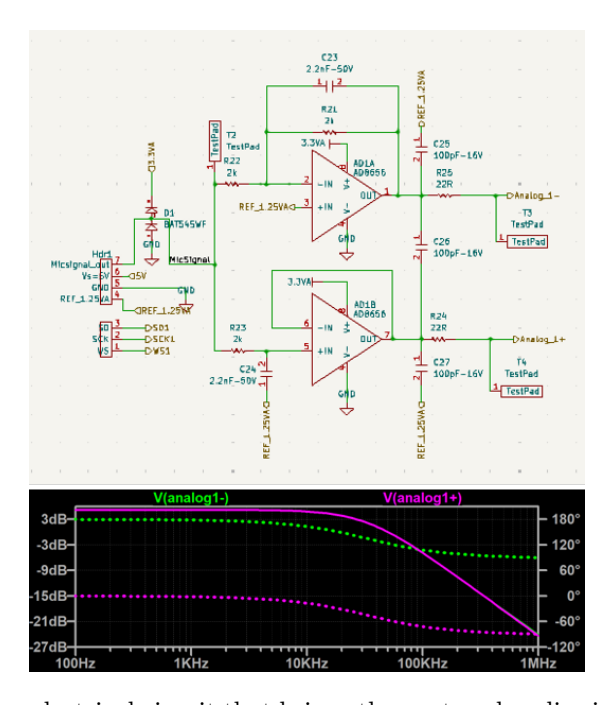


Figure 5.13: Exemplary electrical circuit that brings the captured audio signal into a format that can be fed into the ADC as suggested by the datasheet [28]. The solid line shows the magnitude plot, and the dashed line represents the phase plot. The resulting outputs Analog_1- (green) and Analog_1+ (pink) are phase-shifted by 180 degrees.

Buck converter

The proposed electronic stethoscope is powered by a buck converter that simultaneously supplies the main board circuitry with 3.3 V and the microphone boards with 5 V. In order to determine the specification that the buck converter has to deliver, the total current consumption of the setup needed to be determined. Table 5.3 gives a detailed description of the maximal supply consumption per active component and is subdivided into the individual breakout boards. The electret microphones consume the most current. Consequently, the maximum current drawn by the setup occurs when four electret microphone boards are deployed simultaneously, yielding 127.9 mA + 38 mA = 165.9 mA. According to these specifications, the dual-channel buck converter LT8653S [13] is chosen that provides a maximum of 1A of current per channel and decreases a 12 V input voltage to stable voltage levels of 3.3 V and 5 V respectively. Furthermore, the buck converter generates ultra-low electromagnetic interference, which is crucial to avoid noisy signals.

Board	Component	Mfr. No.	max. supply current[mA]	#	Sum[mA]
Main	Voltage references	REF6025IDGKT	0.9+4	1	127.9
		LT6656BCS6-1.25TRMPBF	0.001+20	1	
	Oscillator	ASEMB-24.576MHZ-XY-T	15	1	
	Microcontroller	PIC32CK2051SG01144	50	1	
	opAmps	AD8656	4.5	4	
	ADC	ADS131A04	20	1	
Electret	Microphone	CMA-4544PF-W	0.5	4	38
	opAmps	AD8656	4.5	2x4	
Piezo- electric	Transducer	CEB-20D64	-	4	36
	opAmps	AD8656	4.5	2x4	
MEMS	Microphone	DMM-4026-B-I2S-R	1	4	4

Table 5.3: Estimated current consumption of the individual PCBs

The schematic for operating the LT8653S was designed with the help of the LTPowerCAD Software by Analog Devices, Inc. The proposed schematic was simulated and modified with LTSpice to meet the above mentioned requirements. The results of the simulation are shown in Figure 5.14. It can be seen that the desired voltage levels are established within a few microseconds. The corresponding operation circuit of the LT8653S can be seen in Figure 5.15. Two load resistors are placed on the board to mimic the power consumption of the whole setup. This approach helps to assess the noise level of the output voltages. The performance of the buck converter board was evaluated in two stages: First, the load resistors were not placed to verify the voltage output levels. These yielded the desired 5 V and 3.3 V. In a second test, the load resistors were placed to measure the noise level. It was shown that there is noise present in the net frequency of 50 Hz. However, it is only a few millivolts in magnitude ranging from 1.6 mV for the 5 V output and 2.5 mV for the 3.3 V channel. The load resistors are removed when the buck converter board is connected to the main board.

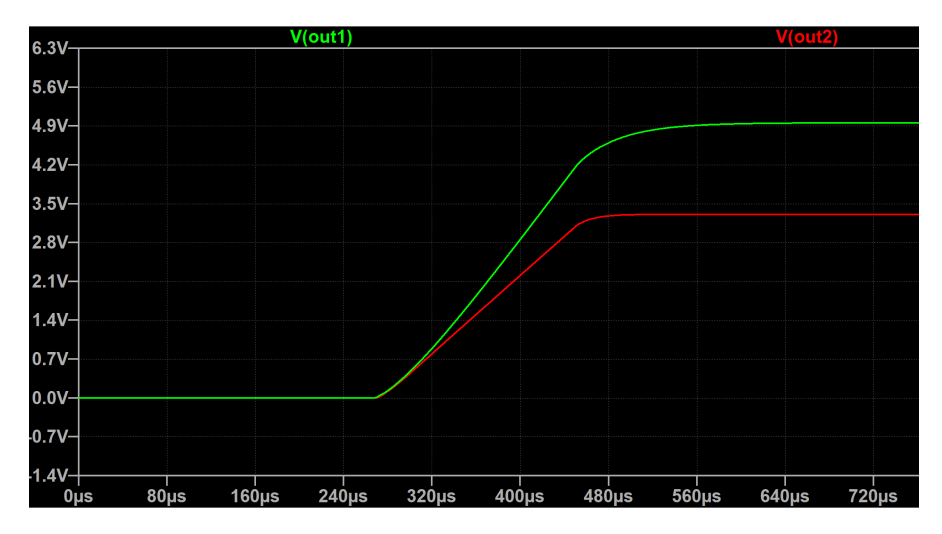


Figure 5.14: Simulation of the operational circuit connected to the buck converter LT8653S showing voltage levels over time. The desired voltage levels of 5 V (green line) and 3.3 V (red line) are reached within a matter of microseconds.

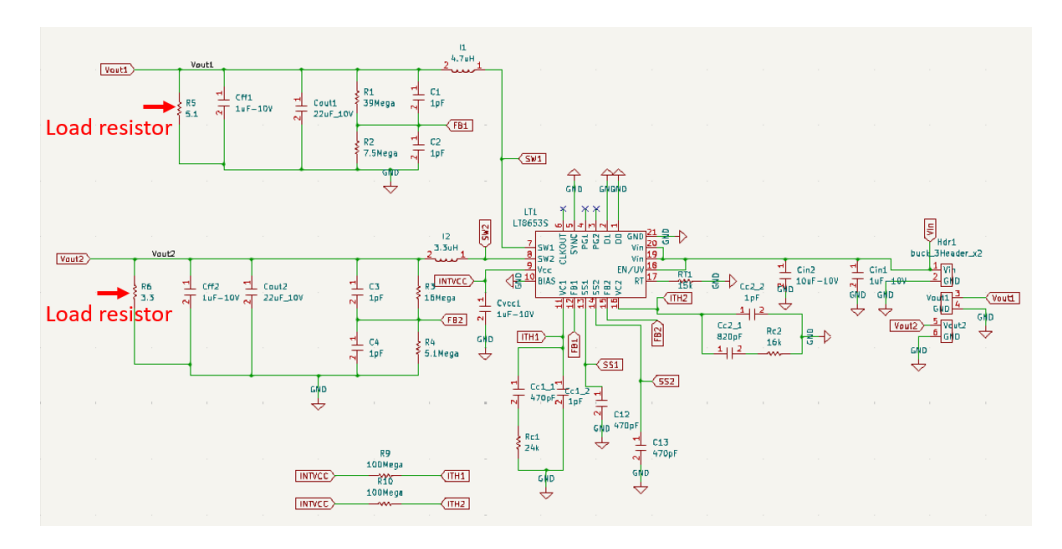


Figure 5.15: Schematic of the buck converter breakout board, the load resistors with values of 5.1 Ω and 3.3 Ω , respectively, are placed for testing the board and are removed when the buck converter is connected to the main board

5.2.3 Digital Back End

The final stage of the signal transmission path is the back end. One of the main goals of this thesis is to establish a versatile platform where the back end can be represented by several computational systems and can be tailored to the needs of the user. For this purpose, the main board provides an interface to the standardized Arduino UNO R3 header pinout.

In the following, some examples that can be used as the digital back end are presented, emphasizing the prototype's diversity. Thereafter, the back end realized in this work is described, highlighting the MCU deployed and explaining the firmware developed.

Flexible Platform Selection

Generally, every platform with Arduino UNO R3 compatibility can be used as a back end. The options that can be used are manifold and range from typical MCUs to high-performing FPGAs. However, commercially available platforms with suitable header configurations exist on the market. The following text briefly summarizes the advantages of different systems.

Microcontroller Units are general-purpose integrated circuits (IC) that incorporate CPU, memory, and I/O pins in one compact chip. They are suited for simple general-purpose applications and are relatively easy to operate. MCUs are available at low cost and are energy-efficient. Some examples of MCUs with Arduino header compatibility are depicted in Figure 5.16. The Adafruit METRO 328 incorporates the ATmega328P and is interoperable with the Arduino IDE, and can be used for simple projects. In Figure 5.16 b) Adafruit provides the ESP32-S3 with Arduino-compatible output headers. This powerful chip supports both WiFi and Bluetooth, making it most suitable for Internet-of-Things (IoT) projects. Next, the ESPDuino is shown in Figure 5.16c) and features an ESP32-WROOM-32. This module is used in this thesis to demonstrate the the prototype's functionality. The ESP32-WROOM-32 chip offers two cores that can be separately controlled and a CPU clock frequency that can be configured in the range of 80 to 240 MHz. Furthermore, it provides both peripheral interface protocols relevant to the prototype, namely SPI, and I2S. And lastly, the module offers Bluetooth and WiFi compatibility. In light of these features, the ESPDuino is the optimal choice for the requirements of the design described in the LORs in Tables 5.1 and 5.2.

Digital Signal Processors are low-cost microprocessors designed to perform efficient signal processing that is crucial for audio applications [18]. The prototype presented herein could serve as a framework for testing and engineering new audio processing technologies, such as digital filters.

System-on-Chips are a combination of multiple computer components in a single IC and can thus execute diverse and more complex tasks. When a desired system with Arduino header compatibility is unavailable, it can be easily mounted on a dedicated bridging board, as [62] has done and is shown in Figure 5.17. With this approach, any possible platform can be connected to the electronic stethoscope developed in this thesis.

Field-Programmable Gate Arrays are reprogrammable and reconfigurable ICs that offer a parallel processing architecture [18]. This makes them a powerful tool to execute the most complex algorithms, such as advanced signal processing or even machine learning algorithms [62]. Figure 5.18 shows two FPGAs that can be found with Arduino compatibility. Combining the developed electronic stethoscope with such a system enables for sophisticated and versatile engineering applications.

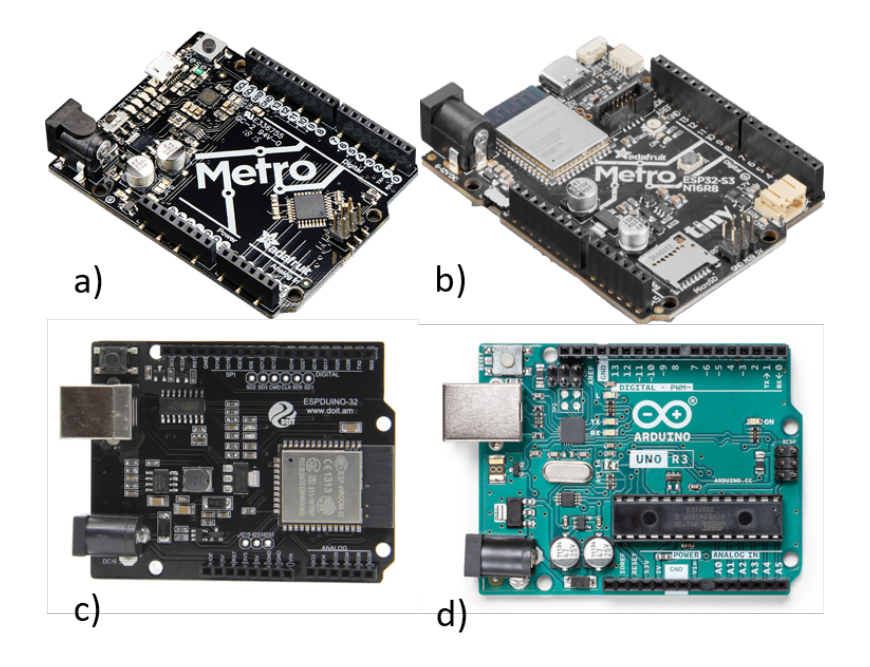


Figure 5.16: Examples of purchasable MCUs with Arduino UNO R3 header compatibility. a) Adafruit METRO 328 b) Adafruit Metro ESP32-S3 c) ESPDuino d) Arduino UNO R3.



Figure 5.17: Infineon PSoC 6 BLE Prototyping Kit (left) with a bridge board to interface the Arduino UNO R3 header as used in [62].



Figure 5.18: Examples of purchasable FPGAs with Arduino UNO R3 header compatibility. Left: Intel DE10-Nano Kit. Right: Xilinx PYNQ Platform.

Firmware

As mentioned previously, the ESPDuino was chosen as an MCU to demonstrate the functionality of the developed prototype. This MCU connects an ESP32-WROOM-32 to Arduino headers and features a wide range of wired and wireless communication. It was opted to perform the wireless data transmission over WiFi in the form of the User Datagram Protocol (UDP) because of its ease of implementation and low latency in data transfer. As mentioned earlier, the ESP32 has to read samples in the I2S and SPI format, depending on whether the data is provided by the digital MEMS microphones or the ADC. The program codes written for the I2S readout and the SPI communication behave similarly and distinguish only in minor differences. This section explains the program structure, how the ESP32 reads samples, and how it forwards them to a PC.

For both communication protocol types, a double buffering program structure was chosen that alternates between filling and sending two buffers, thereby enabling data streaming in real-time without delays. As illustrated in Figure 5.19, after some initialization steps, such as initializing the WiFi connection or configuring the ADC, two tasks run in parallel on the two cores offered by the ESP32. The first task runs on core zero and handles the data transmission over WiFi to the IP address of a PC, while the second task runs on core one and is responsible for filling the two buffers with audio data sent by the main board. Additionally, the program structure includes an interrupt service routine (ISR) whose sole responsibility is to set a flag high whenever a sample is ready. This triggers the data readout of the second task on core one that adds the new sample to the active buffer. When the active buffer is full, the task sets a flag high, indicating that the buffer is ready to be sent to the PC, and switches the active buffer so that the other buffer starts to be filled. This process continues indefinitely.

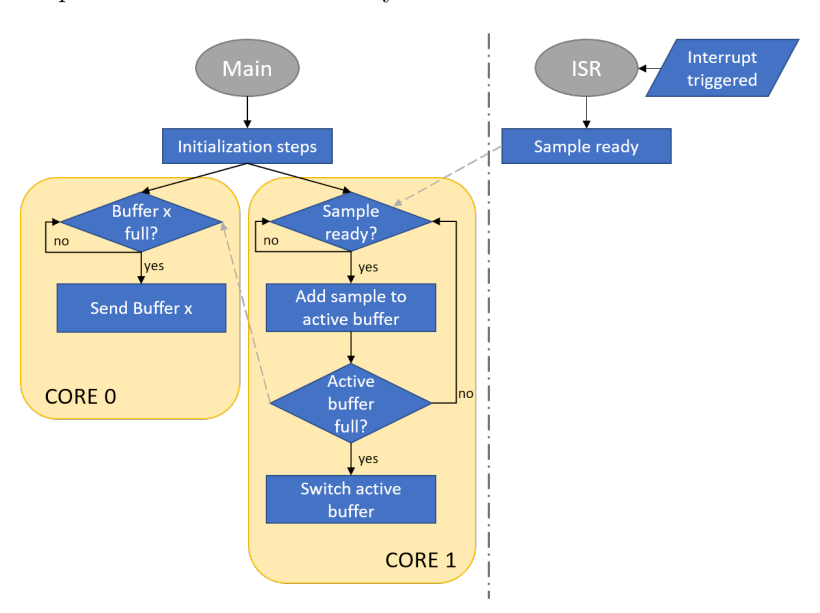


Figure 5.19: Program flow chart of a two buffer program structure to wirelessly transmit data from the ESP module to a PC. An interrupt service routine (ISR) temporarily suspends the CPU's current process and sets a high flag. This flag indicates that samples are ready to be read and can be added to one of the buffers. While one buffer is filled, the other one is sent over WiFi.

The ADC on the main board is configured in asynchronous SPI mode with an oversampling frequency of 128 and a sample rate of 16 kHz. The DRDY pin of the ADC pulsates at the frequency of the sample rate and indicates that a sample from all four channels is ready to be transmitted to the MCU. When the ESP32 receives a high voltage on the DRDY pin, the ISR is triggered, and the sample is read using the regular SPI protocol according to the timing diagram shown in Figure 5.19 on the right.

In contrast to that, the audio data provided in I2S format is read in response to an internal interrupt that triggers at a frequency of 48 kHz. The ESP32 offers two I2S interfaces and can sample from two peripherals for each interface. Therefore, data from four digital MEMS microphones can be read simultaneously. Figure 5.20 on the left side shows the timing diagram of the I2S communication. The word select line WS individually addresses two microphones in one I2S communication by toggling high and low. An audio sample is stored in a 64-bit word, with the first 32 bits from the left microphone and the last 32 bits from the right microphone. On the ESP32 the data is separated into data streams from the individual microphones and stored in the buffer.

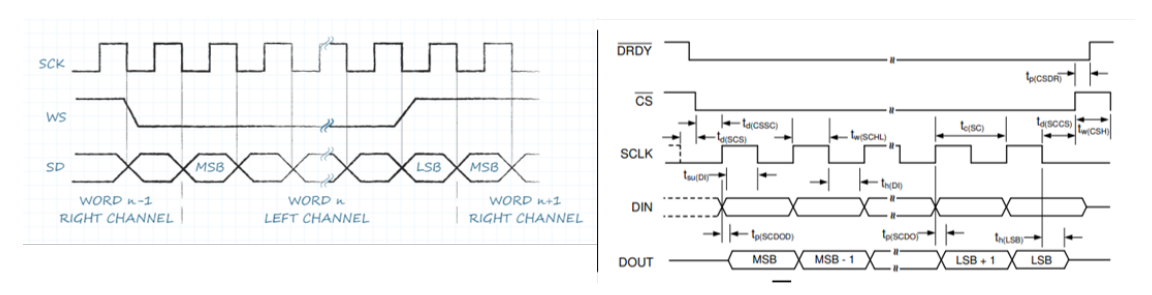


Figure 5.20: Left: I2S communication protocol [61], Right: SPI communication protocol from the datasheet of the ADC [28]

The ESP32 forwards the received audio data to a PC in a uniform format regardless of whether the data comes in through I2S or SPI communication. It acts as the client in the communication model and sends data as UDP packages over the local WiFi router to the desired IP address and port number. The receiving PC is the server and binds to a socket with the same IP address and port number. The user can choose the number of UDP packages to receive, and the acquired data is stored separately as CSV and WAV files for the four microphones.

Some experiments testing the reliability of this wireless communication model revealed that some samples are lost during transmission. This could be due to the chosen transmission protocol because UDP does not include handshakes between the two communicating parties, and hence, there exists no confirmation of reception by the server. Nevertheless, heart signals could be detected in the recordings.

5.2.4 3D Printed Casing

The previous chapters described the developed electronic stethoscope's design and its three essential layers. While the setup can be used as a stand-alone device, a goal of this thesis is to enable simultaneous analog and digital auscultation. For this purpose, a casing was developed that incorporates a conventional chestpiece at the center of the prototype. Figure 5.21 shows an assembly of a typical stethoscope and the main board with two electret microphone boards with tubes, one piezoelectric transducer board, and one MEMS board attached to it. The encapsulated piezoelectric element is illustrated in magenta color.

The housing was designed to meet three requirements:

- All acoustic sensors and the diaphragm of the conventional stethoscope had to be flush to ensure equal detection of heart sounds.
- The design had to be modular and easily exchangeable in case of damage. Therefore, the construction is tied together with screws and can thus be quickly assembled and disassembled. Similarly, the casing for the piezoelement is mounted with screws.
- The casing offers access to the microphone boards to enable for a quick exchange between sensor types.

The PCB of the buck converter is located below the stethoscope tubing for efficient space usage. However, this prevents more than three piezoelectric transducers from being mounted simultaneously.

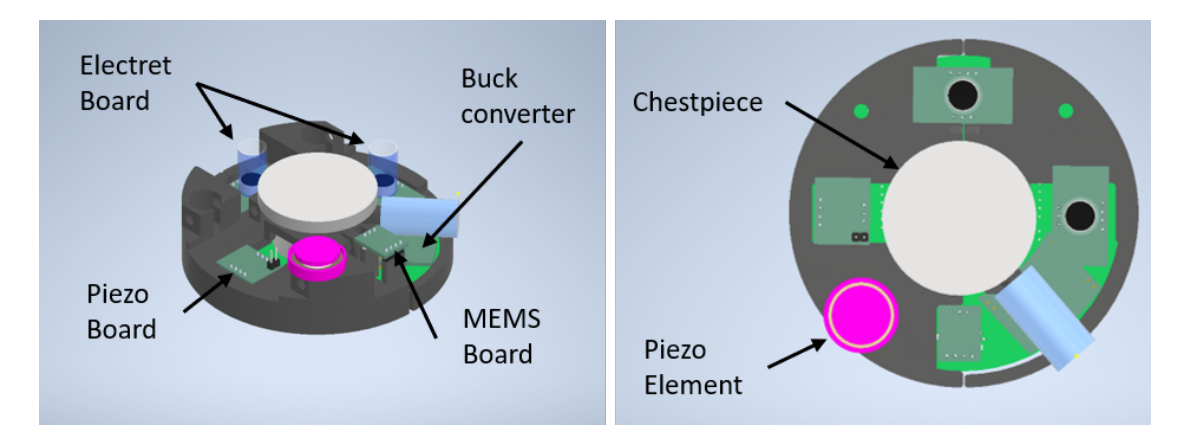


Figure 5.21: CAD model of the 3D printed casing encapsulating the developed electronic stethoscope with two electret microphone boards, a piezoelectric transducer board, and a MEMS microphone board mounted on the main board. A conventional chestpiece is attached to the center of the setup. The piezoelectric transducer is encapsulated in a magenta-colored casing. The left image shows an isometric view of the setup. In the right image, the setup can be seen from the top.

5.3 Demonstrator

The previous sections provided a detailed description of the developed electronic stethoscope by first highlighting its requirements, and secondly outlining its design. The presented prototype can be attached to a typical analog stethoscope, allowing for analog and digital listening. This gives analog stethoscopes an additional purpose and prevents them from being discarded in replacement of a fully digital stethoscope. Above that, all hardware components are designed on individual PCBs, and therefore the design allows for quick exchange and replacement of acoustic sensors. These features make the prototype a sustainable, eco-friendly, and modular device.

Figure 5.22 shows photographs of the final setup in three different configurations with, from left to right, the piezoelectric transducer encapsulated in a magenta-colored casing, the electret condenser microphone boards, and the MEMS microphone boards. The latter two microphones can be operated without housing the prototype. For the piezoelectric transducer, this housing is necessary in order to achieve adequate stabilization of the sensor. However, the main board and the buck converter provide space for no more than three transducers. Nevertheless, the setup's microphone array configurations enable advanced technologies, like sensor fusion, beamforming, or multi-sensor body sound acquisition.

The following section demonstrates the functionality of the developed electronic stethoscope using the example of heart auscultation.







Figure 5.22: Photographs of the three microphone configurations from left to right: the piezoelectric transducer with its magenta-colored casing, the electret condenser microphones, and the MEMS microphones

Chapter 6

Experimental Results

The experiments can be separated into measurements conducted in a controlled environment, i.e. a loudspeaker that emits sound in an anechoic box, and tests performed on the human body. The measurements carried out in the anechoic box are meant to determine the noise floor, the signal-to-noise ratio (SNR), the frequency response, and the sensitivity of each microphone individually. To assess the performance of the developed microphone boards to sense heart sounds, the developed setup was applied in a human heart auscultation scenario. All tests were also performed on the commercial 3M Littmann CORE digital stethoscope to obtain a reference measurement. This stethoscope incorporates multiple signal enhancement steps such as filtering and amplification stages. For the experiments, the 3M Littmann CORE stethoscope was treated as a "black box" as the user does not gain access to the raw data captured by the microphone in the stethoscope. This chapter is structured as follows: At first the measurements performed in the anechoic chamber are presented. These include a sensitivity and noise floor measurement, a SNR analysis, a frequency response evaluation and an experiment on recording a heart beat emitted by a loudspeaker. The second section of this chapter describes the experiments to evaluate the performance of the designed microphones on detecting heart sounds when placed on the human chest.

6.1 Microphone Characterization in the Anechoic Box

Measurements to obtain the noise floor, sensitivity, SNR and the frequency response were conducted in an anechoic box. Additionally, an experiment was performed where the microphones were exposed to a heart beat emitted by a loudspeaker. The left image in Figure 6.1 shows the inside of the anechoic box with the employed loudspeaker. On the right, the measurement setup is depicted. The distance between the loudspeaker and each microphone is 3 cm although it does not resemble the same sound propagation properties, as the heart sound propagates through water-like fluids and not through air as in the experimental setup. Solely, for the sensitivity measurement the microphones were placed at a distance of 50 cm to the loudspeaker.

For the noise floor, the SNR and the sensitivity test, the root-mean-square (RMS) value was chosen as a metric to quantify the effective energy present in the recorded signal. The RMS value for N data points in a signal was calculated as:

$$RMS = \sqrt{\frac{1}{N} \sum_{n=1}^{N} |x_n|^2}$$

and expressed in dB with:

$RMS_{dB} = 20 \cdot log_{10}(RMS)$

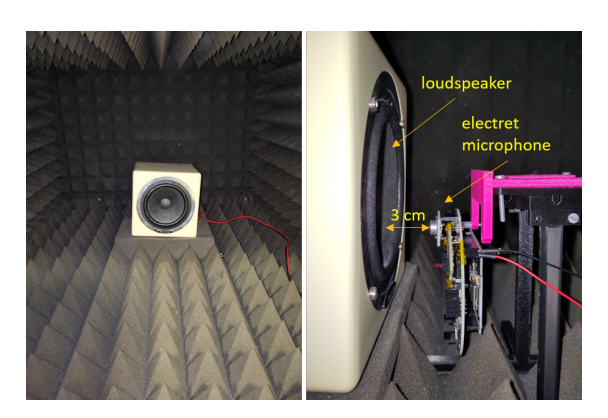


Figure 6.1: Measurement setup in the anechoic box. Left: Inside of the anechoic box with a loudspeaker placed to the back wall. Right: Exemplary measurement setup for the electret condenser microphone for measuring the noise floor, the SNR, the frequency response and a heart beat emitted by the loudspeaker. The same set up was used for every other microphone type and for the 3M Littmann CORE digital stethoscope. All microphone types were attached to the main board which is mounted on a 3D printed holder in magenta color. For the sensitivity test the same setup was used but the distance between loudspeaker and microphone was increased to approximately 50 cm.

The 3M Littmann CORE digital stethoscope was set to "wide mode" as it covers the largest frequency range offered by the stethoscope. It is noteworthy that the commercial stethoscope automatically applies filters and post-processing steps to the recordings and it is not possible to obtain raw signals sensed by the transducer in the stethoscope. In contrast to the developed microphone boards, the commercial stethoscope comes with a generic chestpiece that mechanically increases the sound intensity at the location of the microphone and therefore contributes to the overall sensitivity of the device. The developed acoustic sensor boards do not have such a mechanical amplification.

Furthermore, both the 3M Littmann CORE digital stethoscope and the designed piezoelectric transducer are meant to be used in direct contact with a pulsating surface and could therefore show a weaker performance when exposed to sound waves transmitted through air. However, for the tests presented in this chapter they were treated as if their behavior was equal to a generic microphone to establish a comparability between the test results.

6.1.1 Sensitivity and Noise Floor Measurement

Sensitivity measurements serve to evaluate how changing loudspeaker volumes influence the effective energy of the recorded signals. To determine their sensitivity, the acoustic sensors were placed approximately 50 cm in front of the loudspeaker that emitted a sine wave of 300 Hz. This frequency was chosen as it lies in the range of typical heart sounds (compare Table 2.2). At first, the loudspeaker was configured to output its maximum sound level. Then a 30-second-recording was performed with every microphone board and the commercial stethoscope individually. At the same time a decibel meter measured the sound volume in dB. Subsequently, the volume of the loudspeaker was successively reduced between recordings until it reached its minimal volume.

The captured signals were filtered by a digital Butterworth band-pass-filter with cutoff frequencies 270 and 330 Hz, respectively, to isolate the frequency components that correspond to the frequency that the loudspeaker emitted. Next, the RMS of the signals was calculated and plotted over the sound volume measured with the decibel meter.

In a last step, the noise floor was determined in order to obtain the minimum level of noise that the microphones perceive in the measurement setup. This measured noise can, for example, originate from acoustic noise emitted by the loudspeaker, the ESP32 module, or from mechanical vibrations inside the anechoic box. But also electric distortions, like 50 Hz main hum, can be considered noise. For this purpose, the whole measurement setup was switched on but the loudspeaker did not emit sound. The front door of the box was closed and a measurement of 30 seconds was performed for each microphone and the 3M Littmann CORE digital stethoscope individually. Finally, the RMS of the noise floor signals was added as a green line to the sensitivity curves shown in Figure 6.2.

All graphs show a linear growth for increasing sound levels. To emphasize this trend, a regression model was applied to fifteen data points inside the linear region of the sensitivity curves. The regression line follows the structure of the equation:

$$y_{pred} = e^{m*x+b} (6.1)$$

and the coefficients for every microphone board and the commercial stethoscope are given in Table 6.1. The exponential function in the equation comes from the fact that x is the sound level in dB and thus a logarithmic scale.

Linear Regression	Electret Microphone	Piezoelectric Transducer	MEMS Microphone	3M Littmann CORE
Coefficients		Board	Board	Stethoscope
m	0.11370	0.11096	0.11535	0.11360
b	3.440596	-0.58407	4.60109	-3.81060

Table 6.1: Coefficients for the linear regression model of Equation 6.1 for the three microphone boards and the commercial reference stethoscope.

The sensitivity curves shown Figure 6.2 show the recorded data points in blue, the fitted linear regression line in red and the measured noise floor in green. The noise floor in dB corresponds to the intersection point of the regression line and the noise floor. Hereunder, the graphs are explained in detail for each microphone type individually:

Electret Microphone Board

The sensitivity curve of the electret microphone board is visualized in Figure 6.2A). The graph rises smoothly for increasing sound volumes until it meets the fitted regression line at around 59 dB. The noise floor of the electret microphone board is 48.5 dB, and thereby maintains the highest noise floor among all sensors tested.

Piezoelectric Transducer Board

As can be seen in 6.2B) the recordings made with the piezoelectric transducer board demonstrate a nearly linear sensitivity curve for all sound volumes. The noise floor represented by a green dashed line lies below all measured data points, indicating that the noise floor has never been reached during the measurements. The theoretical noise floor in dB is 37.5 dB.

MEMS Microphone Board

Figure 6.2C) shows the sensitivity curve recorded with the MEMS microphone board. The graph starts with two data points measured at noise floor level. At a sound level of approximately 30 dB the graph suddenly jumps to an RMS of more than 10⁶ and follows a linear trend for increasing sound strength. The rapid increase in RMS value at the beginning of the curve might occur because the output of the MEMS microphone is digital and might therefore intrinsically truncate sound volumes of low-intensity. The intersection of the red regression curve and the green noise floor line indicates a theoretical noise floor level of 14.5 dB when neglecting this truncation.

3M Littmann Core Stethoscope

The sensitivity curve of the commercial stethoscope is shown in Figure 6.2D) and starts with a data point similar to the noise floor level. For increasing sound levels, the curve approximates the regression line. It is noteworthy that the measured data points are located below the regression line, demonstrating a non-linear nature for sound levels lower than 68 dB and indicating a lower signal strength than predicted by the regression model. However, it has to be kept in mind that the stethoscope is not indented to be used for these kinds of experimental characterizations and internal signal processing might explain this behavior. The theoretical noise floor of the 3M Littmann CORE stethoscope is 14.77 dB.

The noise floor levels of every microphone are summarized in Table 6.2, and Figure 6.3 compares the sensitivity curves between the acoustic sensors. It is important to note that in these experiments, the commercial stethoscope and the piezoelectric transducer were treated as typical microphones, although their signal transduction mechanism does not follow the same principle. Therefore, the sensitivity curves might not reflect the genuine performance of these transducers.

The electret microphone board yields the highest noise floor. Conversely, the MEMS microphone board and the commercial stethoscope show comparable performances in the sense of captured background noise.

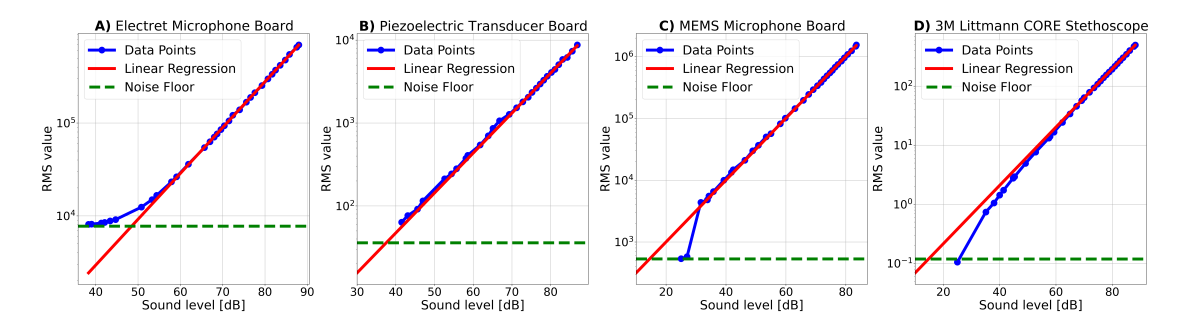


Figure 6.2: Response curves for the developed microphone boards and the commercial reference stethoscope for different sound volumes. The RMS values were calculated from the recorded signals after applying a band-pass-filter of 300 Hz. A regression line was fit to fifteen data points in the linear regions of each curve and is shown in red. Additionally, the RMS of the noise floor measurement was inserted as a green horizontal line.

	Electret Microphone Board	1 102001001110	MEMS Microphone Board	3M Littmann CORE Stethoscope
Noise Floor [dB]	48.5	37.5	14.5	14.77

Table 6.2: Noise floor levels per acoustic transducer deduced from the sensitivity curves shown in Figure 6.2

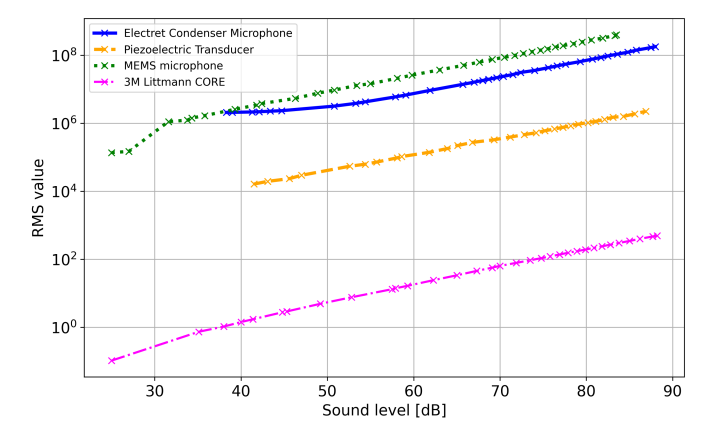


Figure 6.3: Comparison of the digital output range of the acoustic sensing technology for different sound volumes

6.1.2 SNR Analysis

The signal-to-noise ratio (SNR) is the signal over the noise floor and is a good indicator for evaluating the clarity of a signal. Therefore, this section provides the maximal SNR SNR_{max} and a theoretical SNR for a typical heart beat $SNR_{HeartBeat}$ per microphone type. The SNR_{max} is calculated via the following formula:

$$SNR_{max} = 20*log_{10}(\frac{RMS_{max}}{RMS_{noiseFloor}})$$

Here, RMS_{max} represents the theoretical maximum RMS value that a microphone board can output and $RMS_{noiseFloor}$ is the RMS value of the noise floor determined in the previous Section 6.1.1.

To obtain values for RMS_{max} , the subsequent equation was used:

$$RMS_{max} = (2^{24} - 1) * \frac{\sqrt{2}}{2}$$

This equation is composed of two parts: Firstly, the maximum data value that can be transmitted from the developed main board to the ESP is $2^{24}-1$ because the data resolution is 24 bit. Secondly, the RMS value of a sine wave with amplitude one can be estimated by $\frac{\sqrt{2}}{2}$. Therefore, multiplying these two terms approximates the theoretical maximal RMS value.

To determine the microphone's SNR for a typical heart sound, the following procedure was applied: First, an auscultation of a healthy 26-year old woman with a body-mass-index (BMI) of 21.1 was performed with the commercial stethoscope at auscultation point 1. Then, the RMS value of the resulting heart beat signal was determined to be 122.12. The corresponding sound level was calculated with the means of the regression model for the commercial stethoscope provided in the previous Section 6.1.1 and yields 75.8 dB. Inserting this sound volume into the regression models for the developed microphone boards delivers the corresponding RMS value $RMS_{HeartBeat}$ for every developed microphone board.

It should be noted that the chestpiece of the commercial stethoscope acts as a mechanical amplifier. Therefore, the recorded sound volume does not represent the actual pressure level on the skin. Furthermore, for calculating the SNR of heart sounds, only one sole person's heart beat was auscultated. In reality, the sound pressure level of a heart is unique for every person. However, this approach approximates the orders of volume magnitude that can be expected from a healthy heart sound. The $SNR_{HeartBeat}$ can be determined with:

$$SNR_{HeartBeat} = 20 * log_{10}(\frac{RMS_{HeartBeat}}{RMS_{noiseFloor}})$$

The obtained SNRs are summarized in Table 6.3. The highest SNR_{max} is achieved by the piezoelectric transducer board with 110.4 dB followed by the MEMS microphone board with 87.0 dB. The lowest SNR_{max} is reached by the electret microphone board with 63.7 dB. The theoretical maximal RMS of the 3M Littmann CORE can not be determined as 3M does not provide any information about the transfer word size deployed. Therefore, there is no reference SNR available.

Regarding $SNR_{HeartBeat}$ the two analog sensors offer acceptable values, with 27.0 dB for the electret microphone board and 36.9 dB for the piezoelectric transducer. The MEMS microphone board and the commercial stethoscope yield comparable SNRs of 61.4 dB and 60.3 dB, respectively, and are therefore superior in terms of signal strength over noise.

	Electret Microphone	Piezoelectric Transducer	MEMS Microphone	3M Littmann CORE
	Board	Board	Board	Stethoscope
$SNR_{max}[dB]$	63.7	110.4	87.0	-
$SNR_{HeartBeat}[dB]$	27.0	36.9	61.4	60.3

Table 6.3: Signal-to-noise-ratios (SNRs) for the developed microphone boards and the commercial reference stethoscope. SNR_{max} represents the maximal SNR that a sensor can achieve and $SNR_{HeartBeat}$ is the SNR that can be expected for a typical heart sound. The SNR_{max} of the 3M Littmann CORE stethoscope is not available as 3M does not provide the specifications necessary to calculate the SNR.

6.1.3 Frequency Response

The frequency response reveals how the output of a system changes with varying signal frequency and is hence another crucial aspect of microphone characterization. In pursuit of obtaining the frequency response, the microphones were exposed to a chirp signal that covers frequencies from 2 Hz to 20 kHz. During preliminary tests on the reliability of the wireless data transmission over WiFi, it became apparent that some samples are lost. In order to obtain a qualitative frequency response over all frequencies present in the chirp signal, this experiment was repeated three times, and the recorded signals were averaged in the time domain. Subsequently, the DC offset was removed from the averaged signal by subtracting its mean value. Then, the zero-centered signal was normalized by dividing through its maximal value to achieve a comparability between the sensor's signals. In the next step, the signal was converted into the frequency domain by means of a Fast Fourier Transform (FFT). Finally, the spectrum was smoothed out in order to remove noise and fluctuations that obscure the genuine frequency response. For smoothing, an averaging window of 32 Hz was slid across the spectrum.

The spectra obtained for all the sensors can be seen in Figure 6.4. Hereafter, follows a comprehensive analysis of the frequency responses subdivided by the microphone types:

Electret Microphone Board

The sampling frequency of the ADC was configured to 16 kHz. Consequently, consistent with the Nyquist criterion, the electret microphone cannot detect frequencies beyond 8 kHz. The frequency response of the electret condenser breakout board shown in Figure 6.4A) is akin to the simulated Bode diagram of its circuitry shown in Figure 5.3 in Section 5.2.1. A pronounced dip at 50 Hz is caused by the notch filter, and frequencies above 2 kHz are being attenuated due to the low-pass filters applied in the circuit.

Piezoelectric Transducer Board

Similarly to the electret microphone, the maximum perceptible frequency of the piezoelectric transducer is 8 kHz. Its frequency response is depicted in Figure 6.4B) and shows a nearly flat trend for frequencies below 200 Hz. For larger frequencies, the spectrum is highly irregular and shows noticeable peaks at 2.7 kHz, 5.1 kHz and 6.7 kHz. The latter could represent the resonance frequency of the CEB-20D64 piezoelectric element. The low-pass filter designed in the circuitry seems to be insufficient at attenuating frequencies above 2 kHz because high frequencies are more perceptible than those of the cardiac frequency range below 500 Hz. However, it has to be kept in mind that the piezoelectric element should be placed against a vibrating surface, unlike done in this experiment where sound

waves were transmitted over air. This could lead to a deformation of the true frequency response.

MEMS Microphone Board

The MEMS microphones are sampled at a frequency of 48 kHz and can therefore theoretically sense frequencies up to 24 kHz. However, the microphone's data sheet states that the maximum detectable frequency is 20 kHz. Figure 6.4C) reveals that similarly to the frequency response of the electret condenser microphone, the spectrum of the MEMS microphone shows an evident dip at 50 Hz, suggesting that a notch filter was incorporated in its internal circuitry. Apart from that, the frequency response of the MEMS microphone appears non-uniform and shows similar sharp peaks like the piezoelectric transducer at 5.1 kHz, 6.9 kHz and 12.5 kHz.

3M Littmann Core Stethoscope

The sampling frequency of the commercial stethoscope is 4 kHz and the Fourier transform covers frequencies up to 2 kHz. As can be seen in Figure 6.4D), frequencies below 10 Hz are being suppressed. Subsequently, the frequency response follows a fairly flat curve with peaks at 100 Hz, 400 Hz and 670 Hz. Its frequency response is fairly flat in the range of 60 Hz to 750 Hz with peaks at 100 Hz, 400 Hz and 670 Hz. The spectrum begins to decline at frequencies beyond 750 Hz.

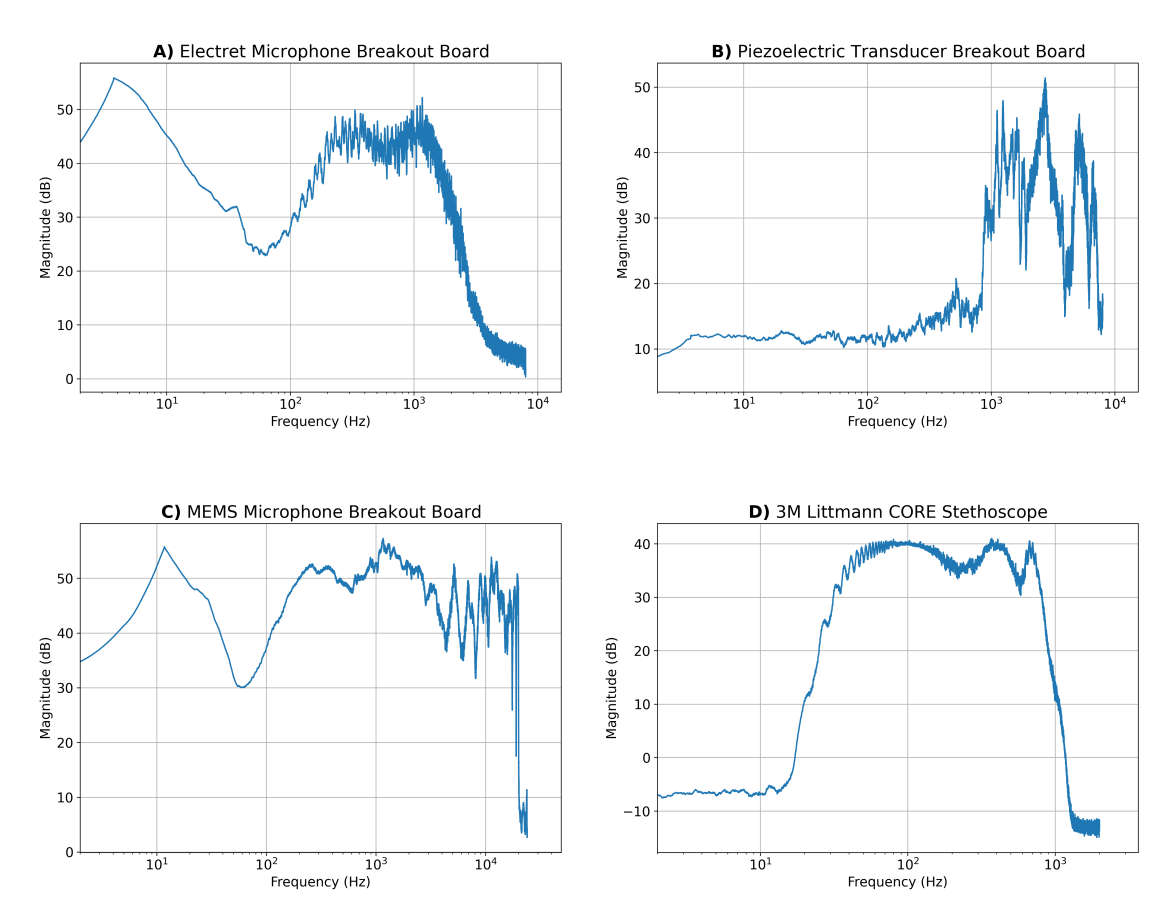


Figure 6.4: Frequency Responses for all developed microphone boards and the commercial reference stethoscope after exposing them to a chirp signal from 2 Hz to 20 kHz. The recorded signals were post-processed by averaging over three recordings, removing the DC components and normalizing the signal. The frequency response was obtained by applying an FFT to the time-domain signals and subsequently smoothing the acquired spectrum by shifting an averaging window of 32 Hz over the spectrum.

6.1.4 Heart Sound emitted by Loudspeaker

As a final measure to evaluate the performance of the microphone boards, the loudspeaker in the anechoic box emitted the beating of a healthy heart. This experiment was done in order to inspect how the different microphone boards react to an identical and reproducible heart beat before applying it to the human chest. For this purpose, the heart beat of a healthy 26-year old woman with BMI 21.1 was recorded with the 3M Littmann CORE stethoscope at auscultation point 1. The same recording was already used for the SNR analysis in Chapter 6.1.1. The sensors were arranged in 50 cm distance to the loudspeaker except for the piezoelectric transducer that was placed against the loudspeaker to detect vibrations. The sensors captured the previously recorded heart beat emitted by the loudspeaker and their recordings were normalized in order to be aligned with the original signal recorded with the digital stethoscope. This procedure was repeated with the 3M Littmann CORE stethoscope. An extract of these recordings showing one full cardiac cycle can be seen in Figure 6.5.

All acoustic sensors are capable of detecting both the S1 and S2 heart sounds. However, in all recordings, the heart sounds contain frequencies that are higher than those of the original signal. The shape of the recordings made with the electret condenser microphone, the MEMS microphone, and the commercial digital stethoscope resemble that of the original signal. In contrast to that, the shape of the signal captured with the piezoelectric transducer declines almost exponentially after a heart sound is detected. Furthermore, the S2 heart sound sensed by the piezoelectric transducer is of a higher amplitude than the S1 heart sound, although in the original signal both heart sounds are almost of the same amplitude. This could be due to the sound transduction mechanism of the piezoelectric transducer or the modified measurement procedure.

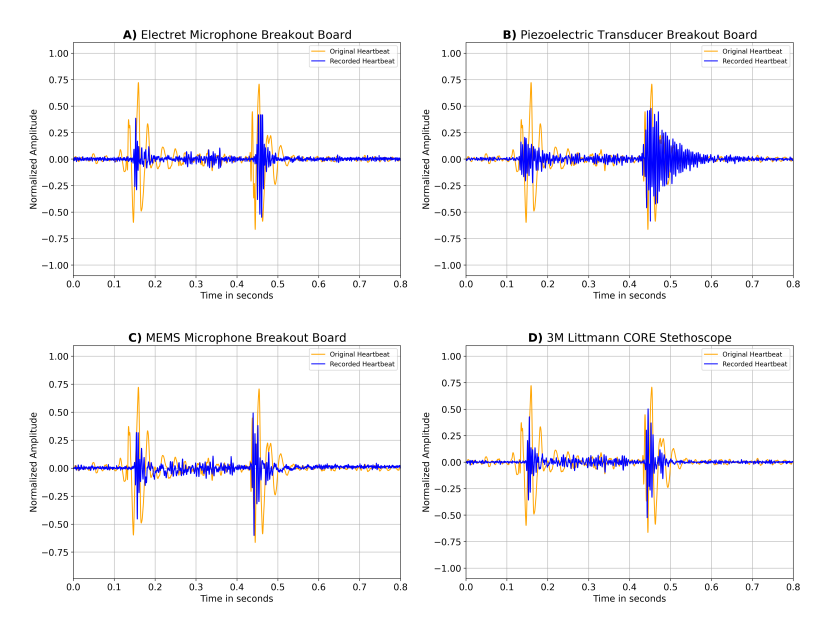


Figure 6.5: Recordings of the loudspeaker in the anechoic box emitting a heart beat of a healthy, 26-year old woman with BMI 21.1. The original signal was recorded with the 3M Littmann CORE stethoscope from auscultation point 1 and was emitted by the loudspeaker. The original signal is shown in orange. The recordings performed with each microphone are shown in blue. The first peak represents the S1 heart sound and the second peak shows the S2 heart sound.

6.2 Microphone Performance on Recording Heart Sounds

After characterizing the microphone boards in a controlled environment, they were applied to a real-life scenario capturing heart sounds at the five auscultation points presented in Figure 2.4. All microphone types were placed individually precisely on the auscultation points and in direct contact to the skin.

All recordings were made in a silent environment. As some microphone boards do not show sufficient sensitivity, for some measurements the subject performed a short exercise of approximately 30 seconds to increase the intensity of the heart sound. This is indicated in the captions of the figures shown below. The resulting signals were analyzed in terms of shape and frequency components and compared to the profile of a reference signal found in the literature (compare Figure 2.3).

6.2.1 Individual Microphone Types applied to Auscultation Points

To evaluate the ability of the microphone boards to capture the heart beat in a real-case scenario, each microphone type was placed on the five auscultation points in direct contact with the skin. A five-second recording of a healthy female heart beat was made. Subsequently, the DC offset was removed from the collected signal by subtracting its mean value, and the signals were normalized to make their amplitudes comparable to each other. The resultant signals per auscultation point along with their corresponding spectrograms can be seen in Figures 6.6, 6.7 and 6.8 for the electret condenser microphone, the MEMS microphone and the piezoelectric transducer, respectively. Hereafter, the results per microphone board are explained in detail:

Electret Condenser Microphone Board

Figure 6.6 shows the signals recorded with an electret microphone board at each auscultation point. The test person performed 30 seconds of exercise to increase the intensity of the heart beat as no heart sounds were detected for a resting pulse. This might be due to the prominent noise floor and the weak SNR of the microphone board (compare Sections 6.1.1 and 6.1.2). Although the heart rate cannot be easily derived from the mere signals, the frequency representations show subsequent vertical lines, representing the major heart sounds and indicating a rate of 108 bpm. In the spectrogram for auscultation point 2 one can even distinguish between the first and the second heart sound. Furthermore, the spectrograms reveal that the major frequency components of the heart sounds lie below 500 Hz. Only the spectrogram for point 3 exceeds this value.

In general, the signals recorded with the electret microphone suffer from noise and it is hard to adequately distinguish heart beats from each other.

Piezoelectric Transducer Board

Heart sound signals recorded with the piezoelectric transducer board and their corresponding spectrograms are shown in Figure 6.7. For auscultating points 1 and 2, the test person performed 30 seconds of exercise, as the intensity of the resting heart beat was too weak to detect a valuable signal. The resting heart rate can be deduced from the signals for auscultation points 3-5 and equals 76 bpm. In the corresponding spectrograms, one can even distinguish the heart sounds S1 and S2 that are illustrated by two successive vertical lines followed by a short pause until the next heart beat starts.

The simplest way to determine the accelerated heart rate after doing some exercise is by inspecting the signal from auscultation point 1 which yields 87 bpm. However, in the corresponding spectrogram only one of the two major heart sounds can be seen clearly.

Similarly, in the signal recorded from point 2 and its corresponding spectrogram, the distinction between the S1 and S2 heart sound is challenging.

The overall frequencies recorded across all auscultation points does not exceed 1 kHz and are more pronounced below $500~\mathrm{Hz}$.

MEMS Microphone Board

The signals recorded with the MEMS microphone board are depicted in Figure 6.8 and clearly show a resting heart beat of approximately 72 bpm at all auscultation points. For this microphone type no physical activity was necessary as the microphone has a sufficiently high SNR. The corresponding spectrograms reveal that the frequency components of the heart sounds go up to 1 kHz with frequencies below 500 Hz being more pronounced.

In the signals collected from auscultation points 3 - 5 both major heart sounds S1 and S2 can be visibly distinct, with the S1 heart sound generating a higher amplitude in the signals than the S2 heart sound. This is reflected in the spectrograms for these auscultation points, where the S1 heart sound appears with a higher magnitude (more yellow) than the S2 heart sound.

In contrast, the signals recorded at auscultation points 1 and 2 suffer from more distortions and noise and show a blurring between the first and the second heart sound in both the signal plot and the corresponding spectrograms. A clear distinction between the heart sounds is not possible.

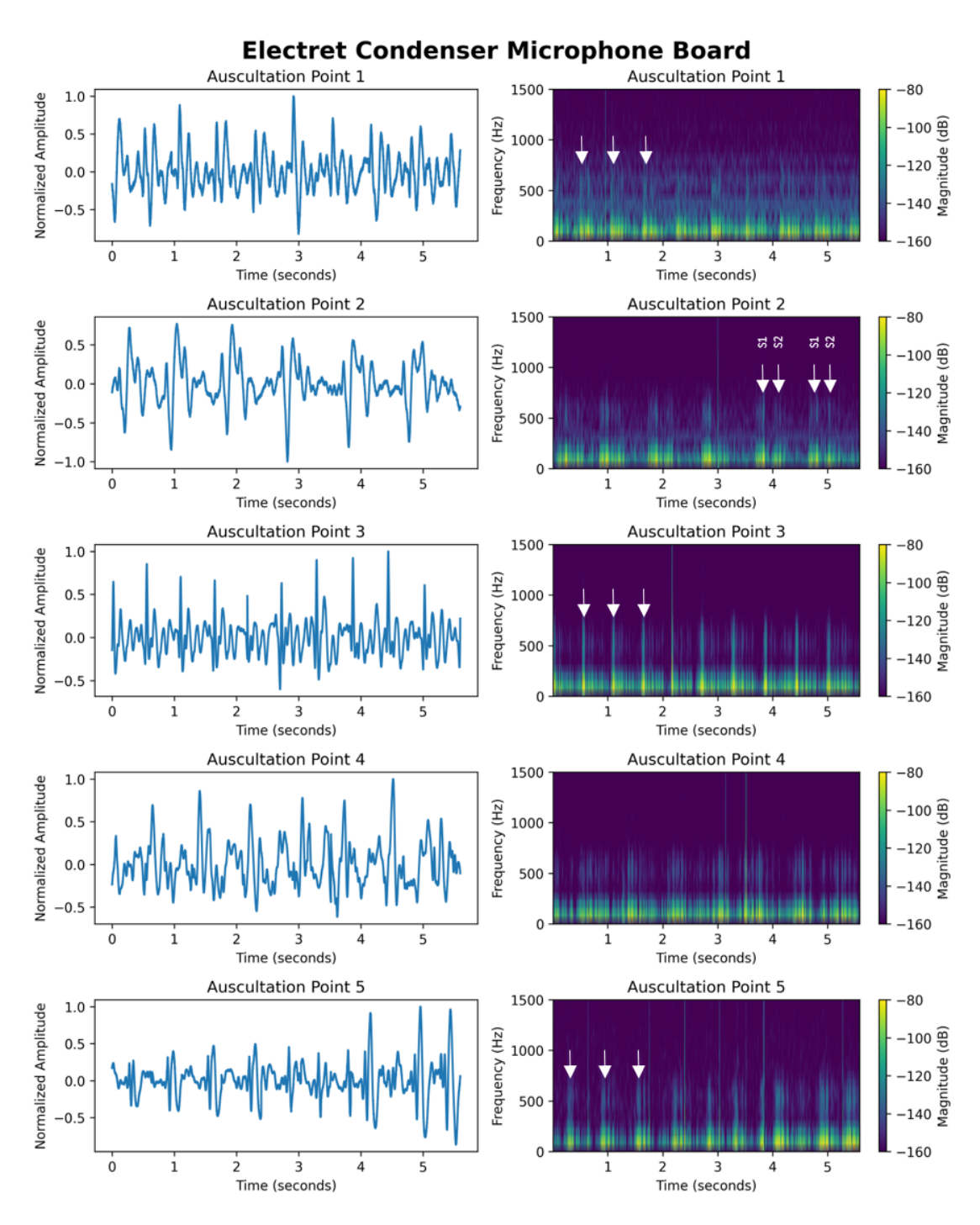


Figure 6.6: Heart sound of a healthy 26-year old woman with BMI 21.1 performed with the electret condenser microphone breakout board at the five auscultation points shown in Figure 2.4. Right: recorded signals of 5 seconds with normalized amplitude for each auscultation point. Left: corresponding spectrogram showing the frequency distribution over time, the colors relate to magnitude of frequencies at a certain time point. For all auscultation points, the subject performed 30 seconds of exercise to increase the heart beat intensity

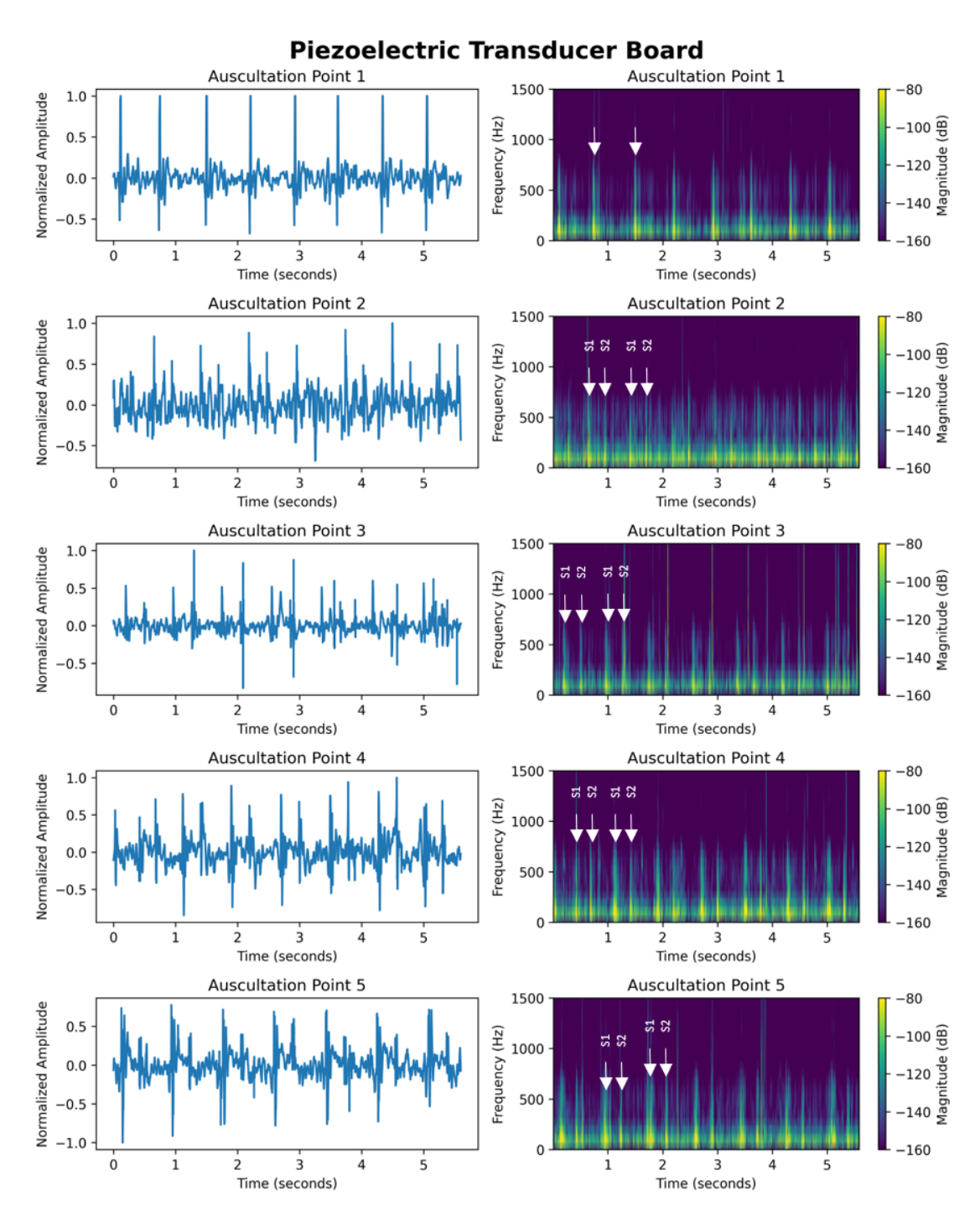


Figure 6.7: Heart sound of a healthy 26-year old woman with BMI 21.1 performed with the piezoelectric transducer breakout board at the five auscultation points shown in Figure 2.4. Right: recorded signals of 5 seconds with normalized amplitude for each auscultation point. Left: corresponding spectrogram showing the frequency distribution over time, the colors relate to magnitude of frequencies at a certain time point. For auscultation point 1 the subject performed 30 seconds of exercise to increase the heart beat intensity

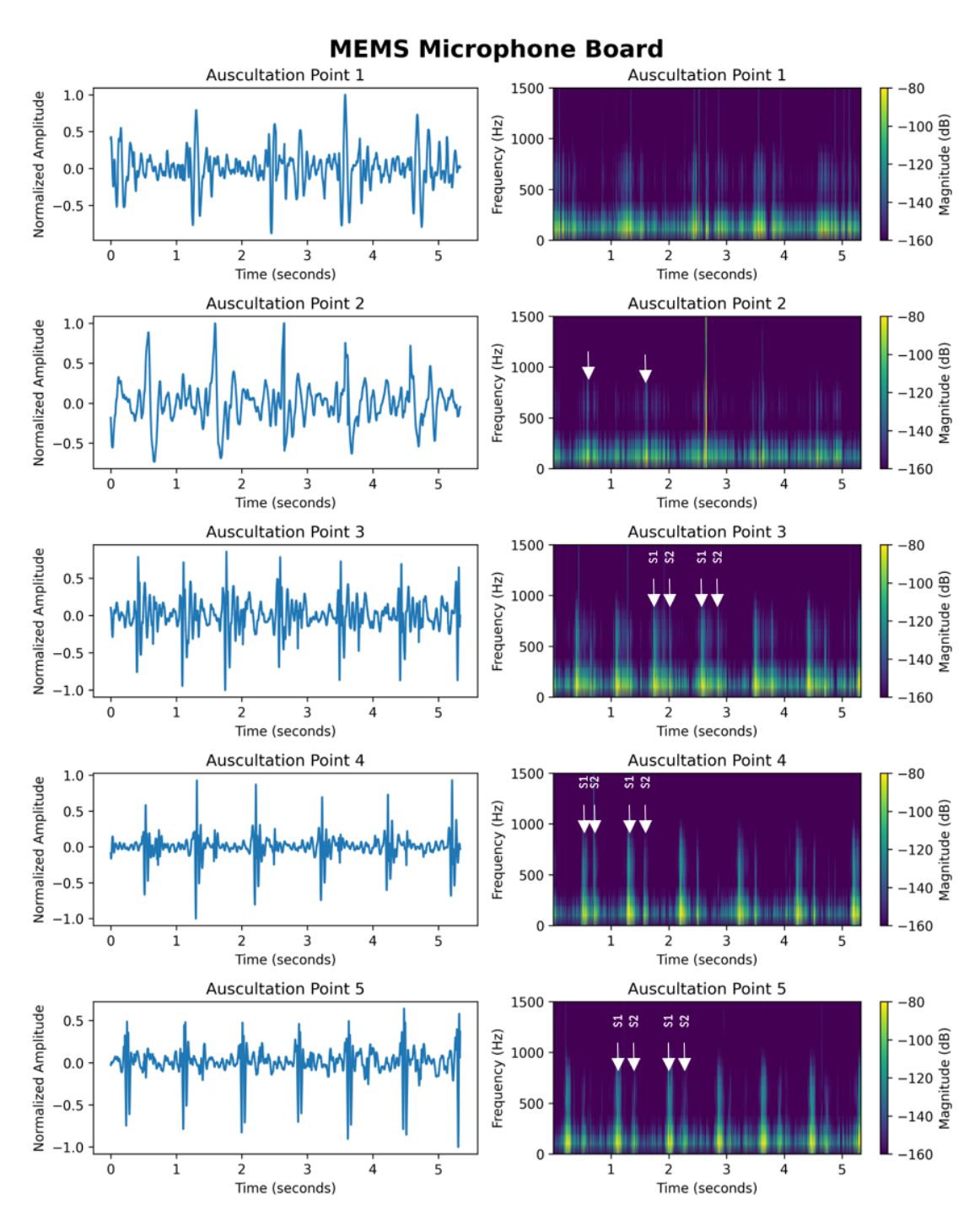


Figure 6.8: Heart sound of a healthy 26-year old woman with BMI 21.1 performed with the MEMS microphone breakout board at the five auscultation points shown in Figure 2.4. Right: recorded signals of 5 seconds with normalized amplitude for each auscultation point. Left: corresponding spectrogram showing the frequency distribution over time, the colors relate to magnitude of frequencies at a certain time point.

6.3 Summary of the Findings

The previous sections in this chapter described in detail the performances of the developed microphone boards and the commercial 3M Littmann CORE stethoscope by thoroughly examining their characteristics ranging from a noise floor and sensitivity measurement over an SNR analysis to a frequency response evaluation. After determining their general characteristics, the microphone boards were tested on their ability to capture heart sounds using two methods: First, the microphones were exposed to a loudspeaker that emitted heart sounds. Secondly, the microphone boards were precisely placed on the five heart auscultation points. The following paragraph briefly summarizes the findings of the aforementioned experiments and is sorted by the sections of this chapter.

The noise floor measurement revealed that the MEMS microphone board senses the least noise level compared to the other two microphone boards and picks up a comparable amount of noise as the commercial stethoscope. In contrast to that, the electret microphone board perceives the highest noise floor.

Figure 6.2 shows the response curves over sound volume of the analyzed sensors. For all microphone boards and the commercial stethoscope, the response curves demonstrate a linear behavior for increasing sound volumes.

While the absolute SNR is the highest for the piezoelectric transducer, the MEMS microphone board exhibits the largest SNR for a typical heart beat and performs similar to the commercial stethoscope in this regard.

The frequency responses of the sensors are depicted in Figure 6.4. The electret condenser microphone board shows a response similar to the simulated Bode plot of its circuitry depicted in Figure 5.3. The piezoelectric transducer follows a flat trend for low-frequency components less than 200 Hz. However, the circuit is more sensitive to high frequency components than to frequencies in the cardiac range below 500 Hz. The frequency response of the MEMS microphone board shows a highly irregular profile and suggests that the circuit incorporates a 50 Hz notch filter. The frequency response of the commercial stethoscope shows a uniform shape and indicates a high sensitivity of the incorporated sensor between 10 Hz and 750 Hz.

When the microphone boards and the commercial stethoscope were exposed to a loudspeaker that emitted heart beats, they were all capable of detecting the two heart sounds in a cardiac cycle. However, the recorded signals show higher frequency components than the original signal. The electret condenser microphone board, MEMS microphone board, and the commercial stethoscope showed comparable profiles while the piezoelectric transducer board showed an exponential decline after each heart beat.

After characterizing the microphone boards in an anechoic chamber, they were exposed to natural heart beats. The microphone boards proved that they are all capable of sensing heart sounds when placed precisely on an auscultation point. However, the signals of the electret microphone board are obscured by noise and the resting heart beat signals are too weak to be perceived by the sensor. Therefore, the subject had to perform physical activity to increase the signal's amplitude. Similarly, for the piezoelectric transducer board, the heart beat at auscultation points 1 and 2 could only be detected after doing some exercise. In contrast to the electret and piezoelectric microphone boards, the MEMS microphone board can accurately detect heart sounds mostly without the need for performing prior physical activity.

Due to the aforementioned reasons, the MEMS microphone appears to be superior over the other two developed microphone boards as it shows the lowest noise floor level, highest SNR for a typical heart beat and was the easiest to operate when conducting an auscultation scenario on a healthy heart.

Chapter 7

Conclusion and Future Work

Stethoscopes are an essential instrument for evaluating body sounds and are prevalent in medical practice. In the early 90s, electronic stethoscopes emerged on the market, striving for an enhanced sound quality and compensating for the varying hearing abilities of physicians. However, they target the human hearing range and thereby ignore the potential of advanced and affordable microphone technology. The thesis proposes an upgrade of analog stethoscopes that allows the recording of body sounds during the traditional auscultation process. This gives fully functional conventional stethoscopes an additional value and prevents them from being discarded in replacement of a new digital stethoscope.

The stethoscope developed in the course of this thesis offers high flexibility regarding microphone technology and is compatible with multiple computation platforms. These can enable the verification and prototyping of algorithms ranging from signal processing techniques to AI models. This makes the device a potential research platform. Furthermore, the device can be helpful in teaching students and professionals about diverse microphone technologies and auscultation techniques.

A modular design approach was chosen that ensures easy replacement and repair of damaged components. These features make the prototype a sustainable and eco-friendly solution for upgrading a conventional stethoscope.

The prototype comes with multiple acoustic sensor types that are arranged in an array, supporting the deployment of advanced processing algorithms, thus potentially improving the accuracy of medical diagnoses.

In essence, the proposed design is an add-on device to a stethoscope's chestpiece that does not interfere with the mechanical appearance of the chestpiece. The device can be easily assembled and disassembled with a conventional stethoscope. The prototype consists of three layers: an analog front end, an interface layer and a back end. The analog front end features three acoustic sensor types, namely, an electret condenser microphone, a piezoelectric transducer, and a MEMS microphone. The signals captured with these transducers are sent to the main board in the interface layer. The main board contains an ADC that converts the analog signals to digital signals and is connected to a buck converter that powers the entire device. Finally, the digital signals are transmitted to the back end that supports a large variety of computational platforms from which the user can choose.

Although the prototype is designed to detect various body sounds, the performance of the acoustic sensors was demonstrated using the example of the heart beat. First, the sensors were characterized in an anechoic box by determining their noise floors, sensitivities, frequency responses, and ability to sense heart sounds emitted by a loudspeaker. The commercial 3M

Littmann CORE stethoscope was analogously analyzed. Secondly, they were applied to natural heart auscultation scenarios.

The MEMS microphone achieved superior results regarding noise floor and SNR compared to the other two acoustic sensors and shows comparable performance to the commercial stethoscope. Beyond that, the MEMS microphones reliably detected resting heart beat signals in real-life auscultation scenarios. The electret condenser microphone appeared to be the worst candidate for heart auscultation due to a high noise level and low SNR. This made it difficult to detect heart beats and to distinguish between the first and second heart sound.

It has to be acknowledged that the device was solely tested on a limited number of subjects and has to be further evaluated in a larger study to assess the full potential of the acoustic sensors.

Currently, the prototype is powered through wires from a power supply, which does not allow for portability. In the next development stage, a rechargeable battery could be incorporated instead

Considering the limited scope of this thesis, the multi-sensor approach still leaves room for plenty of research. The sensors offer heterogeneous responses and can thus potentially be qualified for different auscultation sites. Future work could study the performance categorized by microphone type and body sound.

Furthermore, the microphone array arrangement was not exhausted for signal processing and analysis. In upcoming projects, techniques like sensor fusion or beamforming can be employed, for example, to determine the exact location of the sound source. This could potentially reveal new diagnostic details and eventually lead to more accurate disease identification and characterization. Furthermore, signals from multiple locations surrounding an auscultation point can be a valuable feature for machine learning algorithms.

The prototype is a platform for versatile future research and education. Its flexible back end could initiate various future projects that can range from simple IoT projects to advanced machine learning algorithms. Besides that, it can be implemented in laboratories at universities or training programs. Medical students can benefit from this approach by simply upgrading their pre-existing conventional stethoscope with the presented add-on device. Thereby, they can replay heart sounds repeatedly and learn to pick up on essential diagnostic details.

In conclusion, the modular electronic stethoscope presented herein demonstrates how conveniently and elegantly a conventional stethoscope can be transformed into a digital one, offering multi-sensor technology and capabilities for sensor fusion.

Chapter 8

Societal Reflection

The prototype presented in this thesis is intended to be used as an upgrade for a conventional stethoscope or as an educational and potential research platform. Understanding its full implications on society and the environment is a crucial step towards a comprehensive design. This chapter provides reflection on the consequences that the device might entail by considering ethical, sustainability, safety, and societal aspects.

Ethical Considerations

Body sound recordings are a type of health record and are, therefore, sensitive and confidential data. Currently, the prototype uses WiFi to send sensitive personal data from an MCU to a PC without considering any form of data encryption. This approach was chosen for simplicity reasons, as including data protection would have been outside the scope of this thesis. However, it leaves the setup vulnerable to data theft, which poses a threat to privacy and has to be addressed before the device is used on a larger scale.

Sustainability Factor

The current setup does not incorporate a rechargeable battery, which could make it a more sustainable design. Further, energy efficiency has not been considered within the scope of this thesis and needs to be optimized in future work.

Naturally, an electronic stethoscope can never meet the energy efficiency of an analog stethoscope. However, electronic stethoscopes offer valuable features such as an improved sound quality and the possibility to replay and re-evaluate body sounds. The stethoscope presented in this thesis represents a good compromise between the two worlds and allows physicians to easily upgrade their analog stethoscope. Thereby it could prevent analog stethoscopes from being discarded in replacement of a digital stethoscope.

Therefore, the prototype could potentially lead to a reduction in waste.

Safety Evaluation

The breakout boards that hold the acoustic sensors and that are placed in direct contact with the skin are connected to the power supply and thereby pose a potential safety hazard to the patient. A shielding must be incorporated to adequately isolate the electric circuit from the patient.

Furthermore, the sharp headers on the breakout boards need to be smoothed to ensure a comfortable auscultation scenario for the patient.

Impact on Society and Accessibility

Analog stethoscopes are essential devices that are used in the daily routines of doctors. Therefore, most physicians already own an analog stethoscope. The device presented in this thesis offers a simple but effective upgrade to these stethoscopes while simultaneously allowing the owner to restore the original shape of her or his stethoscope at any time. The device is optimal for individuals who are hesitant to purchase a purely digital stethoscope and for those who are interested in comparing the audio quality of multiple sensors. Furthermore, the device enables to store and send recordings of body sounds to re-evaluate them at a later time or to discuss them with experts. This could possibly result in more accurate identification of diseases and ultimately promote public health.

The prototype can further be of value as an educational platform for both medical and engineering students and professionals to understand advancements made in microphone technology and auscultation techniques. This could additionally boost interdisciplinary collaborations.

Thanks to advances in microphone manufacturing, acoustic sensors are becoming affordable and, therefore, more accessible to the public. Since the prototype can also be used as a stand-alone device, there is no need to possess an analog stethoscope, thus expanding its range of applications.

However, it is important to note that the prototypes' large dimensions make it most likely not suitable for auscultating children. In another version of the device, the size of the developed stethoscope could be reduced by placing the sensors in the array arrangement closer together and thereby adapt it to the dimensions of children's and infants' chests.

Appendix A

Versions of the piezoelectric transducer set-up

When assessing the designed breakout board of the piezoelectric transducer it became obvious that the transducer may not be in direct contact with the human skin due to its electrical conductivity. Furthermore, in order to exploit the piezoelectric effect, the transducer has to be deformed. Therefore, different set-ups encapsulating the transducer were tested ultimately leading to the final version shown and explained in Chapter 5.2.1. This chapter is dedicated to present those set-ups. For all tests, the designed breakout board for the piezoelectric transducer was connected to an oscilloscope. For versions 1 and 2 an amplification factor of 150 was used. In later versions this factor was increased to 1k as this increased the signals amplitude without significantly increasing the noise.

Furthermore, as a first test, the carotid or radial pulses where measured as they are easier to access than the five auscultation points of the heart.

Version 1: Plain transducer in a plastic bag

The first basic trial to decouple the transducer from the human skin was to put it into a plastic bag. With this set-up it was possible to measure the radial pulse (see figure A.1). However, the sensed voltage amplitudes are only of a few millivolts in amplitude and in general this set-up is challenging to operate: A lot of pressure has to be applied to the backside of the transducer and it is cumbersome to find the right spot on the skin to sense an identifiable signal. Heart beats from the five auscultation points presented in figure 2.4 were impossible to detect.

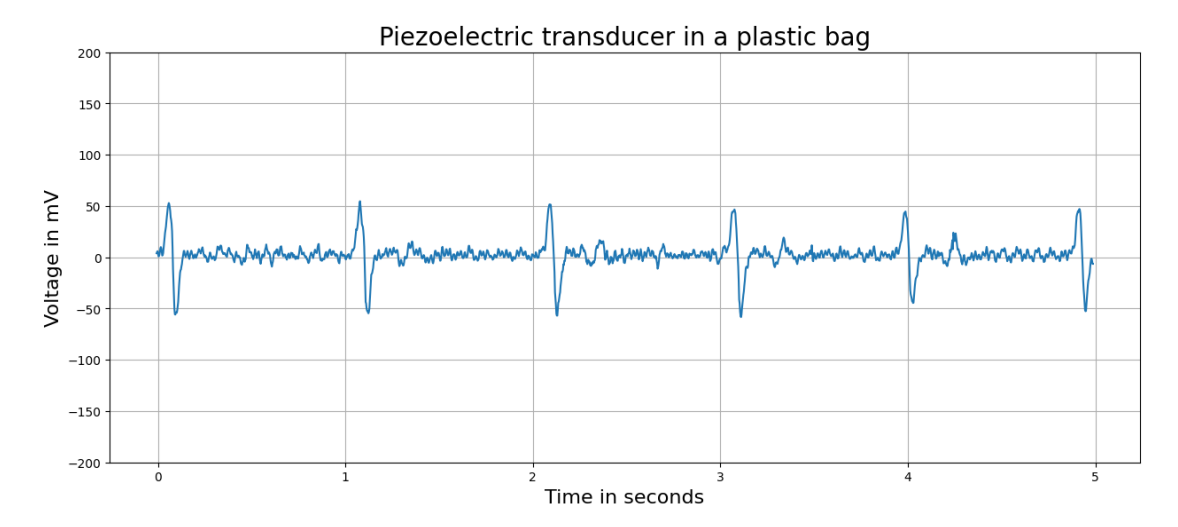


Figure A.1: Heart pulse measured at the left radial artery with the piezoelectric transducer covered by a plastic bag, amplification factor: 150; measured with an oscilloscope

Version 2: Transducer mounted on a chestpiece

The findings from version 1 showed that the transducer has to be mounted by some means. A straightforward approach is to fix it to the diaphragm of a chestpiece to mimic the conventional principle of stethoscope auscultation. An exemplary setup is shown in figure A.2. Three different variations of fixating the transducer were tested: a) the transducer is inserted into a plastic bag which is attached to the diaphragm such that the following layering evolves: stethoscope diaphragm - plastic foil - piezoelectric transducer - plastic foil - tape - human skin. b) same setup but the tape is no longer covering the transducer and c) the transducer is no longer inside the bag; instead only one layer of plastic foil is sandwiched between the transducer and the skin such that the layering transforms into stethoscope diaphragm - piezoelectric transducer - plastic foil - human skin.

The resulting signals measured at the carotid artery are visualized in figure A.3. Their amplitude is still of a few millivolts only and especially version 2 a) is spoiled by noise likely due to multiple layers of plastic and tape. The signal measured with version 2 c) shows a clearer signal similar to a typical carotid pulse. This setup is additionally able to sense heart sounds at auscultation points 4 and 5 (see figure A.4). Heart beats at other auscultation points were not detectable with this setup.

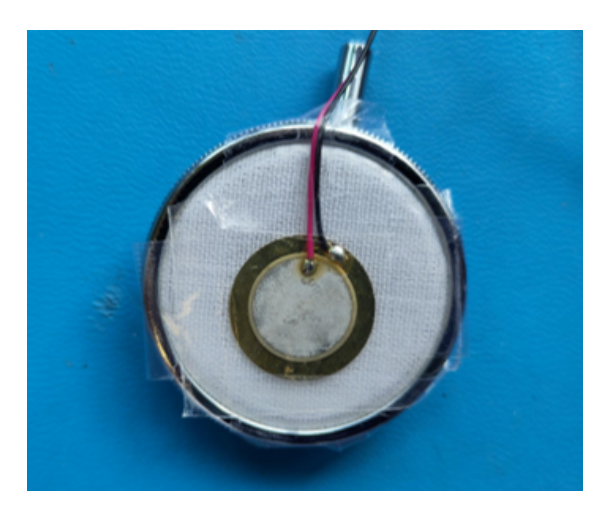


Figure A.2: Piezoelectric transducer mounted on the diaphragm of a stethoscope chestpiece in three different layering variations: a) stethoscope diaphragm - plastic foil - piezoelectric transducer - plastic foil - tape - human skin, b) stethoscope diaphragm - plastic foil - piezoelectric transducer - plastic foil - human skin and c) stethoscope diaphragm - piezoelectric transducer - plastic foil - human skin

Version 3: Transducer mounted on a chestpiece + deformation of transducer

Version 2c) showed the most promising results in the previous chapter and was further equipped with a rubber pen that additionally applied deforming forces to the internal part of the piezo-electric transducer (compare figure A.5). This approach was tested as it might further exploit the piezoelectric characteristic of the transducer. Furthermore, the amplification factor of the measured signals was increased to 1k.

Figure A.6 shows the corresponding signals measured with this setup version. For all auscultation points clear heart beats signal can be sensed.

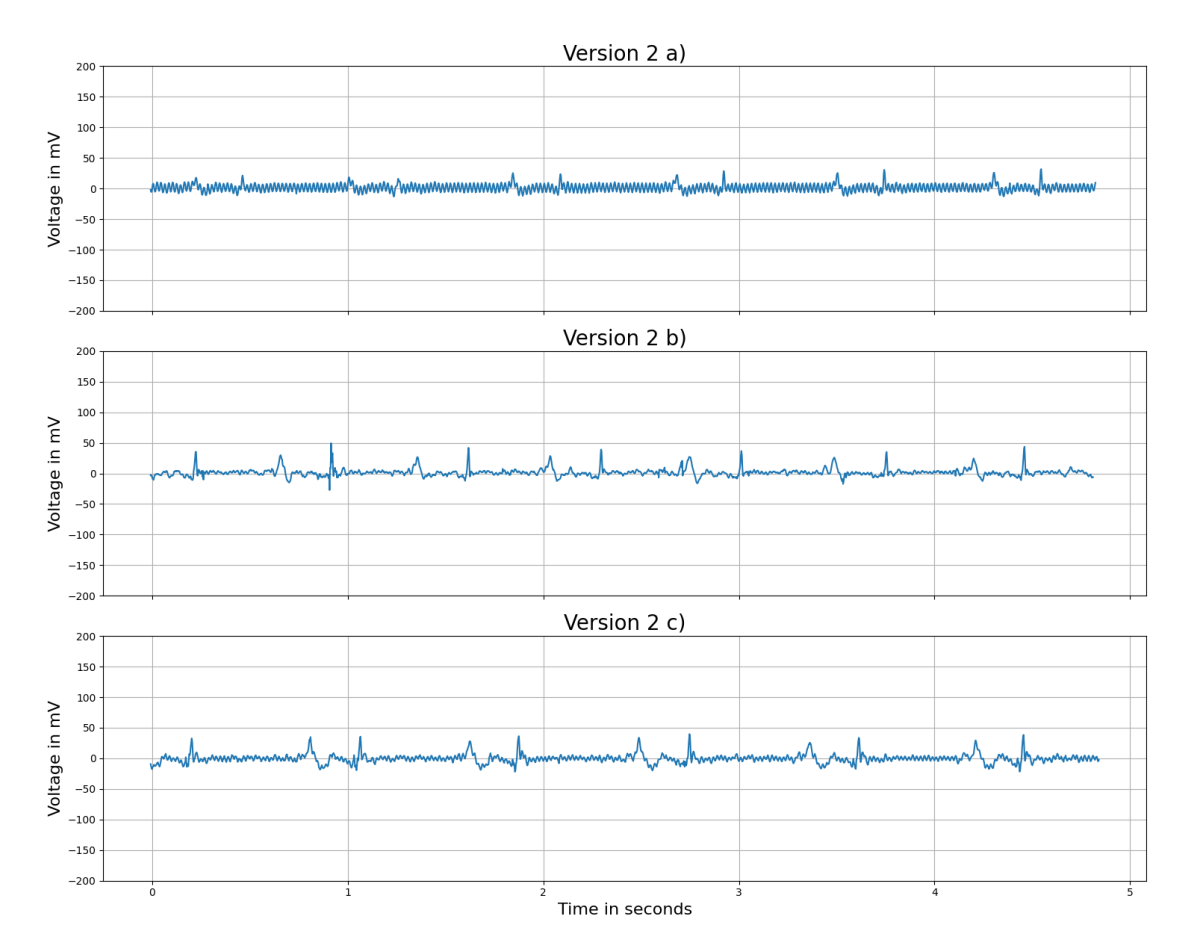


Figure A.3: Carotid pulse measured with the piezoelectric transducer in the set-up presented in figure A.2.

- a) stethoscope diaphragm plastic foil piezoelectric transducer plastic foil tape human skin,
- b) stethoscope diaphragm plastic foil piezoelectric transducer plastic foil human skin and
- c) stethoscope diaphragm piezoelectric transducer plastic foil human skin, amplification factor: 150; measured with an oscilloscope

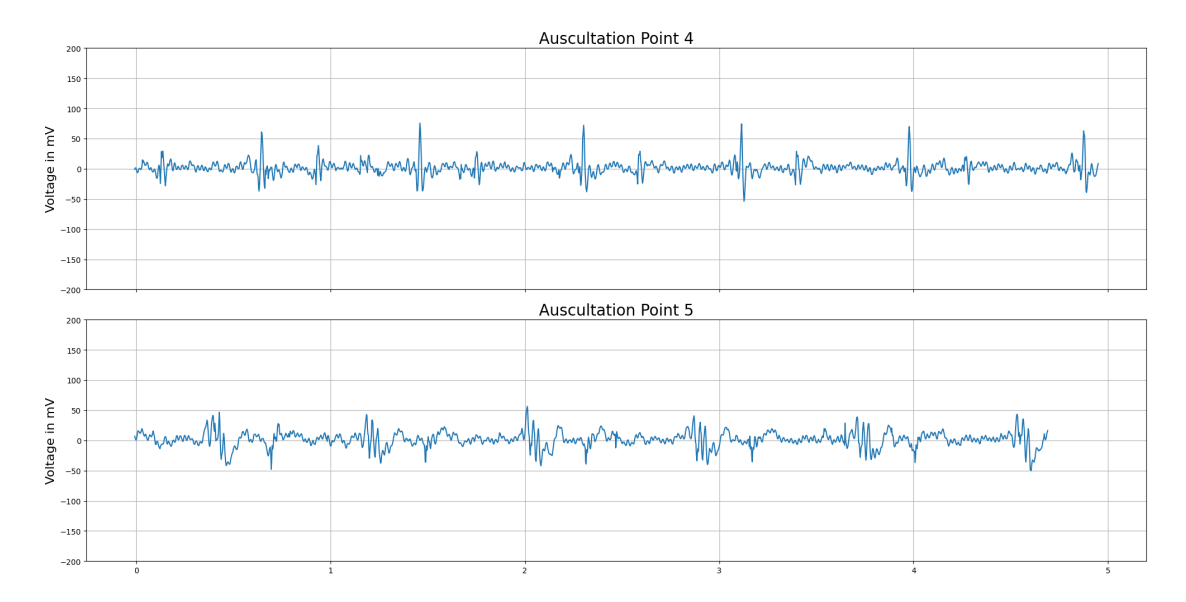


Figure A.4: Heart beat measurements at auscultation points 4 and 5, measured with piezoelectric transducer in the set-up presented in figure A.2, version 2c), amplification factor: 150; measured with an oscilloscope

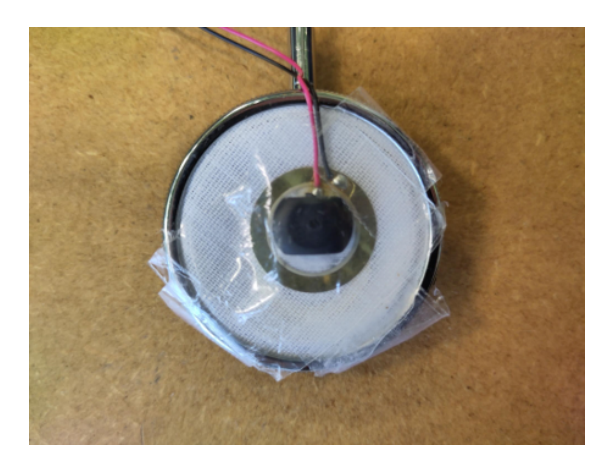


Figure A.5: Piezoelectric transducer mounted on the diaphragm of a stethoscope chestpiece in combination with a black rubber pen deforming the transducer in response to skin vibrations

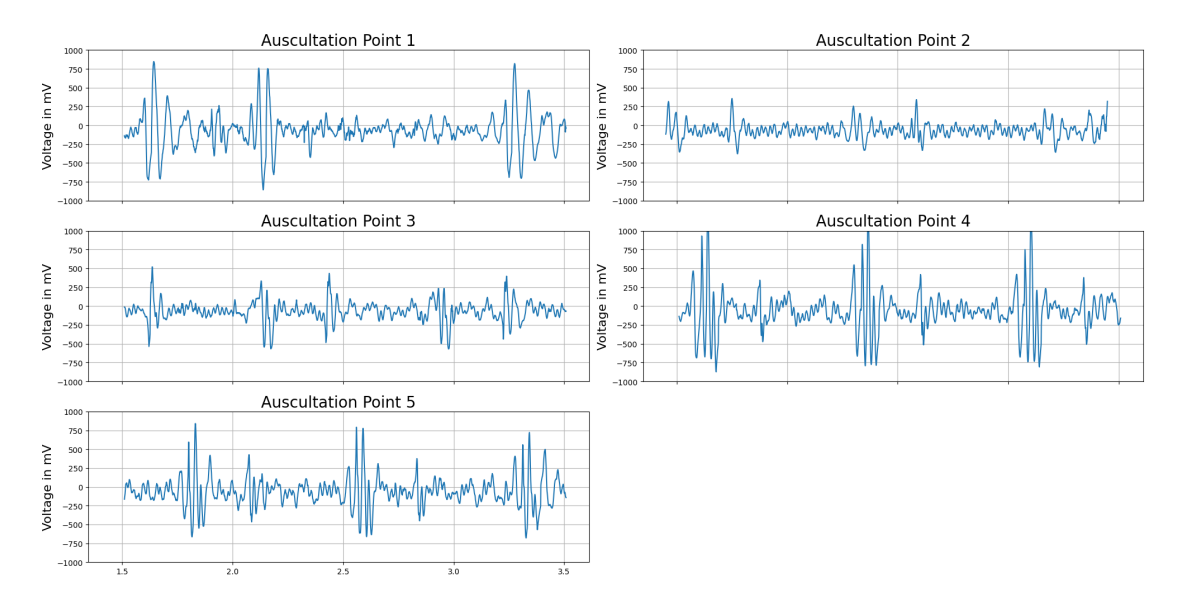


Figure A.6: Heart beat measurements at all auscultation points, measured with piezoelectric transducer in the set-up presented in figure A.5, amplification factor: 1k; measured with an oscilloscope,

Version 4: Transducer mounted behind diaphragm of chestpiece

As with version 3 heart beats at all auscultation point can be sensed, in this approach the transducer is placed behind the diaphragm of the chestpiece as can be seen in figure A.7. However, this approach showed to reduce the signal's strength and it was only possible to sense auscultation points 2, 3 and 4 (compare figure A.8).

Furthermore, setup versions 3 and 4 are rather impractical to operate and there would not be enough space on the diaphragm to install four piezoelectric transducers as intended. Therefore, they do not suite the design specifications of the electronic stethoscope. However, those versions provide information about the features a casing for the piezoelectric transducer might have to have in order to maximize the signal-to-noise-ratio.



Figure A.7: Piezoelectric transducer mounted behind the diaphragm of a stethoscope chestpiece in combination with a black rubber pen deforming the transducer in response to skin vibrations

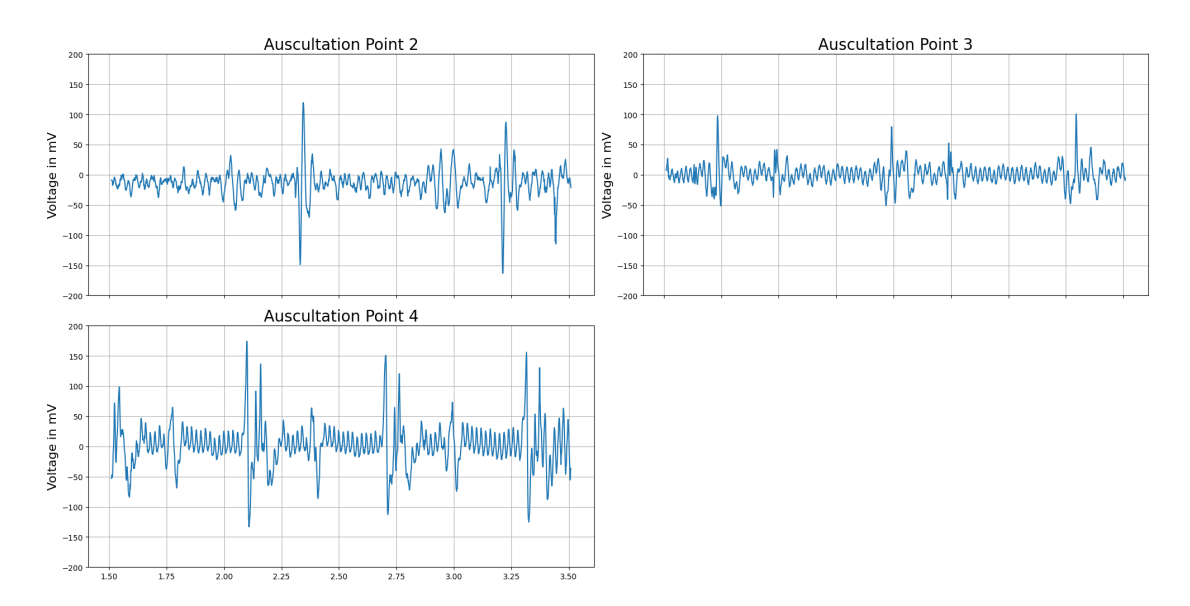


Figure A.8: Heart beat measurements at auscultation points 2, 3 and 4, measured with piezo-electric transducer in the set-up presented in figure A.7, amplification factor: 1k; measured with an oscilloscope,

Version 5: Transducer mounted in a custom, 3D printed casing

From the previous versions it becomes apparent that the plane transducer attached to the human skin does not yield an adequate signal-to-noise ratio. A casing for the piezoelectric transducer must deform it in response to vibration or sound waves. In setup version 5 a casing for the transducer is presented consisting of two parts: a backplane fixating the transducer and a top part that dynamically compresses it and therefore mimics the black rubber pen from setup versions 3 and 4. This version closely resembles the final version of the transducer setup presented in chapter 5.2.1. The two approaches only differ by the cavity present in the final version (Figure 5.7) but not in version 5 that can be seen in figure A.9.

Heart beats at all auscultation points were measured with this setup and are depicted in figure A.10. At all auscultation points both heart sounds S1 and S2 are observable. Furthermore, the setup has a sufficient ease of operability and is space-saving such that four transducers can be simultaneously attached to the electronic stethoscope.

The final casing of the piezoelectric transducer derives from the version presented in this section by adding a cavity below the transducer as to further increase it deformation and consequently the signal's amplitude.

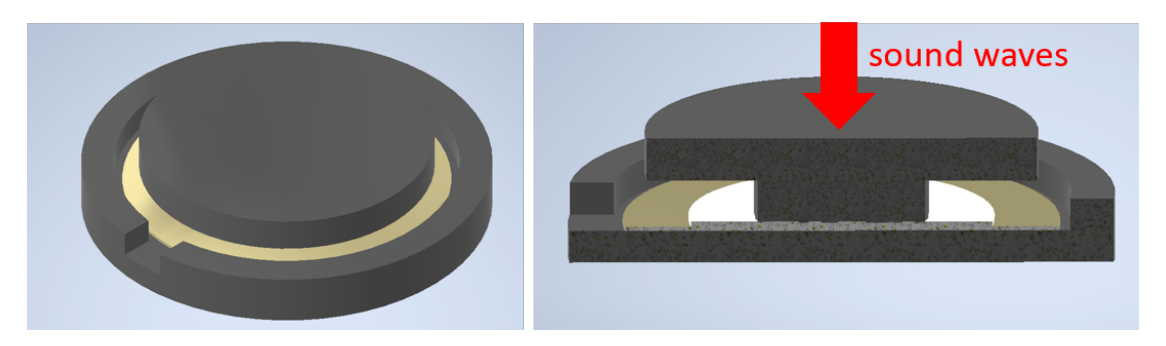


Figure A.9: Piezoelectric transducer (gold-white) encapsulated by a casing consisting of two black parts. Left: Isometric view on the assembly, a notch is left open for the wires of the transducer. Right: cross-section of the set-up, sound waves exert forces on the center of the transducer leading to its deformation and ultimately to an electric signal

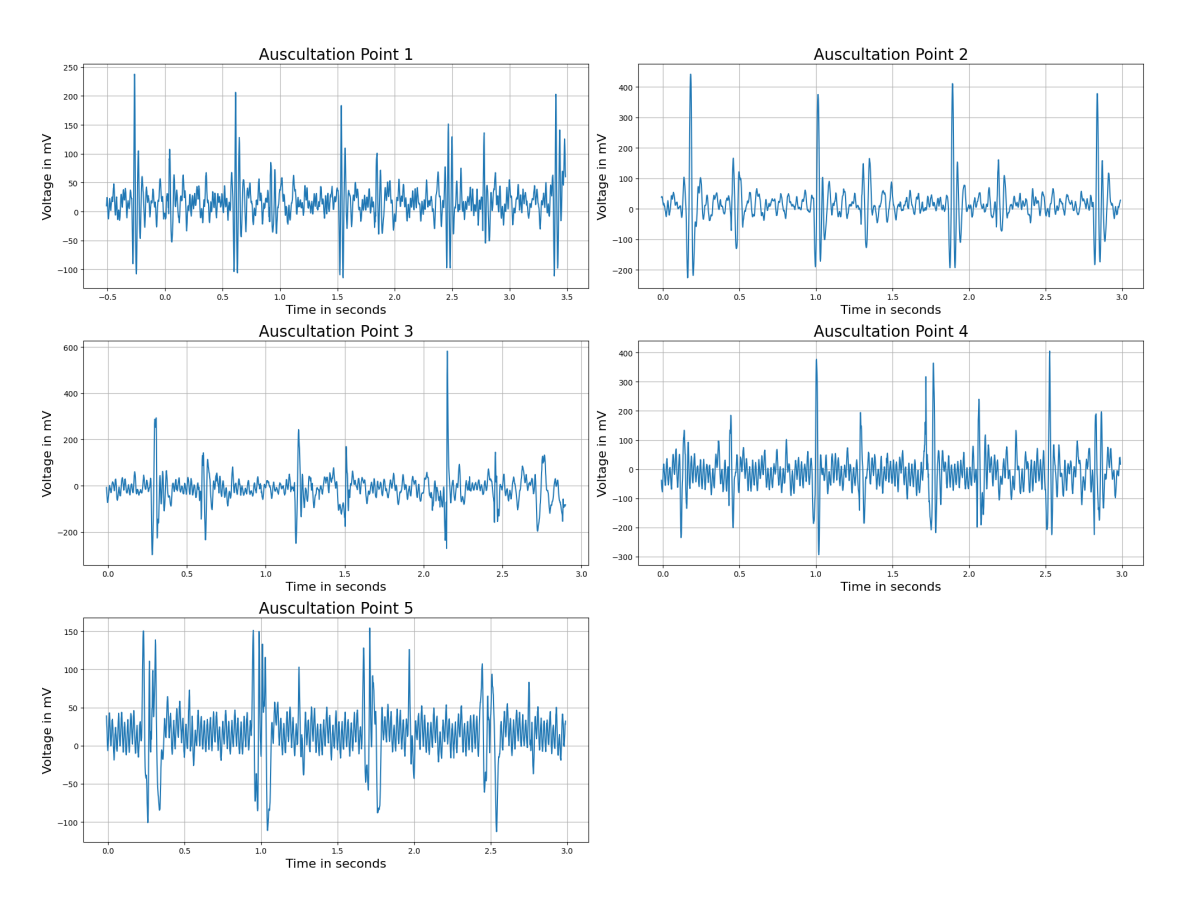


Figure A.10: Heart beat measurements at all auscultation points, measured with piezoelectric transducer in the casing presented in figure A.9, amplification factor: 1k; measured with an oscilloscope

Bibliography

- [1] 3M. 3M[™] Littmann® CORE Digital Stethoscope. URL: https://www.littmann.com/3M/en_US/p/d/b5005222000/. (accessed: 07.11.2023).
- [2] 3M. 3M[™] Littmann® CORE Digital Stethoscope FAQs. URL: https://www.littmann.com/3M/en_US/littmann-stethoscopes/advantages/core-digital-stethoscope/. (accessed: 07.11.2023).
- [3] Abbas K Abbas and Rasha Bassam. "Phonocardiography signal processing". In: vol. 31. Morgan & Claypool Publishers, 2009. Chap. 1, pp. 1–27.
- [4] Antonio Arnau and David Soares. "Piezoelectric Transducers and Applications". In: Springer, 2008. Chap. Fundamentals of Piezoelectricity, pp. 1–37.
- [5] Ayesha Azmeen et al. "Heart sounds: Past, present, and future from a technological and clinical perspective—a systematic review". In: *Proceedings of the Institution of Mechanical Engineers, Part H: Journal of Engineering in Medicine* 237.6 (2023), pp. 669–682.
- [6] Heather Baid. "A critical review of auscultating bowel sounds". In: *British journal of nursing* 18.18 (2009), pp. 1125–1129.
- [7] Dipali Bansal. "Potential of piezoelectric sensors in bio-signal acquisition". In: Sensors & Transducers 136.1 (2012), pp. 147–157.
- [8] Cardionics. Clinical E-Scope® Electronic Stethoscope. URL: https://cardionics.com/en/product/clinical-e-scope-electronic-stethoscope/. (accessed: 08.11.2023).
- [9] Cardionics. Operator's Manual E-Scope® II Electronic Stethoscope. English. 23 pp.
- [10] Muhammad EH Chowdhury et al. "Real-time smart-digital stethoscope system for heart diseases monitoring". In: Sensors 19.12 (2019), p. 2781.
- [11] Rijuven Corp. Cardiosleeve. URL: https://www.rijuven.com/cardiosleeve. (accessed: 08.11.2023).
- [12] Medical Device Depot. Clinical E-Scope Stethoscope. URL: https://www.medicaldevicedepot.com/Clinical-E-Scope-Stethoscope-p/718-7700.htm. (accessed: 08.11.2023).
- [13] Analog Devices. LT8653S. URL: https://www.analog.com/en/products/lt8653s.html. (accessed: 12.01.2025).
- [14] Digikey. CEB-20D64. URL: https://www.digikey.com/en/products/detail/same-sky-formerly-cui-devices/CEB-20D64/412385. (accessed: 12.01.2025).
- [15] Digikey. CMA-4544PF-W. URL: https://www.digikey.be/en/products/detail/cui-devices/CMA-4544PF-W/1869981. (accessed: 08.12.2024).
- [16] Digikey. DMM-4026-B-I2S-R. URL: https://www.digikey.com/en/products/detail/pui-audio-inc/DMM-4026-B-I2S-R/11587483. (accessed: 28.12.2024).

- [17] Digikey. NCP164CSN180T1G. URL: https://www.digikey.com/en/products/detail/onsemi/NCP164CSN180T1G/11592813. (accessed: 29.12.2024).
- [18] Omar Diouri et al. "Comparison study of hardware architectures performance between FPGA and DSP processors for implementing digital signal processing algorithms: Application of FIR digital filter". In: *Results in Engineering* 16 (2022), p. 100639.
- [19] eKuore. eKuore Pro User manual. English. 144 pp.
- [20] eKuore. eKuore Pro Electronic Stethoscope. URL: https://ekuore.com/product/ekuore-pro-electronic-stethoscope/. (accessed: 09.11.2023).
- [21] eKuore. eKuore Trajectory. URL: https://ekuore.com/about/. (accessed: 09.11.2023).
- [22] Ltd. GS Technology Co. JABES Electronic stethoscope Sister Products. English. 2022. 19 pp.
- [23] GST. JABES Digital Electronic Stethoscope. URL: https://cardionics.com/en/product/clinical-e-scope-electronic-stethoscope/. (accessed: 08.11.2023).
- [24] Eko Health. Instructions for Use CORE 500[™] Digital Stethoscope. English. 29 pp.
- [25] Eko Health Inc. 3M™ Littmann® CORE Digital Stethoscope. URL: https://www.ekohealth.com/products/3m-littmann-core-digital-stethoscope?variant=39410642190432&gad=1&gclid=CjwKCAiA3aeqBhBzEiwAxFi0BuEhdp8upEQ9diGMh2xEfmJ-E6DoqE8G1_Sc-gGS38QmZZLcmznVxxoCtxUQAvD_BwE. (accessed: 07.11.2023).
- [26] Eko Health Inc. Eko Core 500[™] Digital Stethoscope. URL: https://www.ekohealth.com/products/core-500-digital-stethoscope?variant=39662120304736. (accessed: 06.11.2023).
- [27] Eko Health Inc. Eko's Story. URL: https://www.ekohealth.com/pages/about-us. (accessed: 12.11.2023).
- [28] Texas Instruments. ADS131A04. URL: https://www.ti.com/product/ADS131A04. (accessed: 30.12.2024).
- [29] Ninik Irawati et al. "Heart rate monitoring sensor based on singlemode-multimode-singlemode fiber". In: *Photonic Sensors* 10 (2020), pp. 186–193.
- [30] Agam Jain et al. "Development and validation of a low-cost electronic stethoscope: DIY digital stethoscope". In: *BMJ Innovations* (2021), bmjinnov-2021.
- [31] Yoojin Jeong et al. "Methods for improving deep learning-based cardiac auscultation accuracy: Data augmentation and data generalization". In: *Applied Sciences* 11.10 (2021), p. 4544.
- [32] Licheng Jia et al. "Design and characterization of an aluminum nitride-based MEMS hydrophone with biologically honeycomb architecture". In: *IEEE Transactions on Electron Devices* 68.9 (2021), pp. 4656–4663.
- [33] Licheng Jia et al. "Piezoelectric micromachined ultrasonic transducer array-based electronic stethoscope for internet of medical things". In: *IEEE Internet of Things Journal* 9.12 (2022), pp. 9766–9774.
- [34] Keith H Johnson and David A Underwood. Recording, digital stethoscope for identifying PCG signatures. US Patent 5,025,809. June 1991.
- [35] Michael Klum et al. "Wearable cardiorespiratory monitoring employing a multimodal digital patch stethoscope: estimation of ECG, PEP, LVET and respiration using a 55 mm single-lead ECG and phonocardiogram". In: Sensors 20.7 (2020), p. 2033.

- [36] Michael Klum et al. "Wearable multimodal stethoscope patch for wireless biosignal acquisition and long-term auscultation". In: 2019 41st annual international conference of the IEEE engineering in medicine and biology society (EMBC). IEEE. 2019, pp. 5781–5785.
- [37] Konstanze Kölle et al. "Data driven filtering of bowel sounds using multivariate empirical mode decomposition". In: *BioMedical Engineering OnLine* 18 (2019), pp. 1–20.
- [38] Steve S Kraman et al. "Measurement of respiratory acoustic signals: effect of microphone air cavity width, shape, and venting". In: *Chest* 108.4 (1995), pp. 1004–1008.
- [39] Rinat K Kusainov and Vladimir K Makukha. "Evaluation of the applicability of MEMS microphone for auscultation". In: 2015 16th International Conference of Young Specialists on Micro/Nanotechnologies and Electron Devices. IEEE. 2015, pp. 595–597.
- [40] KunHyuck Lee et al. "Mechano-acoustic sensing of physiological processes and body motions via a soft wireless device placed at the suprasternal notch". In: *Nature biomedical engineering* 4.2 (2020), pp. 148–158.
- [41] Shuenn-Yuh Lee et al. "Intelligent Stethoscope System and Diagnosis Platform with Synchronized Heart Sound and Electrocardiogram Signals". In: *IEEE Access* (2023).
- [42] Soo Hyun Lee et al. "A wearable stethoscope for accurate real-time lung sound monitoring and automatic wheezing detection based on an AI algorithm". In: (2023).
- [43] Sung Hoon Lee, Yun-Soung Kim, and Woon-Hong Yeo. "Advances in microsensors and wearable bioelectronics for digital stethoscopes in health monitoring and disease diagnosis". In: Advanced Healthcare Materials 10.22 (2021), p. 2101400.
- [44] Shuang Leng et al. "The electronic stethoscope". In: Biomedical engineering online 14.1 (2015), pp. 1–37.
- [45] Jerad Lewis. "Common inter-IC digital interfaces for audio data transfer". In: EDN-Electronic Design News 57.16 (2012), p. 46.
- [46] Shih-Hong Li et al. "Design of wearable breathing sound monitoring system for real-time wheeze detection". In: Sensors 17.1 (2017), p. 171.
- [47] Steven McGee. "Evidence-Based Physical Diagnosis (Second Edition)". In: Elsevier Health Sciences, 2007, pp. 411–471.
- [48] Trang Nguyen Minh et al. "Design of Real-time and Low-cost Electronic Stethoscope". In: 2023 International Conference on Communication, Circuits, and Systems (IC3S). IEEE. 2023, pp. 1–4.
- [49] Roshan D. Modi, Christopher S. Massad, and B. Robinson Williams. "Handbook of Outpatient Cardiology". In: Springer, 2022. Chap. 5 The Cardiovascular Physical Exam, pp. 75–88.
- [50] Maximilian Nussbaumer and Anurag Agarwal. "Stethoscope acoustics". In: *Journal of Sound and Vibration* 539 (2022), p. 117194.
- [51] World Health Organization. *Electronic waste (e-waste)*. URL: https://www.who.int/news-room/fact-sheets/detail/electronic-waste-(e-waste). (accessed: 08.01.2025).
- [52] Geoffrey Ottoy, Bart Thoen, and Lieven De Strycker. "A low-power MEMS microphone array for wireless acoustic sensors". In: 2016 IEEE Sensors Applications Symposium (SAS). IEEE. 2016, pp. 1–6.
- [53] Achilles J. Pappano and Withrow Gil Wier. "Cardiovascular Physiology". In: Elsevier, 2013. Chap. 4 - The Cardiac Pump, pp. 55–90.

- [54] Heejoon Park et al. "Novel Design of a Multimodal Technology-Based Smart Stethoscope for Personal Cardiovascular Health Monitoring". In: Sensors 22.17 (2022), p. 6465.
- [55] Sandra Reichert et al. "Analysis of respiratory sounds: state of the art". In: Clinical medicine. Circulatory, respiratory and pulmonary medicine 2 (2008), CCRPM-S530.
- [56] Rijuven. CardioSleeve: User Manual. English. 2013. 40 pp.
- [57] Muhammad Ali Shah et al. "Design approaches of MEMS microphones for enhanced performance". In: Journal of sensors 2019 (2019).
- [58] Mubashar Hussain Sherazi. "The Objective Structured Clinical Examination Review". In: Springer, 2019. Chap. 4 - The Cardiovascular System, pp. 111–130.
- [59] Clive Smith. Stethoscope and electronic device structure. US20160262717A1. Oct. 2016.
- [60] Clive Smith. Transducer for sensing body sounds. US Patent 6,661,897. Dec. 2003.
- [61] Jeff Smoot. PDM vs. I²S: Comparing Digital Interfaces in MEMS Microphones. URL: https://www.sameskydevices.com/blog/pdm-vs-i2s-comparing-digital-interfaces-in-mems-microphones?srsltid=AfmBOorQ48KbVuqcUhw-vZTsvaz2_i2nOHmpclHLueCz_6cDoxo_lppr. (accessed: 28.12.2024).
- [62] Ángel Solé Morillo et al. "Ppg edukit: An adjustable photoplethysmography evaluation system for educational activities". In: Sensors 22.4 (2022), p. 1389.
- [63] Caitlin N Teague et al. "Novel methods for sensing acoustical emissions from the knee for wearable joint health assessment". In: *IEEE Transactions on Biomedical Engineering* 63.8 (2016), pp. 1581–1590.
- [64] TelehealthTechnology. *Electronic Stethoscopes JABES*. URL: https://telehealthtechnology.org/toolkit/electronic-stethoscopes-jabes/. (accessed: 08.11.2023).
- [65] Thinklabs. Thinklabs ONE Digital Stethoscope. URL: https://www.thinklabs.com/. (accessed: 07.11.2023).
- [66] Thinklabs. Thinklabs One User's Manual. English. 2014. 33 pp.
- [67] Thinklabs. Thinklabs Support. URL: https://support.thinklabs.com/support/solutions/48000449526. (accessed: 07.11.2023).
- [68] Arie Van Rhijn. "Integrated circuits for high performance electret microphones". In: *Audio Engineering Society Convention 114*. Audio Engineering Society. 2003.
- [69] V Nivitha Varghees and KI Ramachandran. "A novel heart sound activity detection framework for automated heart sound analysis". In: *Biomedical Signal Processing and Control* 13 (2014), pp. 174–188.
- [70] Fengle Wang et al. "A flexible skin-mounted wireless acoustic device for bowel sounds monitoring and evaluation". In: Science China Information Sciences 62 (2019), pp. 1–11.
- [71] Tian Wang et al. "Acoustic-pressure sensor array system for cardiac-sound acquisition". In: Biomedical Signal Processing and Control 69 (2021), p. 102836.
- [72] Weidong Wang et al. "A bat-shape piezoresistor electronic stethoscope based on MEMS technology". In: Measurement 147 (2019), p. 106850.
- [73] George R Wodicka et al. "Measurement of respiratory acoustic signals: effect of microphone air cavity depth". In: *Chest* 106.4 (1994), pp. 1140–1144.
- [74] Yu-Chi Wu et al. "Development of an electronic stethoscope and a classification algorithm for cardiopulmonary sounds". In: Sensors 22.11 (2022), p. 4263.

- [75] Chuan Yang et al. "A low-cost, ear-contactless electronic stethoscope powered by Raspberry Pi for auscultation of patients with COVID-19: prototype development and feasibility study". In: *JMIR Medical Informatics* 9.1 (2021), e22753.
- [76] Gürkan Yilmaz et al. "A wearable stethoscope for long-term ambulatory respiratory health monitoring". In: Sensors 20.18 (2020), p. 5124.
- [77] Damjan Zazula, Denis Đonlagić, and Sebastijan Šprager. "Fibre-optic interferometry as a means for the first heart sound detection". In: Advances in applied information science (2012), pp. 31–35.